NEUTRON FLUX AND TEMPERATURE ANALYSIS OF THE SLOWPOKE-2 AND ASSOCIATED CFD MODEL

ANALYSE DU FLUX NEUTRONIQUE ET DE LA TEMPÉRATURE DU RÉACTEUR SLOWPOKE-2 ET DU MODÈLE ASSOCIÉ DE DYNAMIQUE NUMÉRIQUE DES FLUIDES

A Thesis Submitted to the Division of Graduate Studies
of the Royal Military College of Canada
by

Marco Donato Di Giovanni, BSc

In Partial Fulfillment of the Requirements for the Degree of
Master of Science

April 2023

Acknowledgements

I wish to thank Dr. Paul Chan for his supervision and patient guidance throughout this project. I also want to extend my gratitude to Dr. Jordan Morelli for his continued supervision and support. Appreciation must also be extended to Dr. Pavel Samuleev for lending his expertise on the SLOWPOKE-2. In addition, I would like to thank Dr. Bryan van der Ende for his patience and advice with this project. Thanks, as well as to the CNL team including Dr. Krishna Podila, and Dr. Sur Bhaskar for their work. For software used in this project, additional thanks must be extended to CMC Microsystems.

Abstract

The SLOWPOKE-2 reactor at the Royal Military College (RMC) of Canada, has recently undergone refuelling, providing a unique opportunity to investigate core behaviour before and after refuelling. By investigating the temperature differences between the two cores, the energy difference between the two cores is estimated. Furthermore, a sensitivity analysis into the temperature probes in the system reports the uncertainty of these measurements and indicates low power outlet temperature data to have the least error.

Currently, the SLOWPOKE-2 thermal power is estimated by scaling neutron flux data based on an initial calibration during construction that has substantial measurement uncertainties. In order to determine thermal power of the reactor based on measurable operating parameters computational fluid dynamic (CFD) models of the system have been constructed. These models aim to reduce the error and verify the current reported thermal power of the reactor. This accurate thermal output determination in tandem with neutron flux data from various detectors around the reactor should allow enhanced fuel monitoring in the SLOWPOKE-2. This thesis has an application for remote monitoring of reactor power and fissile material of small modular reactors (SMR) and may provide an additional safeguard against nuclear material proliferation.

Keywords: CFD, SLOWPOKE-2, SMR, ANSYS, neutron flux, thermal power, non-proliferation, fuel monitoring, refuelling.

Résumé

Le réacteur SLOWPOKE-2 au Collège militaire royal su Canada (CMR) a récemment reçu une recharge en combustible, ce qui a fourni une occasion unique d'étudier le comportement du cœur du réacteur avant et après la recharge. On a estimé la différence de l'énergie entre les deux cœurs en déterminant leur différence de température. De plus, une analyse de sensibilité des sondes de température dans le système rapporte l'incertitude de ces mesures et indique que les données de la température de la sortie à basse puissance sont les plus précises.

Présentement, on estime la puissance thermique du réacteur SLOWPOKE-2 à partir d'un facteur de proportionnalité appliqué aux mesures du flux neutronique sur la base d'une calibration initiale effectuée durant la construction du réacteur et qui exhibe une incertitude importante. Afin de déterminer la puissance thermique du réacteur sur la base de paramètres opérationnels mesurables, des modèles de Dynamique Numérique des Fluides (DNF) du système ont été construits. Ces modèles visent à réduire l'erreur et à vérifier la puissance thermique du réacteur telle que rapportée couramment. Cette détermination précise de la puissance thermique, de concert avec les données du flux neutronique provenant des divers détecteurs autour du réacteur, devrait permettre une surveillance accrue du combustible dans le réacteur SLOWPOKE-2. Cette thèse comprend une application pour la surveillance à distance de la puissance du réacteur et des matériaux fissiles des petits réacteurs modulaires (PRM), et peut fournir une garantie de sécurité additionnelle contre la prolifération des matériaux nucléaires.

Table of Contents

List of Tables

List of Figures

Statement of Work

The CAD provided for this thesis was created by the modelling team at CNL. The SLOWPOKE-2 reactor operating data was provided by Dr. Samuleev. CFD models using STAR-CCM+ for comparison with model developed by the author was provided by Dr. Podilla (of CNL).

Acronyms

ANSYS	Commercial Analysis System.
BCS	Boron-coated straw neutron flux detector.
CAD	Computer-aided design.
CANDU	CANada Deuterium Uranium
CFD	Computational Fluid Dynamics
CMC	Canadian Microelectronics Corporation
CNL	Canadian Nuclear Laboratories
CPU	Central Processing Unit
CRNL	Chalk River Nuclear Laboratories
GCI	Grid Convergence Index
HTGR	High-Temperature Gas Reactor
IAEA	International Atomic Energy Agency
MSR	Molten Salt Reactor
NRU	National Research Universal
RAM	Random Access Memory
RMC	Royal Military College
SIRCIS	SLOWPOKE Integrated Reactor Control Instrumentation System
SLOWPOKE-2	Safe LOW-POwer Kritical Experiment 2
SMR	Small Modular Reactor

Chapter 1: Introduction

Small modular reactor (SMR) technology has been proposed in recent years as a means to generate clean energy across Canada. The benefits of SMR development include nuclear power deployment in remote communities, faster and cheaper construction than traditional CANDU reactors, and scalable facilities than can easily accommodate more reactors as needed. SMRs are defined as reactors that output electrical power up to 300MW. The SLOWPOKE-2 (Safe LOW-POwer Kritical Experiment) reactor located at the Royal Military College (RMC) of Canada, is defined as a micro-reactor, fits comfortably in this definition as it outputs a maximum thermal power of 20kW.

One of the challenges of large-scale SMR deployment is safeguarding the fissile material against non-peaceful use. A number of safeguard challenges presented by SMRs have been noted in the literature, especially when using enriched fuel [1-2]. As such, additional methods must be employed to safeguard nuclear fuel if SMRs are to gain widespread adoption.

This project contains work on two primary fronts, computational fluid dynamic (CFD) modelling, and data analysis of SLOWPOKE-2 reactor logs before and after refuelling. Within these two major tasks there are many goals that must be met before both aspects of this project can come together for the ultimate goal of creating an enhanced fuel monitoring system in the SLOWPOKE-2 facility. As such, Figure 1 shows a flowchart of the project, and the order of goals the project must meet.

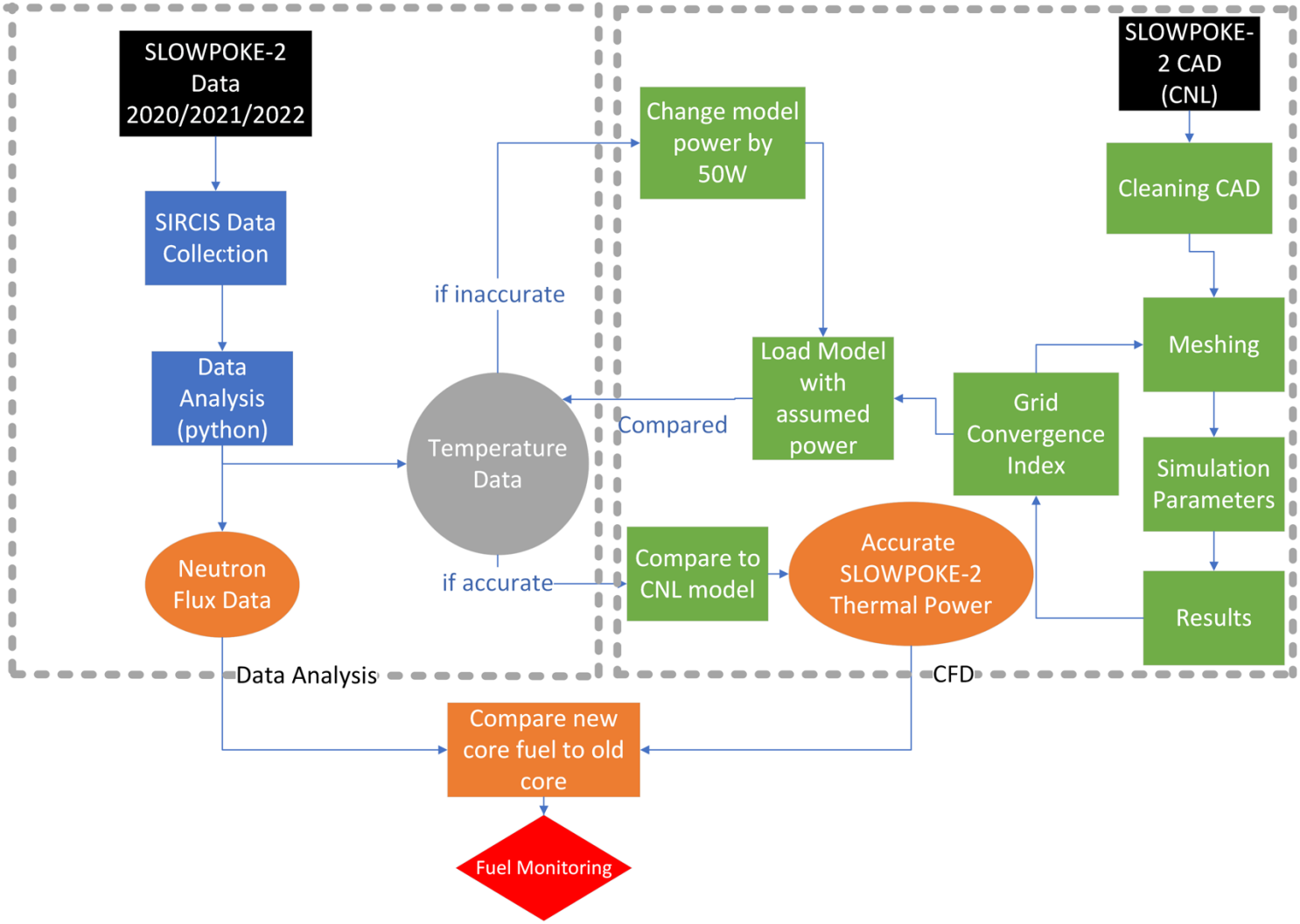

Figure 1: Project flowchart.

The approach outlined in Figure 1 is explained in depth in Chapter 3. As a general overview of the project, the data analysis was conducted first primarily due to the data being available at the beginning of this project whereas the CAD has only been available since April 2022. The data analysis was also conducted first, as a comparison of experimental results to CFD results requires experimental temperature data.

The CFD modelling aspect of this project was done primarily through CMC Microsystems' compute cluster for lower computation times. With this resource, simulations could be done in under 24 hours allowing many different models to be tested. Moreover, the low computation time for the SLOWPOKE-2 system indicates CFD modelling is a useful technique that other experiments involving the SLOWPOKE-2 can take advantage of.

Figure 1 shows the typical project flow for a CFD model. Importantly, after the Grid Convergence Index (GCI), once a converged model is created the simulated results are compared to the experimental results. This will not be the case in all CFD projects; however, because there is experimental data of the SLOWPOKE-2 operation temperatures, this comparison can be done as part of the validation process.

1.1 SLOWPOKE-2 Design

The SLOWPOKE-2 is a pool-type research reactor located at the Royal Military College (RMC) of Canada in Kingston Ontario. The SLOWPOKE-2 is the second iteration of the SLOWPOKE reactor design, a very similar reactor which had been constructed at the Chalk River Laboratories and at the University of Toronto. The SLOWPOKE-2 reactors were commissioned at the University of Alberta, Dalhousie University, Saskatchewan Research Council, Nordion (Kanata), the University of the West Indies Jamaica, and Polytechnique Montreal. Many of these have since been

decommissioned. Details of the SLOWPOKE-2 design given below are from Pierre [3] and Duchesne [4].

The SLOWPOKE-2 reactor is cooled via the natural convection of light water, which also acts as the moderator. The reactor's primary safety features are its negative temperature and void coefficients, giving the reactor high passive safety. As temperatures in the reactor increase, the reactivity decreases. This allows the reactor to be self-limiting and does not require conventional shutdown systems. Furthermore, the reactor can be run for long periods without constant supervision.

The core of the SLOWPOKE-2 contains a fuel cage constructed of a zirconium alloy, Zircaloy-4 [3]. This material is also used in the cladding of the SLOWPOKE-2 fuel, due to the low neutron absorbing cross-section, and adequate material properties including structural integrity and corrosion resistance. The fuel cage consists of two circular plates connected by a hollow spool in the middle, which allows for the insertion of a control rod, and additional structural support cylinders connecting the circular plates at the edge of the plates, as shown in Figure 2. The circular plates contain holes allowing for the insertion of the ends of the fuel pins; however, it is important to note not every hole in the fuel cage is filled with a pin. Coupled with the open sides of the fuel cage, water can flow through the fuel cage and around the fuel rods to provide cooling.

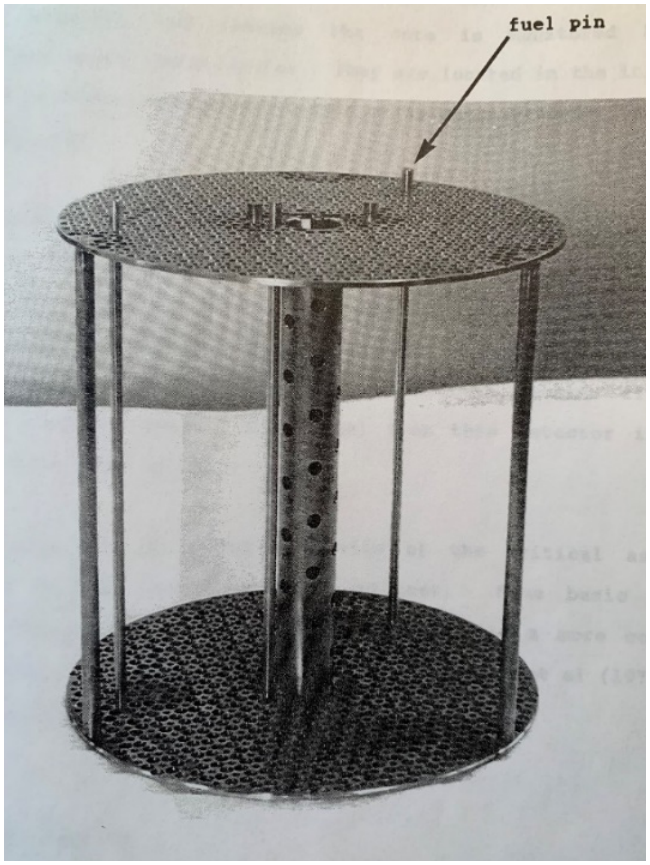

Figure 2: Fuel cage of SLOWPOKE-2 with 3 fuel pins inserted [4].

The centre spool of the cage allows for the insertion of a cadmium control rod. Cadmium is used to regulate the neutron flux, and therefore power, of the reactor due to its very high thermal neutron capture cross-section. This control rod is suspended with a cable attached to a winch atop the reactor allowing for precise movement of the control rod and can be fully removed from the fuel cage for maximum reactivity, or fully inserted. The position of the control rod during reactor operation is also recorded as part of the reactor operating logs.

The reactor core is housed in a closed container filled with water, called the reactor container, which is submerged in a larger external pool. Inside the reactor container, the fuel cage is surrounded by beryllium reflectors as seen in Figure 3. An annular beryllium reflector surrounds the reactor cage on the side, and above the fuel

cage is an aluminum shim tray which allows for the insertion of beryllium shims. Shims are additional beryllium reflectors added to compensate for fuel burnup in aging fuel. Beneath the fuel cage is a lower beryllium reflector. The gap between the lower beryllium reflector and the annular beryllium reflector (beryllium annulus Figure 3) is called the inlet gap, this is where water enters the fuel cage to cool the core. Similarly, between the annular beryllium reflector and the top support plate holding the shim tray is the outlet gap. The temperature of the fluid at both gaps is measured constantly with thermocouples recording data at an interval of every second. The fluid mechanics of the system are discussed further in Section 1.2.

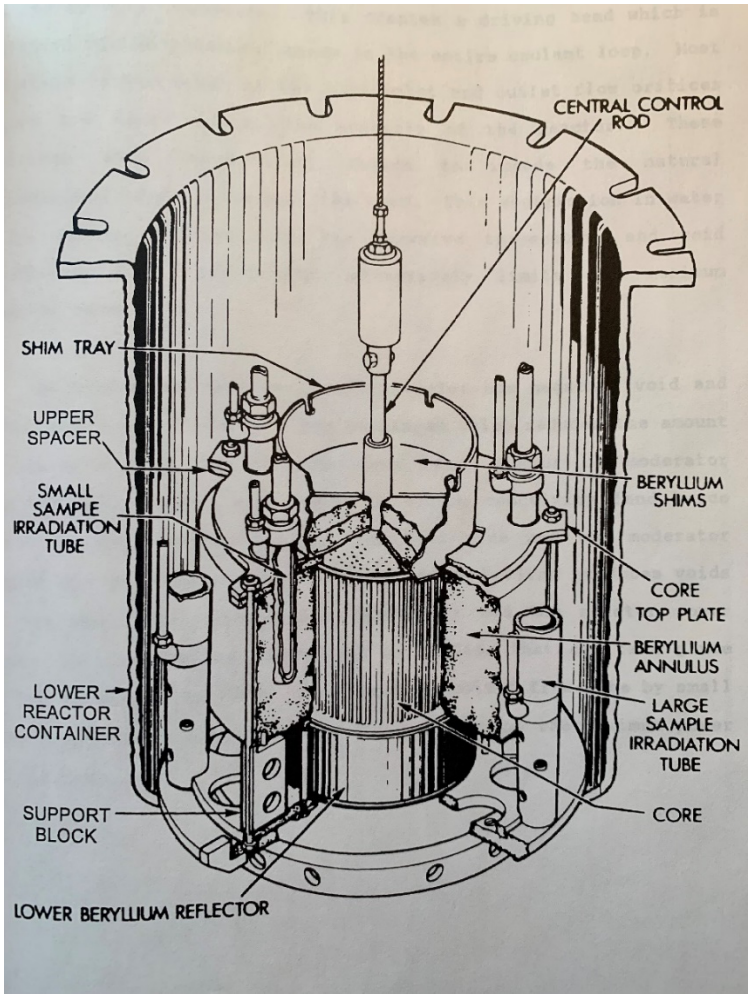

Figure 3: Isometric SLOWPOKE-2 core [4].

The fuel used in the SLOWPOKE-2 is high-density uranium oxide (UO_2) pellets [3]. The pellets follow the same design philosophy as those in CANDU (Canada Deuterium Uranium) reactors; however, a shorter end pellet at the ends of the fuel rod is not used in the SLOWPOKE-2 as used in CANDU. The pellet design both in CANDU and SLOWPOKE-2 are cylindrical high-density pellets, 95-97% theoretical density, with CANDU pellets having slight concave faces. Theoretical density being the maximum achievable density assuming no internal voids. The pellets are placed in the Zircaloy-4 fuel sheaths and designed such that there is a diametral clearance between the pellets and the sheath allowing for the production of gaseous fission products without critical rod swelling, cracking, or failure [4]. In part due to the high theoretical density of the fuel, highly enriched uranium is not required [3]. The uranium oxide fuel is only enriched to approximately 20% U-235 making the reactor a Low Enrichment Uranium (LEU) design [3]. The design of the SLOWPOKE-2 was originally intended for the use of High Enriched Uranium fuel (HEU), but due to proliferation concerns, the SLOWPOKE-2 system was converted to a low-enrichment fuel [3].

To monitor the operation of the SLOWPOKE-2, several detectors have been placed in and around the system. Primary detectors which have been integrated into the SLOWPOKE-2 since its creation involve three temperature probes and an internal neutron flux detector. The thermocouples are located in the inlet gap, outlet gap, and in the external pool, close to the reactor container. The interface in the reactor room records the real-time values from these detectors, and the data from these detectors are recorded in the reactor logs. In addition to temperature data, the rector logs include data from the internal flux detector which is located beside the fuel cage. The readings from this flux detector are constantly compared to the neutron flux setpoint by the reactor control system. In other words, when the reactor is operated, the power level the reactor is operating at depends on the neutron flux setpoint to which the reactor operator has set the reactor within 1.5%. This ensures the reactor remains operating at the appropriate thermal power. With reduced distance to the fuel, and reduced moderator/barrier between the fuel and the detector the readings from the internal flux detector are very large in

magnitude compared to the neutron counts from the external neutron detectors in the SLOWPOKE-2 facility. The data from the internal flux detector remain relatively constant throughout reactor operation, with slight variations accounting for control rod movement. This data will be discussed in depth later in this project.

Additionally, a compensated ion chamber has been added to the system attached to an arm that allows for repositioning in the external pool (henceforth referred to as the pool). Radially the detector can move from 0.79 cm away from the core capsule to 40.96 cm away. Axially the detector can move from 0 cm to 18.2 cm away from the plane passing through the centre of the core. Due to the design of the compensated ion detector, gamma detection does not seem to be possible; however, neutron flux can be determined.

In addition, large area He-3 and B10+ neutron detectors were installed in the ceiling above the reactor and in the reactor control room, respectively, for stand-off monitoring of the neutron level in the reactor. The He-3 detector works by recording the output pulse of the detector based on the following process-

$$^{3}He \quad + {}^{1}_{0}n \rightarrow {}^{1}H \quad + \ {}^{3}H + Q,$$

where Q is approximately 764 keV of energy released. Therefore, the He-3 detector is an excellent tool for measuring the thermal neutron flux. The B10+ is a hybrid detector, utilizing both the He-3 detection process described above, as well as neutron capture by B-10,

$$^{10}B + \ {}^{1}n \rightarrow \begin{cases} {}^{7}Li(0.84\ \text{MeV})+\alpha(1.47\text{MeV}) \ \ 94\% \\ {}^{7}Li(1.01\ \text{MeV})+\alpha(1.78\ \text{MeV}) \ \ 6\% \end{cases}.$$

1.2 Natural Convection

The process of natural convection, sometimes also called free convection, occurs due to the changes in buoyancy forces that arise due to the changes in temperature within

the fluid. In the SLOWPOKE-2 the water inside the reactor container is heated by the fuel pins. As the fluid is heated, it decreases in density, and as such rises through the fuel cage and travels out the outlet gap where its temperature is recorded. It then travels up toward the top of the reactor container where it cools, and increases in density, thereby falling to the bottom of the reactor container. From here it will enter the inlet gap, and its temperature will be recorded before being heated by the fuel pins again. This leads to the circulation of water and cooling of the SLOWPOKE-2.

1.3 Power Calibration

The calibration of the RMC SLOWPOKE-2 first began with the power calibration of the original SLOWPOKE reactor. During the commissioning of the original SLOWPOKE an Am:Be source was placed in the empty core, and the flux was measured with an ion chamber adjacent to the core. Afterwards, a water-cooled coil was placed inside the thermally isolated reactor container, and the reactor was operated at approximately 5kW steady-state. The amount of heat removed via the cooling coil was used to determine the heat balance of the original SLOWPOKE. With the measured heat balance and neutron flux data, the ion chamber adjacent to the core was calibrated. Finally using the calibrated ion chamber, the effective power of the Am:Be source was measured and found to be 1.47×10^{-8} kW [4].

During the commissioning of the RMC SLOWPOKE-2 a new Am:Be source was used that had been measured against the original Am:Be source; the new source's effective power was found to be 1.16×10^{-8} kW [4]. The source was placed in the middle of the empty fuel cage and the ion chamber adjacent to the core was calibrated. From this, when the SLOWPOKE-2 was fuelled and run, the reactor power could be calibrated from the ion chamber, and a relationship between neutron flux and reactor power was determined.

There are several problems immediately evident with this calibration method, and its propagation to the current SLOWPOKE-2. First is the assumption that the original heat balance results of the SLOWPOKE are directly applicable to the SLOWPOKE-2. Secondly the Am:Be source used for the ion chamber calibration of the RMC SLOWPOKE-2 was not the same source or the same effective power as the source used in the calibration of the original SLOWPOKE. Finally, the ion chamber signal from the Am:Be source was near the lower end of the detector's sensitivity range. This meant that for the calibration there was a large amount of background which led to large uncertainties at the time. It has been proposed that this power calibration process for the SLOWPOKE-2 could be ± 25% accurate at the most favourable estimates [4].

1.4 SLOWPOKE-2 Refuelling

The refuelling process began in August 2021 and was finished in September 2021. The old core before refuelling consisted of 198 fuel pins; after refuelling the core now has 195 fuel pins. Due to this, the core geometry has changed slightly, as has the weighted isotopic composition of the core. The weighted isotopic composition of the ore is the weighted sum of the isotopes in the core composition depending on each isotope's contribution to in-core neutron flux per unit thermal power [5]. Data from before and after refuelling were investigated to determine the differences between the two cores. However, the CFD model being presented is primarily focused on the old core geometry. It should be noted that due to the fuel pin loading pattern of the SLOWPOKE-2 the new core contains pins in the same location as the old core [6]. The new core simply has three fewer fuel pins in the outer side of the fuel cage. According to estimates made by collaborators at Canadian Nuclear Laboratories (CNL) the weighted isotopic composition of the fuel between the old core and the new varies by approximately 2% [7].

1.5 Problem Definition

Nuclear fuel proliferation is a risk that must be safeguarded against to ensure the peaceful use of nuclear materials. SMRs present new challenges to ensure that nuclear material is properly safeguarded, as such, new methods must be put forth to address these challenges [1-2]. The first seven SLOWPOKE-2 cores used highly enriched uranium (HEU); however, proliferation concerns lead to two SLOWPOKE-2 cores being converted to use low-enriched uranium, such as the core located at RMC. While using low-enriched fuel, as opposed to highly enriched fuel, is beneficial in safeguarding against proliferation, more can be done to safeguard against the possible diversion of fuel in next-generation SMRs. For the safe and sustainable future of nuclear energy, more effective fuel monitoring systems must be researched and installed.

The current guidelines by the International Atomic Energy Agency (IAEA) require various safeguard measures in nuclear facilities to detect the diversion of fissile material from peaceful purposes and to determine if proliferation has occurred. In the event of nuclear proliferation, IAEA guidelines require loss of Pu, HEU, U-233 in irradiated fuel to be detected in under 90 days [5]. This process may involve manual inspection of the material which may be costly and time-consuming. Furthermore, the IAEA has designated a high priority towards the goal of developing instruments and techniques for early detection of nuclear material misuse [8].

According to research by van der Ende et al. by using neutron flux detectors and the theory outlined in the State-of-Knowledge chapter, an additional safeguard against proliferation can be placed in nuclear facilities. This safeguard involves using neutron flux data, and reactor thermal power to monitor the amount of fissile material in the core [5]. This may allow for the remote monitoring of the fuel and indicate proliferation within 90 days of its occurrence. SMRs which are typically designed with sealed cores make conventional safeguards and inspection of nuclear material for verification purposes difficult. This thesis, building on the fuel monitoring system put forth by van

der Ende et al. aims to circumvent this issue by making verification of fissile material possible from the outside using neutron flux and reactor thermal power [5].

As part of remote monitoring fuel via neutron detectors, accurate thermal power of the reactors is required to lower the error on calculations determining if proliferation has occurred [5]. It is especially important if thermal power can be related to observable and measurable parameters of the reactor. This would allow for real-time accurate thermal energy monitoring as opposed to using scaling factors on the neutron flux based on an initial calibration of the reactor, as the SLOWPOKE-2 currently does.

The thermal power output as reported on the reactor monitoring computers must be considered a "best" estimate, built off the scaling factors from the initial calibration as described in the Power Calibration section. Changes since the initial calibration of the SLOWPOKE-2 system include refuelling with a different core layout, 195 pins versus 198, and the addition of shims. These changes may have little to no change on the current thermal power estimation, as it is a scaling of the neutron flux as determined via the internal flux detector and the changes described would also affect the internal neutron flux. However, for the fissile material monitoring method put forth by van der Ende et al. having accurate thermal power with low uncertainty is key to getting useable results of the fissile content of the core. In the past efforts have been made to determine accurate thermal power of the SLOWPOKE-2, such as by Duchesne, using mass flow rates, water temperatures, and frictional losses [4]. In this project determining an accurate thermal power will be done by constructing a Computational Fluid Dynamic (CFD) model of the SLOWPOKE-2.

Applying a CFD model to the SLOWPOKE-2 and relating reactor power to variables such as inlet and outlet temperature, provides an introductory study into using means other than neutron flux from a calibrated ion chamber to measure reactivity, allowing for verification between the two readings. Two methods of determining the power output of the reactor could be beneficial for additional safety of the reactor as well. However, due to the computational time required to simulate the SLOWPOKE-2

system, it is unlikely real-time verification of the SLOWPOKE-2 power will be possible. Furthermore, CFD modelling by its nature will provide insight into turbulence within the SLOWPOKE-2 and the cooling efficiency of the past core geometry.

1.6 Objective

There are three primary objectives in this thesis. First, to analyze the SLOWPOKE-2 operating data including the temperature probe data, internal neutron flux, and external neutron flux data for both the old and the new cores. Secondly, to create an accurate thermal power detection system for the SLOWPOKE-2 using a CFD model. Within this objective are many milestones that must first be met. The steps of this process will be discussed in depth. Lastly, the final objective is to use the neutron flux data and the accurate thermal power data to compare the isotopic composition of the two cores and to determine if differences can be detected using the enhanced fuel monitoring system.

Before analysis and post-processing of the CFD model, several sets of experimental data must be cleaned. The data sets must be converted to csv file formats and the temperature and internal flux data must be merged to a single file. Details about data cleaning and preparation are discussed in Section 3.1. Data sets will be taken from before refuelling, and after refuelling. Comparing several data sets to the CFD model will allow for investigation into possible confounding variables such as ambient temperature and time of year the data was recorded. The SLOWPOKE-2 pool is kept at a controlled temperature, and as such external temperature variables are not expected to alter the results. However, because of the quantity of SLOWPOKE-2 data available for this project, data sets taken from approximately the same time of year can be used.

The creation of the CFD model is the largest task of this project. The first step in this task is to create the CAD of the SLOWPOKE-2 core. RMC was not permitted by

CNL to create the CAD from the reactor drawings. As such, CAD was provided by CNL for this thesis.

Before the simulation work of the CFD model begins, the CAD must be appropriately meshed. However, the SLOWPOKE-2 geometry is not symmetrical as originally thought and has areas of complex geometry. Therefore, symmetry simplifications cannot be used to decrease computation/meshing time. Moreover, areas of complex geometry may need to have the meshing technique and mesh size manually adjusted in these areas. The details of the SLOWPOKE-2 geometry must be appropriately captured, as these details will affect the fluid flow and turbulence in the model. Appropriate mesh resolution will be discussed in depth.

Due to the size of the core, the required resolution of the mesh, and the complexity of the problem, the simulation computations were offloaded to a server hosted by CMC Microsystems. This server uses 32 CPU cores for computation, as such all the computation times given in this project will reflect this greater computation power compared to the average workstation. The journal files and Linux code used to offload the CFD simulations to the CMC server are provided in Appendix C.

Once the CAD is meshed the simulations will begin on the old core layout. The first goal of the CFD model will be to obtain useable results without any unrealistic cold/hot spots in the model. To do this, correct mesh resolution must be used, which in turn means conducting a grid convergence index (GCI) test. In addition, the correct settings in ANSYS must be used to ensure the model is solved correctly, without any unrealistic solutions. As part of this project, all ANSYS Fluent settings have been recorded and are logged in Appendix D for all simulations shown in this paper.

The final objective of this project is to test the enhanced fuel monitoring system on the SLOWPOKE-2 that was originally tested at the National Research Reactor (NRU) reactor at Chalk River by van der Ende et al. This process involves using external neutron flux data and accurate thermal power from the CFD model. Using this process, the isotopic change in core composition due to refuelling should be detected.

Chapter 2: State-of-Knowledge

The issue of inaccurate SLOWPOKE-2 thermal power is well known; it has been a problem investigated by individuals such as Duchesne and De Wit [4, 9]. De Witt approached the subject by investigating excess reactivity versus uniform core temperature, which followed the same trend as calculated by Chalk River Nuclear Laboratories (CRNL) but exhibited significant differences [9]. Duchesne, whose thesis is more applicable to this project, used convective equations and numerical methods to determine equations relating the inlet and outlet temperatures to the accurate thermal power of the core [4].

Duchesne concluded that the SLOWPOKE-2 thermal power could be related to neutron flux (as measured by the internal neutron detector) via a proportionality constant [4]. This relationship was noted later in a study on enhanced neutron monitoring by van der Ende et al. wherein it was demonstrated that changes in thermal neutron flux per unit thermal power could be used to follow changes in fissile isotopic content of the reactor core [5]. Duchesne's method was found to have lower uncertainty than the thermal power as calculated previously from the original calibration [4]. The relation found by Duchesne used not only inlet and outlet temperatures but also flow rate and pressure loss from frictional forces [4]. These calculations are most applicable to the old core.

As mentioned previously, the relation put forth by van der Ende et al. as the cornerstone for the enhanced fuel monitoring system is as follows [5]-

$$n_{det} \propto n_{pop} \propto \frac{\langle \phi \rangle}{\langle v \rangle} V, \tag{1}$$

where $\langle \phi \rangle$ is the average neutron flux in the reactor core, $\langle v \rangle$ is the average neutron speed, and V is the core volume. This relation states that neutron detection rate outside of the reactor core, n_{det}, is proportional to the neutron population, n_{pop}, of the core, which is, in turn, proportional to the ratio of neutron flux in the core to the average speed of neutrons in the core multiplied by the volume of the core. Knowing that the

SLOWPOKE-2 is a thermal reactor and that most fissions occur in the thermal neutron range this relationship can be further expanded. Using the monoenergetic rate of volumetric fission $\Sigma_f \phi$ where Σ_f is the macroscopic fission cross-section, the atom density N, and taking ϕ in the thermal range we can determine the following relation [5]-

$$P_{tot} = V\langle\phi\rangle \sum_i \langle\Sigma_{f,i}\rangle E_{f,i} = V\langle\phi\rangle \sum_i N_i \langle\sigma_{f,i}\rangle E_{f,i} \quad (2)$$

where P_{tot} is the total thermal power of the reactor the summation accounts for the different isotopes populating the reactor, $E_{f,i}$ is the energy released per fission of the i^{th} isotope, and the macroscopic cross section has been converted to the microscopic fission cross section $\sigma_{f,i}$. Each fissile isotope in the core will have a weighted effect on the neutron flux. In the National Research Universal (NRU) reactor, a 1 kg increase of U-235 mass was estimated to increase the neutron flux per unit power by 4%, whereas a 100g increase of Pu-239 mass was estimated to have a 0.5% increase [5]. Equation 2 also shows a linear relationship between reactor thermal power and in-core neutron flux; noting the proportionality between neutron detection rate outside of the reactor core to in-core neutron flux (Equation 1), this linear relationship is demonstrated in Figure 4(c).

Rearranging Equation 2 shows that the relationship with respect to neutron detector count per unit reactor power is proportional to $\frac{\langle\phi\rangle}{P_{tot}}$ [5]-

$$\frac{\langle\phi\rangle}{P_{tot}} = [N_A \sum_i \frac{m_i \langle\sigma_{f,i}\rangle E_{f,i}}{w_i}]^{-1}, \quad (3)$$

which uses Avogadro's number N_A, along with microscopic fission cross-section $\sigma_{f,i}$, mass m_i, and atomic weight w_i for the i^{th} isotope. Equation 3 shows that the neutron count rate per unit reactor thermal power and the relative weighted fissile isotopic composition of the core is linear. This is the relation that allows for determining changes to the isotopic core composition based on neutron flux normalized by reactor thermal power. From data shown in Figure 4(b), the slope found between measured neutron flux per unit power (with background subtracted) and the weighted isotopic composition of the core was 1.08 +/- 0.13 [5]. Using the ratio of neutron flux detected to reactor power is

important for comparing changes in this ratio to a base measurement, known to have the expected amount of fissile material.

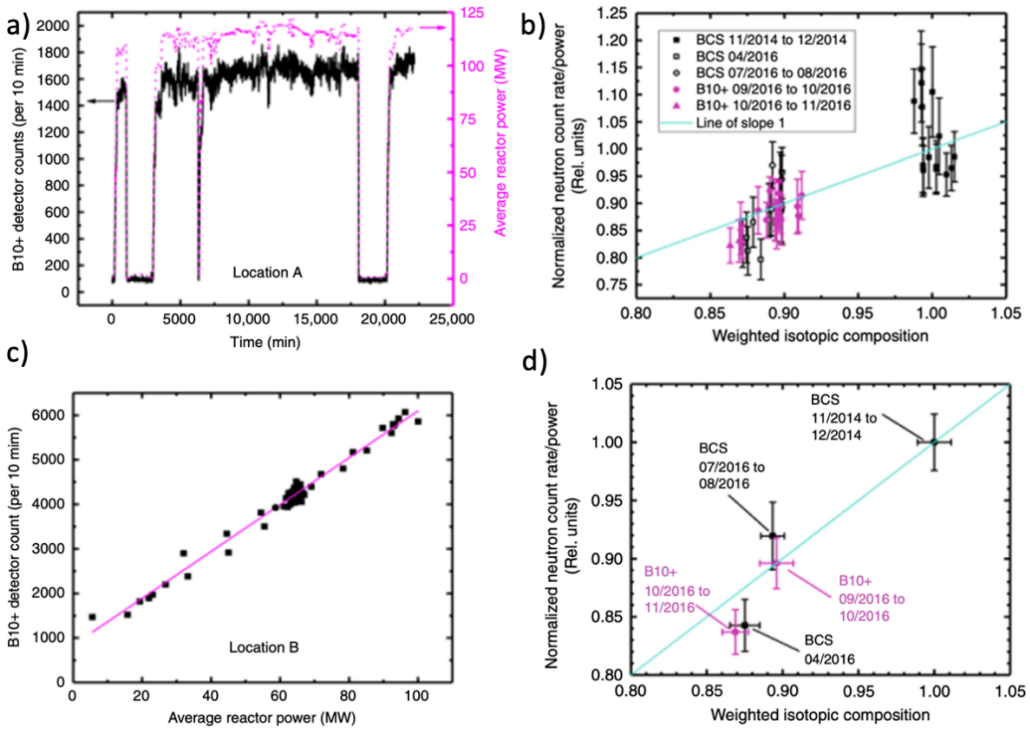

Figure 4: a) Comparison of B10+ detector counts and reactor thermal power (MW) over time averaged over 10 min. intervals. b) Measured neutron count rate per unit reactor power versus weighted isotopic composition of the core from different detectors and multiple time periods. c) B10+ detector count averaged over 10 min intervals versus reactor thermal power during startup with a linear fit. d) Averaged data from b) showing error bars. Figures taken from Ref. [5].

As seen in Figure 4, testing the enhanced fuel monitoring system at the NRU involved using both calculated and measured data. It was found that the accuracy of this method of monitoring was limited to a change of less than 5% in neutron flux to reactor power ratio [5]. This limitation was from environmental and operational variations. It should be noted that this fuel monitoring method was able to detect changes to the fissile content within the IAEA guideline of 90 days to detect the diversion of one significant quantity of Pu (8 kg) from irradiated reactor fuel [5]. This method falls well within this

timeframe, as the historical data used in this investigation were taken over 4 weeks, and the monitoring system detected the change with over 95% confidence.

As expected, that study found that variation in detector location and detector type gave different neutron flux values. Therefore, it is important to remain consistent with detector type and placement throughout the duration of the fuel monitoring. Significant count differences were found between the B10+ detector and the boron-coated straw (BCS) detectors employed in the study, partially due to placement in the reactor surroundings, but also due to differences in their detection efficiency. The differences in placement and detection efficiency between the He-3 and B10+ detectors are also present at RMC; therefore, a similar count discrepancy is expected for this project. For this project, only data from the He-3 detector is used as a source of external neutron flux, although it is possible to use data from the B10+ detector as well.

As mentioned, this technique has possible application to other cores, given the background theory (Equations 1, 2 and 3) is the same for all thermal reactor cores, including Molten Salt Reactors (MSR) and High-Temperature Gas Reactors (HTGR) which were also investigated by van der Ende [5]. Moreover, since this method uses a baseline measurement system of neutron flux per unit reactor power, the calibration of new reactor types is mitigated as an issue; hence, proper baseline calibration is essential.

2.1 CFD Theory

CFD software simulates systems by solving the governing equations of mass (continuity), momentum, and energy when selected. The conservation equations for mass, momentum respectively are as follows [15]-

$$\frac{\partial \rho}{\partial t} + \nabla \cdot (\rho v) = S_m \tag{4}$$

$$\frac{\partial}{\partial t}(\rho \vec{v}) + \nabla \cdot (\rho \vec{v} \vec{v}) = -\nabla p + \nabla \cdot (\bar{\bar{\tau}}) + \rho \vec{g} + \vec{F} \tag{5}$$

Where S_m is the mass added from dispersion due to phase change, p is static pressure, $\bar{\bar{\tau}}$ is the stress tensor, $\rho\vec{g}$ and $\vec{F}$ represent forces from gravity and external forces respectively [15]. These equations define the flow while also ensuring continuity, that mass is not gained or lost throughout a closed system. It should also be noted the momentum equation presented is for non-accelerating reference frames, like the SLOWPOKE-2 system. For heat transfer problems ANSYS solves the following energy equation to determine temperature in the system [10]:

$$\frac{\partial}{\partial t}(\rho E) + \nabla \cdot \left(\bar{v}(\rho E + p)\right) = \nabla \cdot \left(k_{eff}\nabla T - \sum_j h_j \bar{J}_j + \left(\overline{\bar{\tau}_{eff}} \cdot \bar{v}\right)\right) + S_h \quad (6)$$

Where k_{eff} is effective thermal conductivity, $\bar{J}_j$ is the diffusion flux of species j where species j is fluid of the model that can be changed via mixing, multiphase changes, or chemical reactions. In the case of the SLOWPOKE-2 the only species is light water. $S_h$is the volumetric heat source if defined [10]. Notably, the first three terms of the right-hand side of this equation solve for conduction energy transfer, diffusion, and viscous dissipation respectively [10].

Other equations such as turbulence will also be solved at the cost of computation time if selected. Used briefly in this paper is the Spalart-Allmaras turbulence model, which solves the least computationally intensive turbulence equation Fluent offers. The turbulent transport equation solving for the turbulent kinematic viscosity $\tilde{\nu}$ is as follows [15]-

$$\frac{\partial}{\partial t}(\rho\tilde{\nu}) + \frac{\partial}{\partial x_i}(\rho\tilde{\nu}u_i) = G_\nu + \frac{1}{\sigma_{\tilde{\nu}}}\left[\frac{\partial}{\partial x_i}\left\{(\mu + \rho\tilde{\nu})\frac{\partial\tilde{\nu}}{\partial x_i}\right\} + c_{b2}\rho\left(\frac{d\tilde{\nu}}{\partial x_j}\right)^2\right] - Y_\nu + S_{\tilde{\nu}} \quad (7)$$

Where G_ν is the production of turbulent viscosity, Y_ν is the destruction of turbulent viscosity that occurs due to wall effects and viscous damping, $\sigma_{\tilde{\nu}}$ and c_{b2} are constants, and $S_{\tilde{\nu}}$ is a source term [15].

Regardless of density-based or pressure-based solver type the velocity field is calculated from the momentum equations. However, in density-based solvers, the density

field is calculated via the continuity equations whereas, in pressure-based solvers, the pressure field is found by calculating the pressure correction equation. Pressure-based solvers have been selected for this project due to the low fluid velocity of the SLOWPOKE-2, as will be discussed in Sections 3.3 and 4.3.

Solving the various equations and scalars the CFD model consists of dividing the domain into a large number of small control volumes, or cells. Within these control volumes, algebraic equations are constructed to solve for the discreet variables of velocity, temperature, pressure etc. These discreet variable equations are linearized and solved for the new variable values. These fundamental calculations occur in both the density-based and the pressure-based solvers.

Several volume mesh types are available in ANSYS Fluent. These include tetrahedral, hexahedral, polyhedral, pyramidal, or wedge cells. Using a combination of these cells is also possible. According to Fluent documentation it is recommended to use quadrilateral/hexahedral for simple and moderately complex geometries, triangular/tetrahedral for relatively complex geometries, and pure triangular/tetrahedral cells for very complex geometries [15]. In this project the volume is meshed via a combination of polyhedral and hexahedral cells. The SLOWPOKE-2 geometry may be considered moderately complex, with areas of extreme complexity. As such, hexahedral mesh is used with a combination of polyhedral mesh to improve meshing time.

An overview of the steps that occur within each iteration of a pressure-based solver is as follows. First, the fluid properties are updated based on initial values or values of the last solved iteration. From the updated values, or initial values if the simulation has just started, of pressure and mass, the momentum equation (Equation 5) is solved. From the updated values and momentum equation the pressure correction equation, mass flux, pressure field, velocity field, and the optional turbulence (Equation 7) or energy equations (Equation 6) can all be found. The variable values can be updated, and the convergence of the equations checked.

In contrast, the density-based solver attempts to solve the continuity, momentum, energy, and species equations simultaneously after the variables have been updated, as opposed to the pressure-based solver which solves momentum first, followed by the field, energy, and turbulence equations [10, 15].

For this project, second-order upwind solver schemes were used. These solvers provide higher-order accuracy at the faces of the control volume via a series of Taylor expansions [10]. Upwind and upstream refer to the direction of the fluid flow through the volume cells. These Taylor expansions are done from the cell-centered solution allowing for a gradient upstream from the cell with higher accuracy at the faces [10, 15]. Changing this solver may affect the numerical stability of the simulation.

The numerical stability of the solution will be investigated further for the models used in this project in Section 4.4. Residual plots show the value of the residuals, which is a numerical value of the difference between the variables in a cell (continuity, energy, kinematic viscosity, velocity, etc.) and those same variables in the neighbouring cell. This is discussed in depth in Section 4.4. If these values change radically in the last 200 iterations, do not converge, or oscillate, this may indicate poor numerical stability of the models.

Chapter 3: Methods

As stated in the Introduction, a major objective of this work is constructing a CFD model of the RMC SLOWPOKE-2 that would allow an accurate determination between observable reactor temperature parameters, and the reactor thermal power. CFD modelling for this project focused on the old core layout. This layout includes three more fuel pins than in the current core. Due to the loading procedure of the SLOWPOKE-2, the 195 pins in the current core should occupy the positions of 195 of the pins in the old core. Therefore, all pin locations should be the same between the two cores, the new core is simply missing 3 fuel pins which were last in the loading order to be inserted [6].

The main challenge of this project is the verification and validation process of the CFD model. The data contained in the reactor logs, which will be used as data to compare against results from the CFD model, are temperature data from the inlet, outlet, and pool thermocouples, and the internal neutron flux. Reactor power is not given; however, as discussed previously, reactor power is set based on the neutron flux setpoint the reactor is operated at. This relationship is expected to change with burnup of the core; however, shim insertion should mitigate this issue. This data recording method, in tandem with the SLOWPOKE-2 power calibration, makes validation of the CFD results difficult.

Given the information in the data logs, there are only two variables, temperature, and neutron flux, that can be used to load and validate the model. The neutron flux is directly related to reactor power. Therefore, the reactor thermal power is set as an input in ANSYS, and the temperature output given by ANSYS is compared to the experimental temperature data. Importantly, the reactor thermal power is possibly inaccurate, leading to the difficulty in validating the CFD model, which is comparing the simulated data to the experimental data. This issue, along with the construction of the CFD model will be described in detail in the CFD subsection.

3.1 Data Analysis

The data analysis for this project will be conducted using Python. The data sets presented in this project are from the SLOWPOKE-2 in 2020, 2021 and 2022. This time frame allows for the investigation into reactor behaviour before and after refuelling. Note that for all data analyses conducted, the same time interval is used. For example, if the before-refuelling dataset ran for three hours, and the after-refuelling data set ran for five hours, the after-refuelling data set would be limited to three hours so that it matched the same operating time as before-refuelling.

In addition to limiting the reactor operating times to match before and after refuelling, it is also important to ensure the data being compared has as few confounding variables as possible. For example, if the reactor was recently run consecutively, the pool temperature will be higher, and therefore this reactor run cannot be reasonably compared to a reactor run where the reactor had been operated from its coolest steady-state. Additionally, there was a period when the chillers that operate in the external pool of the reactor were not functioning, leading to the pool temperature, and therefore internal reactor temperatures, being warmer for longer periods of time after the reactor had already shut down. The data sets investigated in this project are run from the coolest steady-state temperature, with the chillers working.

3.1.1 Data Collection

One aspect of the data analysis in this project involved the conversion of reactor logs to readable csv files, as opposed to the LabVIEW file type the data logs are recorded as. Converting the LABVIEW files to csv files made several problems immediately evident with the SLOWPOKE-2 Integrated Reactor Control & Instrumentation system (SIRCIS) data collection of the SLOWPOKE-2. First, and most notable, is the data

collection differences between the temperature data and the neutron flux data. The temperature data, taken from each of the three thermocouples are recorded every second. Therefore, there are 86400 data points for each day for each of the thermocouples. However, for the neutron flux data, whenever the neutron flux drops below a certain value the data log stops recording. This means there are not 86400 data points in the neutron flux data per day, there may only be a few thousand from when the reactor was operating. This leads to issues combining the two datasets and that must be surmounted. When the SIRCIS data collection code is rewritten, it is recommended to have neutron flux data recorded for every time interval of recorded temperature data. If the neutron flux is below detection threshold, the software should input zero or a null value.

The second problem that occurs when converting from the LabVIEW file to csv format via Excel is the date changes during conversion. Excel will take the year from the LabVIEW file and record it as the day, making 2020 the 20th day of the month. While this is easy to fix within Excel, during a code rewrite the date format should agree between software types so that when exporting the data from LabVIEW (typically to software such as Excel), the dates match without additional work.

The final change recommended in a code rewrite of SIRCIS would be the ability to export neutron flux data and temperature data together so both data sets are natively in the same csv file. Currently, the two csv files containing neutron flux data and temperature data must be manually merged into the same file using Excel, Python, or similar software, and the incorrect date is changed via the find and replace function.

3.2 CFD

The CFD software used in this project is ANSYS Fluent [11]. This software was chosen over alternatives such as COMSOL, due to the parallel meshing feature in ANSYS, an important feature given the size of the geometry in question [11, 12].

Furthermore, Fluent was chosen over the CFD software of CNL (STAR-CCM+) as using different CFD software would allow for a unique comparison between the models. Parallel meshing is the feature by which multiple computer cores can be used to mesh the geometry, greatly decreasing computation time. For CAD as large and complex as the SLOWPOKE-2 system, parallel meshing is an important feature to utilize. As such, meshing took approximately 30 minutes for the finest mesh. However, before meshing the geometry can begin, the geometry first must be imported into ANSYS. The act of importing a file, especially a heavily compressed file can cause issues in the geometry. These issues must be resolved before meshing can begin.

After importing the CAD into ANSYS, the CAD geometry must be checked. This can be done in either DesignModeler or SpaceClaim modules of the ANSYS workbench that allow for checking, cleaning, and repairing geometry. Some of the translation issues that can occur include split edges, small faces, and sharp angles that will lead to meshing failure. Most errors can be automatically fixed via the software in question however some geometry errors such as split edges require manual intervention and will be corrected on a case-by-case basis. An example of a split edge can be seen in Figure 5, showing a screenshot of the SLOWPOKE-2 geometry in ANSYS before being repaired.

As mentioned earlier, the CAD for this project is provided by CNL and contains the entire SLOWPOKE-2 geometry, including the reactor capsule. However, the CAD that modified in this thesis only extends to the reactor capsule and as such the external pool is not modelled. Given the size of the pool and the computation time required to also determine heat transfer within this large volume, the pool not being modelled is an appropriate and efficient modelling choice. The CAD provided was in the universal Parasolid file format.

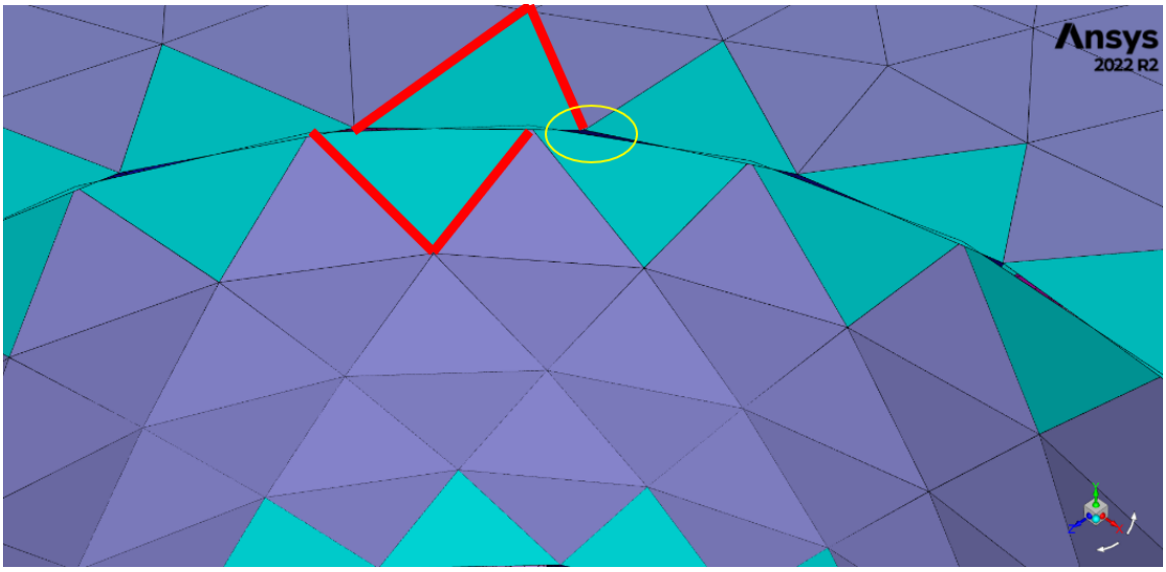

Figure 5: Nonconformal mesh on split edge geometry fault where the solid fuel pin meets the fuel cage. Non-conformal mesh is highlighted in red, and an example of a gap shown from a split edge is circled.

In Figure 5, not only is the nonconformal split edge visible, but the failed surface mesh is also visible. Fixing these errors not only ensures the CAD can be properly meshed but also ensures the CAD is watertight. It should be noted that double precision should always be used when meshing and solving in CFD software for more accuracy in temperature calculations.

Once the geometry is completely meshed, there can still be errors that occur in the meshing stage due to difficult geometry. One such error occurs when the mesh cannot properly model a sharp corner. The mesh elements in that area of difficult geometry will get smaller and smaller to capture the corner but will never converge, leading to a singularity. This means the number of cells required to capture this specific corner never converges, and as such the mesh either fails or the CAD is slightly altered to remove the singularity. The meshing software may also have difficult meshing faces that are very close together but not touching. This error occurred in the spacers of the SLOWPOKE-2, the geometry that creates the outlet gap. This geometry was fixed by ensuring the edges that joined the faces were properly connected. During the meshing process, this region needed to be manually edited to ensure proper mesh quality.

To capture the local geometry appropriately, different meshing techniques may have to be manually set to different parts of the geometry. For example, the SLOWPOKE-2 fuel pins are rather small and cylindrical, so it is most appropriate to model these using a curvature mesh sizing. As mentioned above the small outlet gap is most appropriately meshed using the proximity mesh sizing function. After appropriately surface meshing the geometry, the geometry must be described before the fluid volume can be meshed. In the case of the SLOWPOKE-2 geometry the CAD is shell modelled covering only the solid regions.

The geometry used for this project only models the solid regions as shell structures, meaning the open area of the CAD is either filled with fluid or a void region. As such the geometry can be simply described and the software moves on to volume meshing. The type of volume mesh must be chosen, in this case, poly-hexacore mesh was chosen due to its speed, but adequate modelling of the geometry. The maximum size of volume mesh cells can also be chosen, if not explicitly selected, the program will choose an appropriate maximum for the geometry in question. Part of the volume mesh procedure is choosing the appropriate amount of boundary layers. Boundary layers are thin layers in the mesh that occur where the surface of the solid geometry meets the volume mesh, this can be seen in Figure 6. When there are very large, very fast changes in temperature in a specific area there may need to be more boundary layers in this area to appropriately capture the changes in temperature. It is not recommended to have less than 3 boundary layers when CFD modelling. Boundary layers and poly-hexacore mesh can be seen in Figure 6.

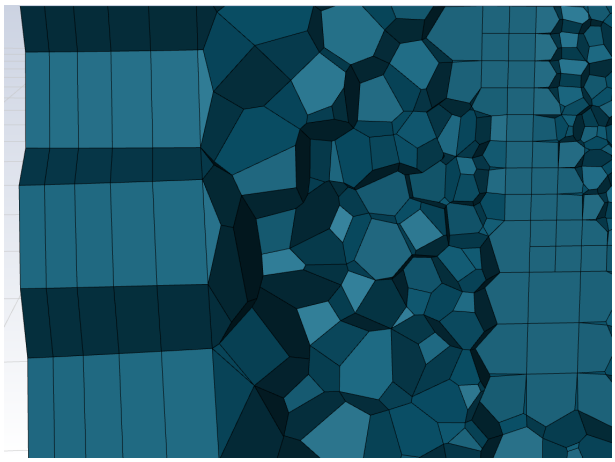

Figure 6: Five boundary layers on the reactor container wall, with poly-hexacore mesh elements visible.

Adjusting the boundary layers and mesh size was a key factor in this project for accurately capturing temperature changes in the SLOWPOKE-2, this will be discussed in depth in Chapter 5.

Once the meshing is completed the model can proceed to the simulation loading stage and CFD solution. Before the loading and CFD defining begins, the mesh should be checked using the automatic built-in function to ensure there are no errors, such as left-handed cells. Once any issues with the mesh are found and fixed the solution portion of the CFD model can begin. This portion of CFD involves loading the model with the appropriate initial temperature values, choosing the turbulence mode, and choosing the heat flux and temperatures, among other settings (see Appendix D for a listing of settings used) to define the model.

During this process, the mesh quality can be evaluated to determine if the quality of the mesh is good enough to capture the temperature changes in the model. The quality of the volume mesh is given as an orthogonality value, with 0 being the lowest quality and 1 being the highest. Typically, models should not have cells of lower orthogonal quality than 0.2 and should have an average mesh orthogonality of 0.7. Although in some cases mesh cells with an orthogonality lower than 0.2 will still generate a reasonable solution. In the solution section of ANSYS Fluent, the lowest user-inputted percentage of

mesh cells can be improved over a number of user-inputted iterations. For this project, the lowest 10% of cells were improved over 10 iterations.

During the simulation some areas of the geometry, or mesh cells, will not capture the temperature changes appropriately, and as such will automatically be limited by the software. Such limited cells are limited by default at 5000 K and 0 K and usually occur at sharp corners or difficult geometry. While these cells may not affect the fluid mechanics at the areas of concern, the inlet and outlet, it is difficult to conclude this with certainty as the calculations ANSYS conducts during the simulation may take these cells into account in significant ways. Refining these areas, coarsening the mesh, improving mesh quality, or adjusting the Fluent solver settings such as under relaxation factors may solve these issues. Section 3.4 describes Fluent solver settings and their effects in depth.

Appropriate grid resolution was a major obstacle in this project. As such, many meshes were created to appropriately capture the SLOWPOKE-2 behaviour. By coarsening or refining the mesh of the model while keeping the ANSYS settings the same, behaviours and temperatures of the models can be easily compared. These comparisons form the basis of the Grid Convergence Index (GCI) and will be discussed in detail in Chapter 5.

The meshes tested ranged from most coarse at 12 million volume cells to finer meshing with 30 million cells. Various mesh sizes allow for the comparison of results to determine if the solutions from ANSYS are independent of mesh resolution. Models of different mesh resolutions are shown in order of increasing mesh count in Figure 7, however, only the 27216708, 23230824, 19629240, and 12171151 cell models are shown. While it may be difficult to see differences between the models, around the edges and in the fuel cage the increased resolution may change the output of the simulations.

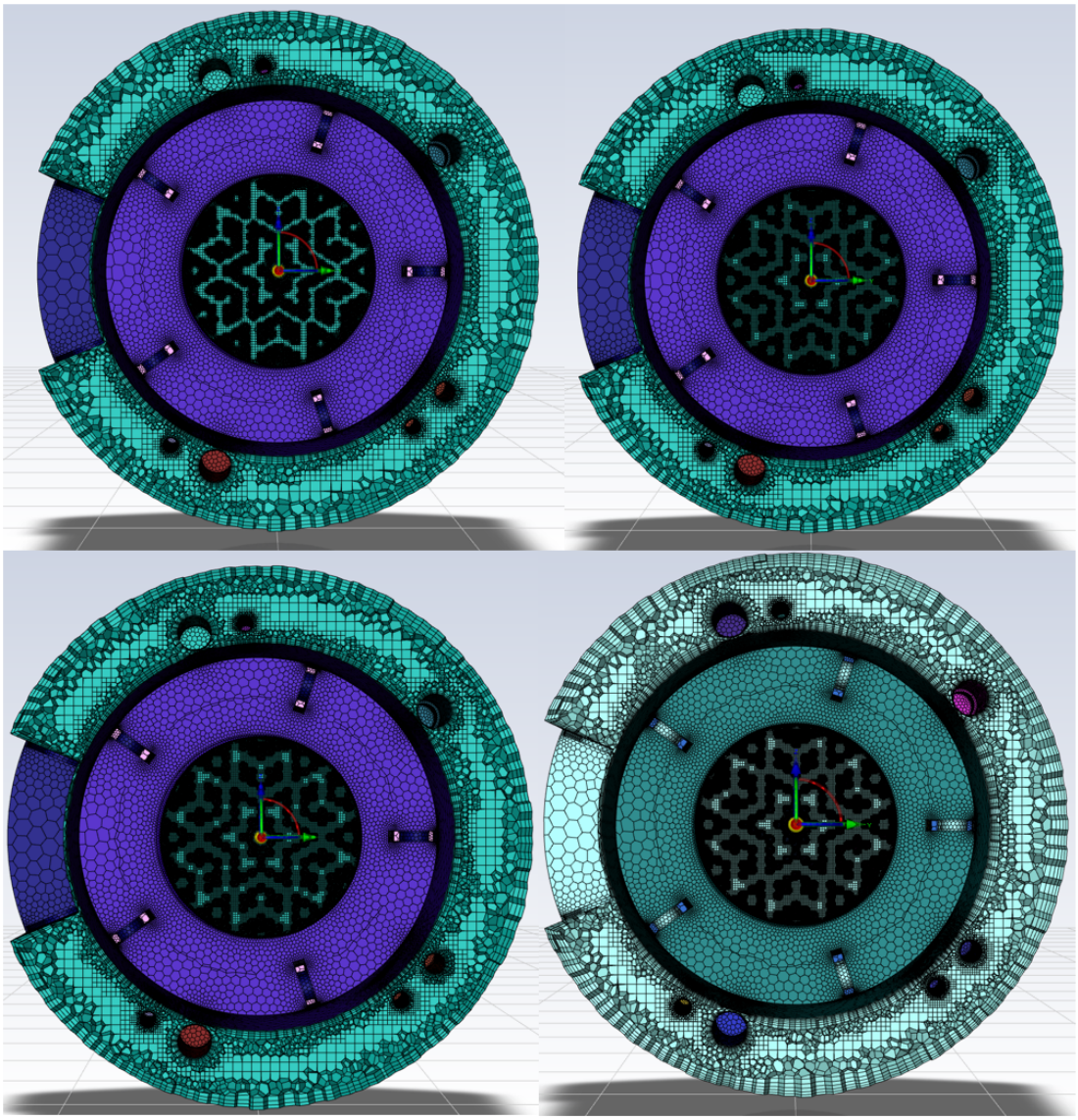

Figure 7: SLOWPOKE-2 core cross section CFD models using mesh resolutions of 12171151, 19629240, 23230824, and 27216708.

Once the mesh has been created, checked, and improved, the simulation settings must be selected. For ease of comparison, all simulations in this project were run at half-power. According to the reactor control room computer, the power associated with the half-power thermal neutron flux ($5x10^{11}$) for the inner irradiation sites is approximately 8.5kW. To set this power level in the simulation, fuel pin walls were set with a thermal heat flux of 11668.3 W/m^2.

3.2.1 Mesh Quality

Mesh quality can be evaluated in many ways depending on if the cell under consideration is either a surface cell (2D) or a volume cell (3D). If the cell being evaluated is a volume cell, the type of volume cell poly-hexacore, tetrahedral, polyhedral etc. also matters. In addition, cell density needs to be considered in complex areas of the geometry, and generally, no flow passage should be meshed with less than 5 cells [10].

Cell skewness defines the difference between the shape of the cell and the shape of an equilateral cell of the same volume or area depending on if the cell is 2D or 3D. Cells with a large skew towards a vertex can affect the solution stability. Maximum skewness should be kept below 0.95 with an average of around 0.33 [10]. Skewness is generally calculated by determining the difference of the ideal quality cell volume to the actual cell volume. A skewed cell example and aspect ratio is shown in Figure 8.

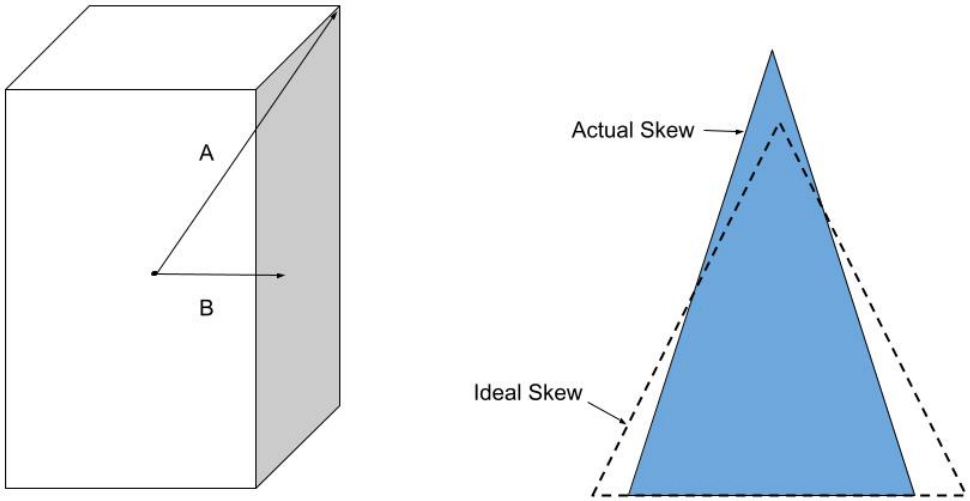

Figure 8: Aspect ratio (A/B) and skewness.

Figure 8 shows the maximum aspect ratio is the distance from the vertex of the cell (A) to the distance of the cell face (B) as measured from the centroid. This value can go very high, but it is recommended to be kept below 35:1 [10].

Note that changing the under-relaxation factor may help numerical stability in models with high cell skewness. Relaxation factors are used to numerically stabilize solutions at the cost of computation time by updating the temperature by a fraction of the change. The result of the simulation will reach the same temperature but take longer to do so by under-relaxing the variables.

Orthogonality is the measure of the angle between the normal vectors of each face of the cell and the centroid vector. The centroid vector being the fluid direction vector at the centroid of the cell. In other words, faces with sharp angles from the cell centroid have low orthogonal quality. Ideally, the orthogonal quality should be as close to 1 as possible, and above 0.15 [10]. This is the main measure of mesh quality in this project for volume cells, as poor orthogonality likely indicates poor aspect ratio and skewness. It should be noted due to dimensionality, skewness is the primary measure of quality for 2D surface cells.

3.2.2 Physical Properties

The CFD model also requires material definitions for the fluid and solid regions. Typical properties of light water were used and defined as constant (see Appendix D). Importantly, the density of water was not set to be constant, as changing density is needed for natural convection and appropriate modelling. Instead, the Boussinesq approximation was used on the base density of saturated light water at 25°C, which is 997 kg/m^3 [14].

The Boussinesq approximation is useful in calculating small changes to the density of a fluid, and as such is typically used in convective heat transfer problems. This

approximation holds true when the ratio of change in density to the density of the fluid is much less than 1, which in the case of the SLOWPOKE-2 holds true.

Defining the material properties of the solid region in the SLOWPOKE-2 requires the material properties of Zircaloy-4 to be available through the CFD software material library or must be manually added. The exact values of the material properties of Zircaloy-4 used in this project can be found in Appendix D. The other material used in the solid region of the SLOWPOKE-2 is aluminum, specific material properties can be found in Appendix B. Zircaloy-4 is only defined on the fuel pins, for the rest of the structure high-quality aluminum (1050a-h19) was used.

3.2.3 Fluent Settings

When configuring ANSYS Fluent for simulating the SLOWPOKE-2, several decisions had to be made regarding the parameters of the simulation. First, one must choose the type of solver being used for the simulation. There are two broad categories of solver technologies, pressure-based and density-based. In Fluent 2022 both solvers should be applicable to most flow problems, however, pressure-based models are traditionally used for incompressible flows [10]. Whereas density-based solvers were traditionally used for high-speed (Mach number above 0.3) compressible flows and as such may see more accuracy when solving these fluid behaviours [10]. Given this background using a pressure-based solver is ideal for the simulation of the conjugate heat transfer of the SLOWPOKE-2. However, simulations were also done using a density-based model for comparison.

Additionally, the system must be loaded with appropriate gravity. Since the SLOWPOKE-2 system is cooled via natural convection which occurs due to the flow arising from density differences in heated water, gravity must be turned on to ensure natural convection occurs. Depending on the orientation of the CAD, gravity must be loaded in the minus y direction with an acceleration magnitude of 9.8 m/s^2.

Another important setting is choosing between a steady-state solver versus a transient solver. As implied by its name, the steady-state solver assumes the system is in a steady-state and the flow properties do not change over time. As such, this solver is typically much faster and calculates average temperatures, whereas the transient solver solves for instantaneous values of each property. If run for long enough, the SLOWPOKE-2 can enter a quasi-steady-state where there is not a dramatic change in temperature at the areas of interest. As such, all simulations for this project are done in the steady-state; however, for future work on this project, transient simulations of the SLOWPOKE-2 should be conducted as part of the validation process to ensure the simulated results match experimental data of how quickly the SLOWPOKE-2 heats and cools during start-up and shutdown operations. If the simulated transient data match the experimental results this would indicate the validity of the CFD model.

ANSYS Fluent also allows for choosing the velocity formulation solver to be absolute or relative. An absolute velocity formulation is solved assuming that the fluid flow in the domain is not rotating, whereas relative velocity formulation assumes the fluid is rotating. While the convective movement of the SLOWPOKE-2 may be considered rotating as it rises and falls, the relative velocity formulation setting is used in cases such as large rotating mixing tanks. As such, absolute velocity formulation was selected for all simulations and should have the necessary numerical stability needed.

Moving on from general Fluent settings, more specific model settings must be adjusted. First, the SLOWPOKE-2 system is not a boiling water reactor [4], as such the multiphase setting should be turned off as all fluid movement will be in the liquid state without phase change. The main motivation behind this model is to investigate the heat transfer and thermal power of the system, thus the energy equation setting must be turned on. However, because most of the heat transfer is convective and conductive, the radiation setting can be turned off as energy transferred via radiation is negligible. All other model settings can remain the default, except for the turbulence setting.

Choosing a turbulence model for CFD modelling is not a straightforward process, as this setting will affect the heat transfer, numerical stability, and time to solve; the factors this project is mainly concerned with. For most of the simulations run in this project, laminar nonturbulent flow will be chosen. Using this setting there are no turbulence equations to solve, greatly reducing the computation time. The assumption of laminar flow in the reactor must hold true or affect the results to such a small degree that it is not worth the greater computation power required to run the turbulence model. For comparison, and to validate the assumption of laminar flow a turbulent model will also be simulated using the one equation, and therefore low computation cost, Spalart-Allmaras Turbulent model which solves a kinematic eddy turbulent viscosity equation [10]. Laminar flow does not calculate or solve for kinematic viscosity.

For all models tested a coupled pressure-velocity scheme was used. Furthermore, pressure, momentum and energy spatial discretization were all set to be second order upwind. Second order solvers provide more accurate values via the expansion of a Taylor series as discussed in Section 2.1, and upwind refers to the fluid flow in the model. Several relaxation factors were tried in the creation of the CFD models, originally set at 0.75 this was later adjusted to 0.5. Relaxation factors as discussed in Section 3.3 are used to numerically stabilize solutions. The result of the simulation will reach the same temperature but take longer to do so by under-relaxing the variables.

For analysis of the model at the areas of interest temperature probes must be placed at the inlet and outlet locations, the approximate locations of these detectors are displayed on the CAD in Figure 9.

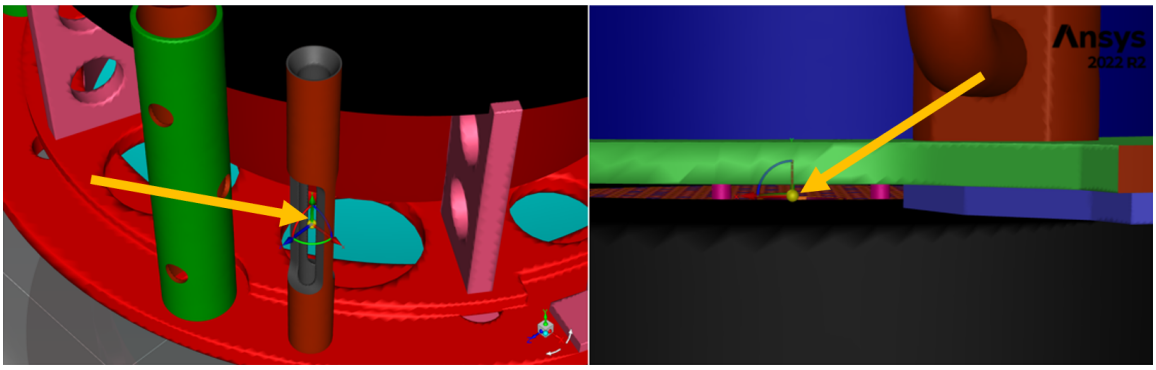

Figure 9: Inlet thermocouple assembly towards the bottom of the reactor container (left) and outlet thermocouple location in the gap between the beryllium annular and top reflector (right).

In addition to monitoring the temperature at these locations, shown in Figure 9, the total heat transfer at the fuel pins should be measured to ensure the correct amount of energy enters the system.

Geometric details in the CAD were kept in the model for comparison purposes to CNL. To simplify the simulation as much as possible instead of simplifying the geometry, assumptions were made to simplify the Fluent solver itself. These assumptions included laminar non-turbulent flow in the model, constant heat flux, etc.

Initialization for the models in this project was done via standard initialization, with no initial velocity at 273 K. Operating conditions of the reactor were set to be standard atmospheric pressure, and 288 K, which matches the pool temperature and internal temperatures during long periods of inactivity. It should be noted that hybrid initialization or different initialization values should not change the outcome of the simulation if operating conditions and heat sources remain the same.

Two sources of heat transfer were defined in the CFD models. The first was the heat flux delivered by the fuel pins themselves. The heat flux on the fuel pins was defined on the walls of the fuel pins with a heat flux of 11668.3 W/m^2. This was chosen by taking the reactor power the model was simulating, approximately 8.5kW, and dividing this thermal power by the surface area of the fuel pins, approximately 0.7285 m^2

as given by the CAD. It is important to note this heat flux is uniformly applied, whereas in reality the heat flux can vary along the length of the fuel pin. In contrast, the CFD model of the SLOWPOKE-2 created by CNL using STAR-CCM+ uses a varying heat flux along the length of the pin [13].

The second source of heat transfer in the system is on the outer wall of the reactor container, where heat transfer occurs to the external pool. This is a major source of uncertainty at this stage of the project, as the exact heat transfer at this wall is unknown. At the recommendation of CFD engineers from CNL, as well as for comparison purposes between the models, the heat transfer coefficient at the wall was set to 5 W/m^2K. Also of note, this condition was only set on the annular wall.

At this point, the simulation is ready to be run after it has been initialized with the conditions outlined above. However, before running any simulation, ANSYS Fluent has a feature called “Check Case” that will automatically check the simulation to determine if errors or issues are detected before the simulation is run. This is very useful given the size and complexity of the simulation in question and the time it will take to solve. The simulation can take up to 24 hours to solve, therefore problems in the case may not be detected until manually inspecting the results after 24 hours of computation.

Comparison of the CFD model created in this project using Fluent, to the model created by CNL using STAR-CCM+ will be compared to determine differences between the models, either due to software or model conditions. As stated previously model conditions will be the same for comparison, such as the reactor container wall heat flux, with a major difference being the fuel rod heat flux which varies along the length of the fuel rod for the CNL model. The time to compute, thermal power, temperatures and temperature delta will be compared between models.

All computation for this project was done on the CMC Microsystem computer cluster. This system utilizes 32 cores of an Intel Xeon Gold 6130 CPU, with 384 GB of RAM. Scripts used to upload simulations are shown in Appendix C.

Chapter 4: Results

The results for this project come primarily from analyzing the SLOWPOKE-2 data before and after refuelling, as well as a sensitivity analysis of the thermocouples in the system. The results from the temperature data show that in its current state SLOWPOKE-2 thermal power error is not small enough to provide reasonable fuel monitoring results. As will be shown in this chapter, the SLOWPOKE-2 power reading does not differ between the old and new cores however the external neutron flux does. This is not consistent with the theory outlined in Chapter 2. However, by investigating the temperature probe values before and after refuelling a reasonable estimate of the average energy difference between the cores can be reported.

The CFD results in this thesis showcase the viability of using CFD to monitor or ascertain reactor parameters. Models of the SLOWPOKE-2 could be simulated in less than 24 hours. The CFD results are promising, and with future validation and verification work, could reasonably be used to estimate the thermal power of the reactor. Fluid dynamics, pressure changes, density changes, and temperature changes other than at the thermocouples can also be found using CFD modelling, indicating the applicability of CFD to other projects and generally to a greater understanding of the SLOWPOKE-2 system.

4.1 Temperature Data

The temperature curves for the average power levels of the SLOWPOKE-2 before refuelling are shown in Figure 10. The most common power level for the SLOWPOKE-2 to be run at is half-power, which according to the reactor control system corresponds to approximately 8.5 kW. This setting is called half-power as the neutron

flux setpoint for this power level is $5x10^{11}$ neutrons cm^{-2} s^{-1}, thereby making full power at the flux setpoint of $1x10^{12}$ neutrons cm^{-2} s^{-1}. Units of nv are neutrons $cm^{-2}s^{-1}$.

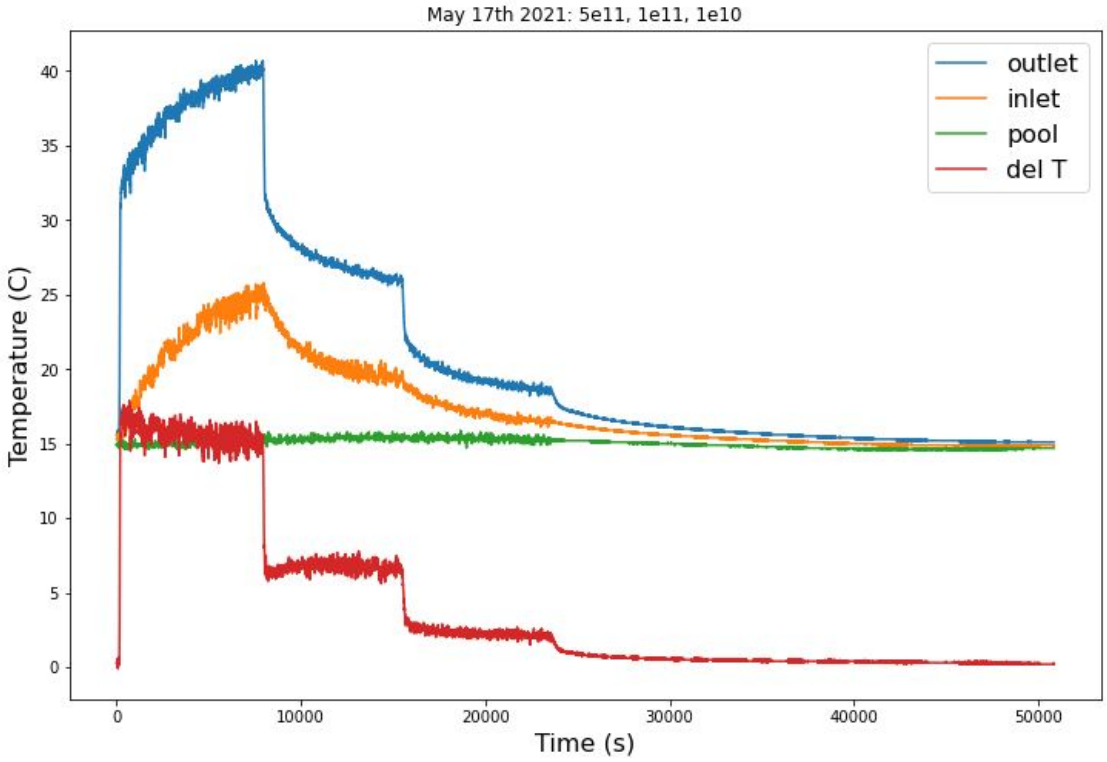

Figure 10: Typical temperature curves of various SLOWPOKE-2 power levels. Outlet represents outlet temperature, inlet represents inlet temperatures, pool represents the external pool temperature, and del T represents the temperature difference between the outlet and inlet.

Figure 10 shows the raw temperature curves given by the inlet, outlet, and pool thermocouples of the SLOWPOKE-2 for half, tenth and hundredth power. Figure 10 introduces many concepts of the SLOWPOKE-2 data collection and data analysis that are important in understanding this paper. Immediately noticeable is the noise in the temperature data. Large amounts of noise in the data may make comparison of the experimental SLOWPOKE-2 data to the simulated SLOWPOKE-2 data difficult. As such, an investigation into the temperature probe noise will be discussed in Section 6.1.

Another trend that must be examined in the SLOWPOKE-2 data is the shape of the temperature curves themselves. It can be seen in Figure 10 and the rest of the Figures

containing temperature curves in this paper that the rate of temperature increase is much higher when the reactor has just been set to a flux point. However, after some time the rate of temperature change in the reactor will decrease, entering a quasi-steady-state. The temperatures in this quasi-steady-state will still increase, but at a much slower rate than when the reactor was first set to this power level. This trend can easily be seen in Figure 11 which shows temperature curves in the old core set at half-power.

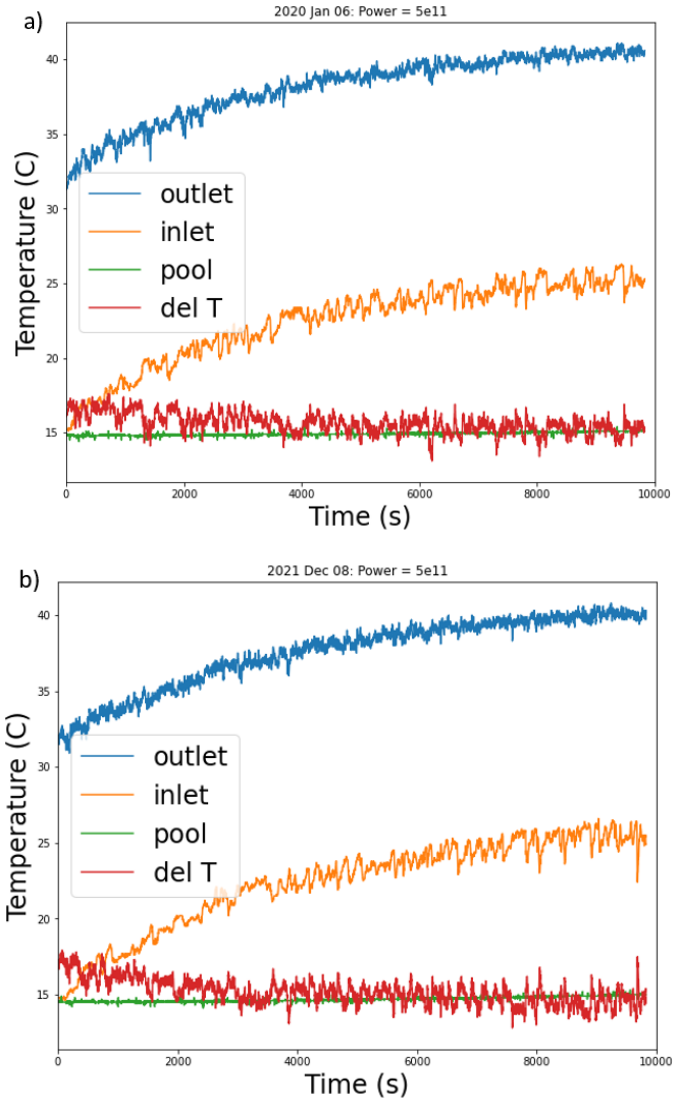

Figure 11: Showing the reactor entering the quasi-steady-state at half-power a) before and b) after refuelling.

From Figure 11 it is evident that the reactor enters a quasi-steady-state over time with temperatures changing less rapidly in the quasi-steady-state. Unless otherwise stated all temperature comparisons done in this project between the old and new core are done using quasi-steady-state temperatures to ensure the most accurate comparisons. For example, to compare the data in Figure 11a to data from the new core, the new core data was also taken in the steady-state and truncated such that both data sets had matching time frames, approximately 2 hours and 46 minutes. This data from the new core is shown in Figure 11b. It is worth noting data sets are taken when the pool temperature in the systems is comparable, and not abnormal due to the improper function of the chillers.

Using these two datasets, the data from January 6th, 2020, before refuelling, and December 8th, 2021, after refuelling, we can compare the temperature data between the two cores for a half-power reactor run. Figure 12 shows the histogram of the difference between the outlet and inlet temperature probes.

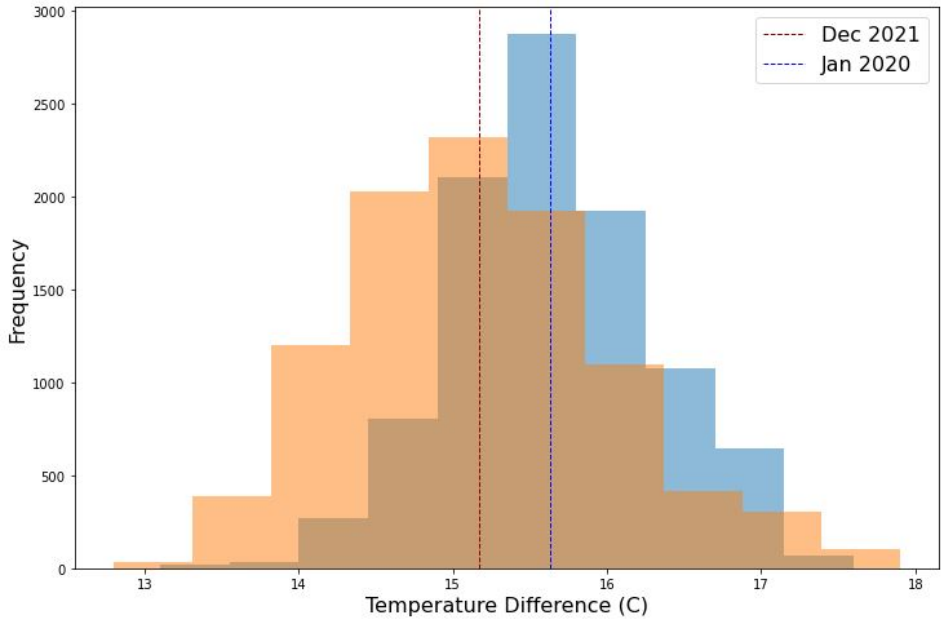

Figure 12: Temperature difference between the average Delta T before (blue) and after (orange) refuelling.

As we can see from the dotted lines on the figures indicating the average temperature difference values, the new core has a slightly lower temperature difference than the old

core, by approximately 0.46°C. To investigate this further the data showing the temperature difference between the outlet and inlet (referred to in the figures as del T or ΔT) have been fitted linearly and via a curve optimization fit. As seen in Figure 13 the line of best fit does not capture the data appropriately, however, the curve of best fit indicates the trend of these data sets.

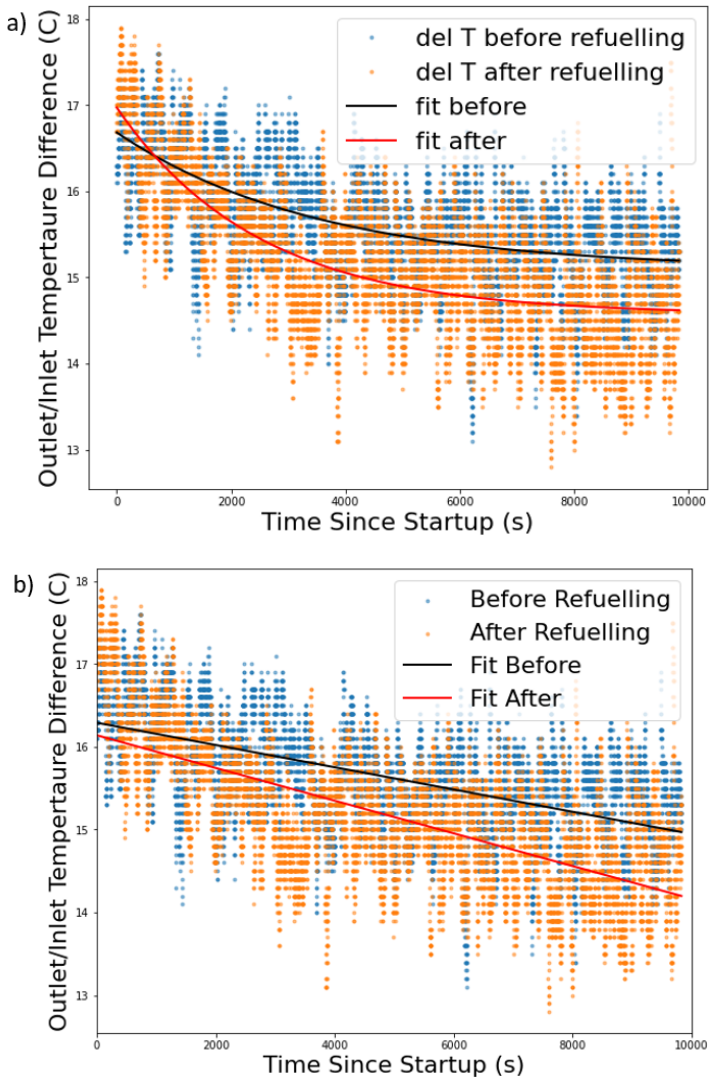

Figure 13: Data of the Delta T between old (blue) and new (orange) reactor cores. a) shows a curve fit of the data b) shows a linear fit of the same data.

As seen in Figure 13 the temperature difference between the outlet and inlet in the new core stays lower than in the old core as the reactor enters the quasi-steady-state. This

lower temperature difference between the two thermocouples in the SLOWPOKE-2 indicates the new core has less thermal power at the same neutron flux point. From Figure 13 it is evident a curved fit best captures the data.

Using another dataset from the old core, the possible thermal power difference between the two cores can be further investigated. Data taken from the quasi-steady-state of half-power operation on June 30th, 2021, and Dec 8th, 2021, the temperature probe data can be graphed individually and compared. The histograms shown in Figure 14 compare the inlet and outlet temperature differences between the old and new cores.

To determine if the ΔT difference between the cores is caused primarily by changes in the inlet or outlet temperatures, histograms of both the inlet and outlet temperatures are shown. If the ΔT difference between the cores is caused primarily by a difference in the inlet temperatures, while the outlet temperatures remain the same between the two cores, this indicates the change in ΔT is not caused by a change in thermal power. Instead, if the inlet temperatures are different while the outlet temperatures are the same this may indicate an increased cooling efficiency of the new core due to an increase in fluid volume cooling the core caused by the fewer fuel pins in the new core. However, if the ΔT between the cores is caused primarily by the difference between the outlet temperatures, this clearly indicates a difference in thermal power between the cores. Figure 14 shows the temperature differences of the inlet, outlet and ΔT between the two cores.

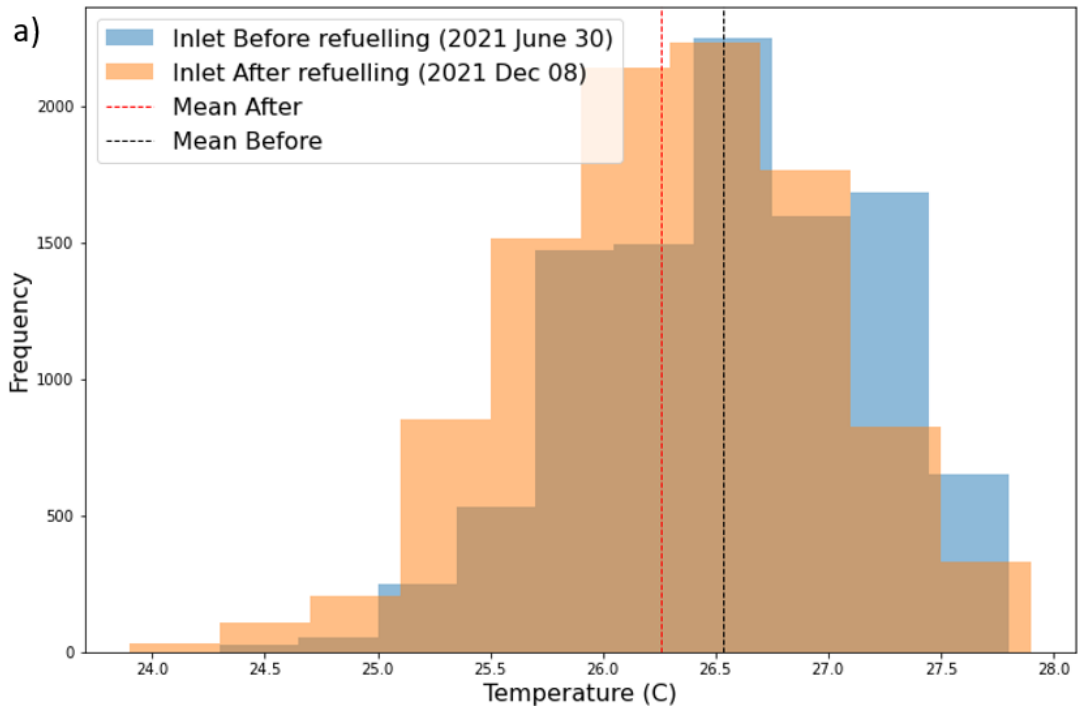
a)
Inlet Before refuelling (2021 June 30)
Inlet After refuelling (2021 Dec 08)
Mean After
Mean Before
Frequency
Temperature (C)

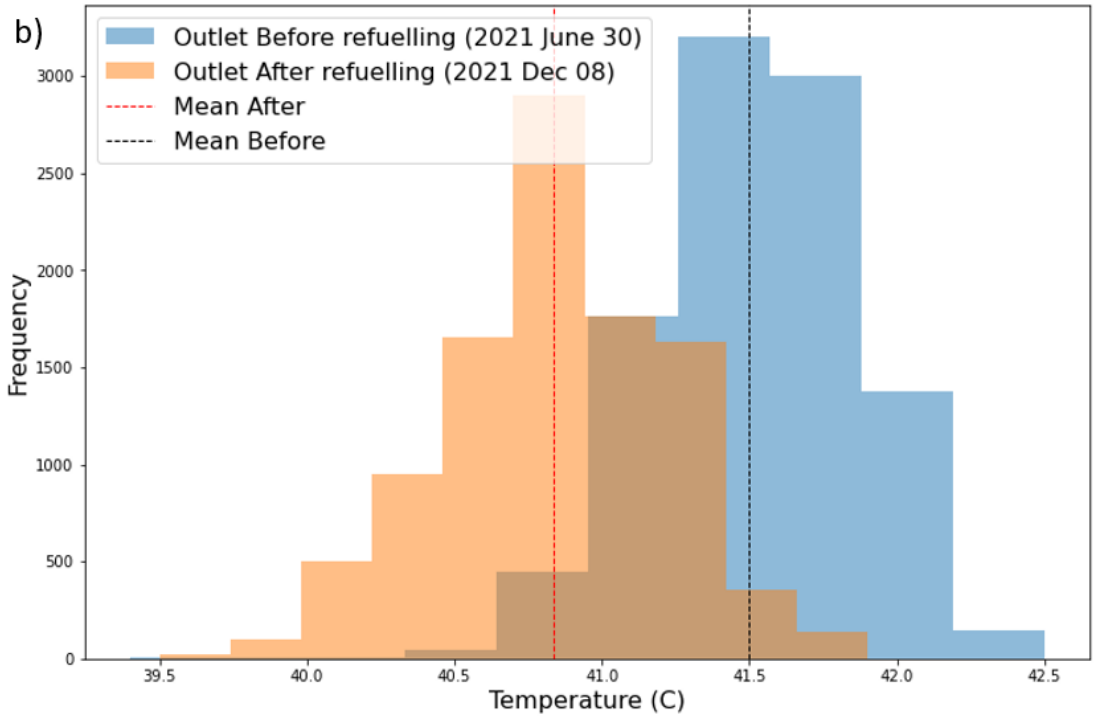
b)
Outlet Before refuelling (2021 June 30)
Outlet After refuelling (2021 Dec 08)
Mean After
Mean Before
Frequency
Temperature (C)

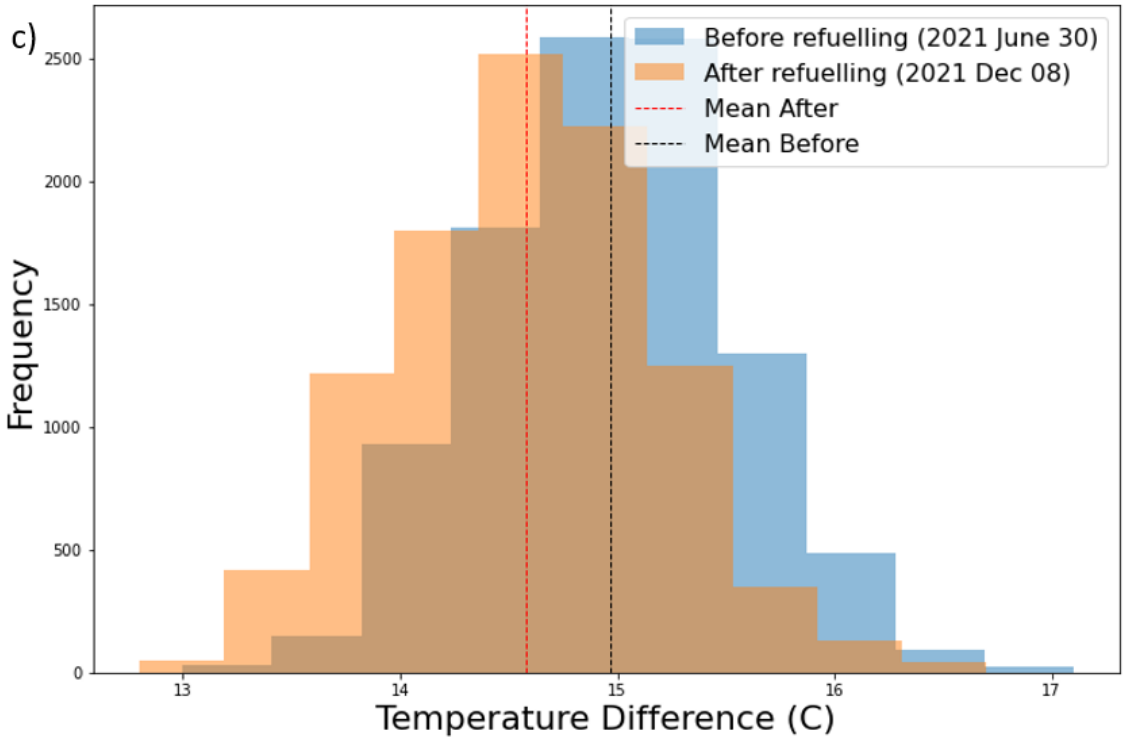

Figure 14: Average temperature differences between the new (blue) and old (orange) core for the a) inlet, b) outlet, and c) delta T.

As we can see from Figure 14, the average inlet temperatures between the two cores are much closer than the average outlet temperature between the two cores. This indicates the ΔT difference between the cores is likely caused by a difference in thermal power, not from increased cooling efficiency. Note that the temperature difference between the two cores varies by approximately 0.39°C. It should also be noted that the covariance of the datasets shown in Figure 14 for ΔT values before and after refuelling is 0.321, with a correlation coefficient of -0.0367 and p-value of 2.422×10^{-4}. These statistical measures are important consider for calculations in this paper using these datasets, specifically for the large uncertainties shown in Chapter 7. These histograms indicate that as expected the temperature difference between the outlet and inlet is analogous to the thermal power of the core, and the thermal power of the new core is slightly lower for the same neutron flux level, and the same time period.

The power level (neutron flux setpoint) for these data sets compared were set to the same value, half-power, $5x10^{11}$ neutron flux. This is the first indication of the inaccurate power readings given by the SLOWPOKE-2 operating computers, which as previously discussed calculates the SLOWPOKE-2 power level by scaling the internal neutron flux, in the case for half-power, $5x10^{11}$. Therefore, if the internal neutron flux and power level are the same between the two cores the same temperature values given by the thermocouples should be expected as well. While burnup in the core and fuel age may affect reactivity and therefore temperature values, beryllium shims are added on top of the SLOWPOKE-2 to compensate for this reactivity change. The higher temperatures in the old core and therefore additional thermal power may be from the full shim tray above the core, as opposed to the empty shim tray in the new core.

Despite the shim insertion, Figure 14 shows the SLOWPOKE-2 at half-power (approx. 8.5kW) for both cores. From the temperature difference between the cores, and therefore the inferred thermal power difference between the cores the new core has slightly lower thermal power. However, the internal neutron flux reported by the SLOWPOKE-2 reactor computer does not change between cores at half power, despite the temperature difference indicating a change in power. Since the reactor power is calculated from scaling the internal neutron flux (based on initial calibrations discussed in Section 1.3) the thermal power of the reactor as calculated by the reactor computer does not change between the cores. Therefore, since the internal neutron flux reported and thermal power calculated by the SLOWPOKE-2 reactor computer does not change between the cores, the system currently does not have the resolution necessary to properly employ the enhanced fuel monitoring technique. This leads to the motivation for a CFD model. Furthermore, if the temperature values between the new and old core vary there should be similar variation seen in the neutron flux between the two cores for the fundamental theory of fuel monitoring to hold true. With the insertion of shims, the internal neutron flux values should also change to indicate the reflection of neutrons in the core, and therefore the neutron flux scaling from initial calibration should remain the

same. It is also worth noting that the additional reactivity from shim insertion may not have been accounted for in the original calibration process.

Using the temperature difference between the ΔT values of the two cores while the reactor is operating at steady-state, a simple thermodynamic equation,

$$Q = mc\Delta T \tag{8}$$

can be used to estimate the Q energy difference between the two cores, m being the mass of fluid, and ΔT being the temperature difference. The heat capacity (c) of light water used in the reactor at approximately 20°C is 4182 J/kg°C, and the volume of water in the reactor container can be estimated using the CAD and CFD models of the reactor [14]. According to the CFD model, the fluid region of the reactor container contains approximately 0.17 m^3 of light water (assuming the volume difference caused by three fuel pins is negligible). Converting this to 170 kilograms and taking 0.4 °C (14.58 °C average ΔT after refuelling, and 14.97 °C average ΔT before refuelling) to be the approximate temperature difference of the ΔT, we can estimate the Q difference between the cores to be approximately 284.4 kJ, or 80 Wh. Given the simplicity of this calculation and the assumptions used in the calculation of the energy difference between the two cores, this value should be considered a starting point for comparison between the two cores in the CFD simulations.

4.2 Neutron Flux Data

Having shown the thermal power discrepancy between the two cores according to the temperature probe data, the neutron flux data can be analyzed to determine if the discrepancies are visible. As mentioned in Chapter 1, the neutron flux monitoring of the SLOWPOKE-2 is done primarily by an internal neutron flux detector located in the reflector region of the core. This detector is used to control the neutron power level of the

core. Figure 15 shows the neutron flux data from the internal neutron flux detector for the associated temperature plot shown in Figure 10.

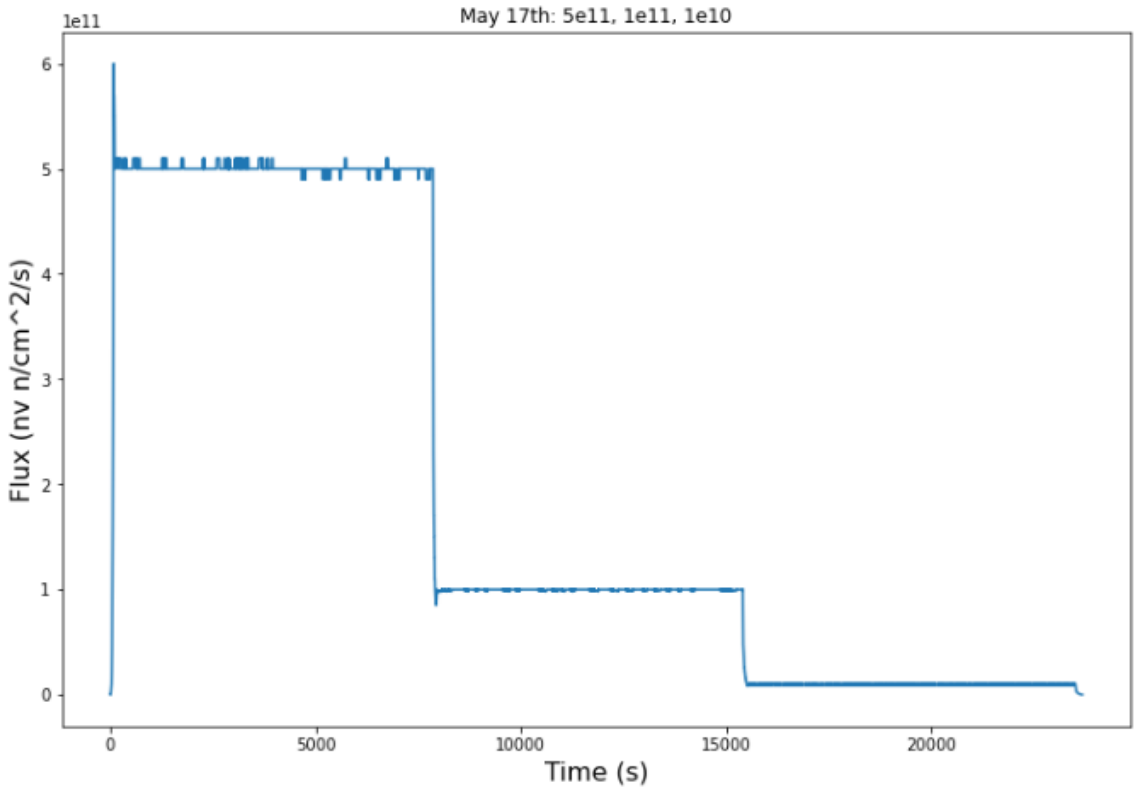

Figure 15: Thermal neutron flux data measured in the inner irradiation site during operation of the SLOWPOKE-2 reactor at RMC with control system flux set points of 5×10^{11}, 1×10^{11}, and 1×10^{10} n/cm^{2}s on May 17th, 2021 (old core).

As seen in Figure 15, the neutron flux according to the internal flux detector remains constant over the reactor operation with small fluctuations due to neutron poisons formation which in turn leads to control rod movement to maintain the neutron flux setpoint within 1.5%. This is not surprising as the internal neutron flux detector determines if the reactor has reached the neutron flux setpoint, and the reactivity of the reactor will be adjusted to ensure it stays at the neutron flux setpoint as determined by the internal flux detector.

In addition to the internal neutron flux detector, He-3 and B10+ neutron flux detectors have been added to the SLOWPOKE-2 facility, in the ceiling above the reactor

and in the reactor control room. These detectors which are shielded by the water in the reactor and located significantly further away from the core than the internal neutron flux detector, show neutron count rates on the order of thousands per 600 s. The internal neutron flux detector which records in units of neutrons cm^{-2} s^{-1} records flux values on the order of 10^{11}, as shown in Figure 15. While these two detection methods are not directly comparable due to different units being used, the external neutron counts show detectable differences between the two cores while the internal neutron flux does not. This is likely due to the distance from the core the external neutron count detector is placed at but may also be due to the units being used. As such, the external neutron detectors can determine slight variations in the neutron count of the core that would be lost on the internal neutron flux detector due to the magnitude of neutron flux, or units used.

Figure 16 shows the internal neutron flux from December 08, 2021 and the external neutron count from the same day. This reactor run is the same reactor operation that was graphed in Figure 14 to show temperature and thermal power differences. The units of internal neutron flux are nv while the external neutron count is measured in neutrons detected per 600 s, it is still reasonable to compare the plots to determine the trends of each. The neutron count discrepancy found between the old and new core shown in Figure 16b will not be seen in the internal neutron flux due to the system being operated at the given neutron flux setpoint and adjusting control rod movement to stay at this value. Therefore, Figure 16 simply shows the difference between comparing datasets taken from the external neutron count detectors versus the internal flux detector, and how using the external neutron counts shows a clear difference between the two cores.

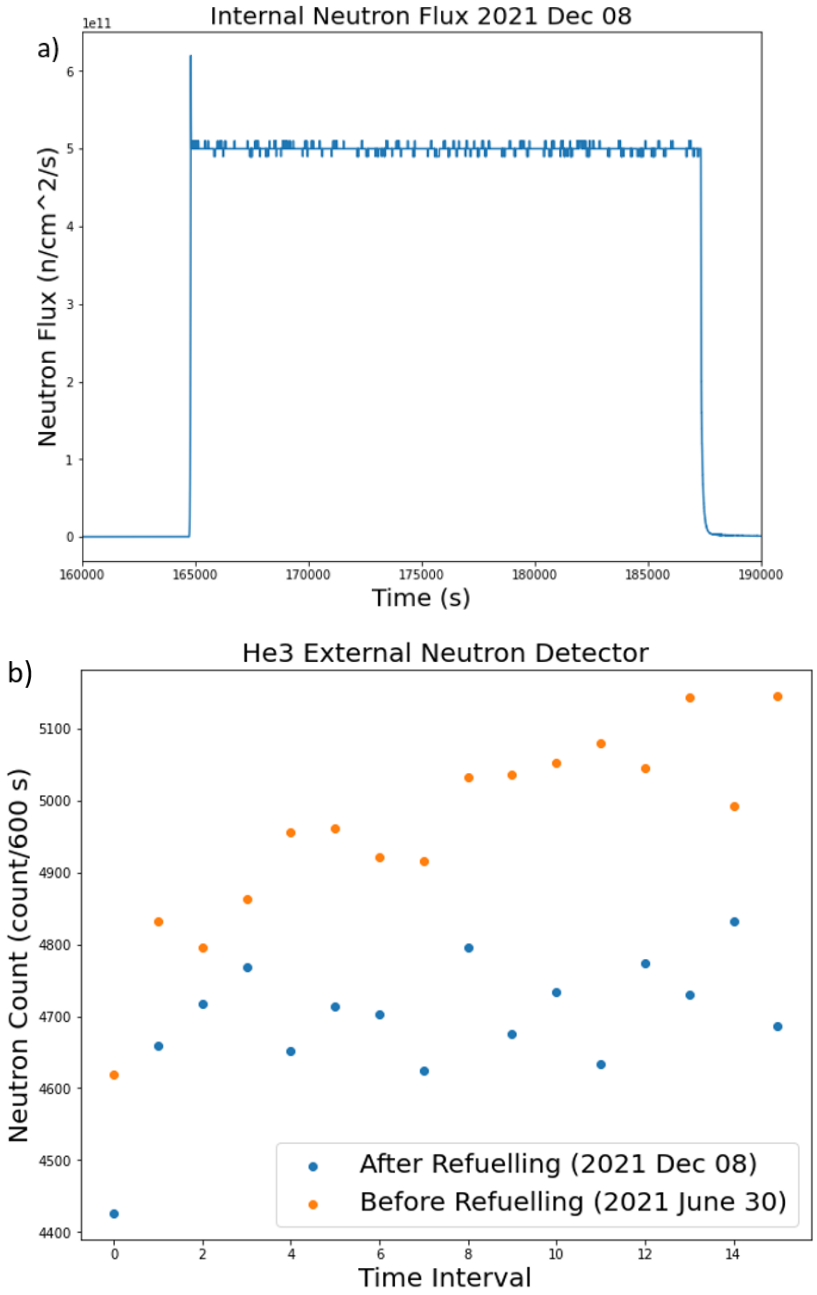

Figure 16: a) Internal neutron flux of the new core. b) External neutron counts of old (orange dots) and new (blue dots) cores per 600s time interval.

These figures show that consistently over the course of the reactor operations considered in Chapter 4.1, the new core has a slightly lower neutron flux as measured by the He-3

external detector. However, the differences in neutron flux between the cores is not visible based on the internal neutron flux detector readings.

This external neutron flux data in tandem with the temperature data is a key result indicating the applicability of the enhanced neutron monitoring capability in the SLOWPOKE-2 facility. According to the theory laid out by van der Ende et al. on enhanced fuel monitoring, the thermal power of the core is proportional to the external neutron flux detected [5]. The new core clearly has a lower thermal power according to Figure 13. The new core also has a lower external neutron flux count. Without normalizing the external neutron flux count with accurate thermal power, conclusions on the fissile content cannot be made. However, if the thermal power decreased and the neutron count increased, or remained the same as before refuelling, this would indicate an increase in fissile material. Moreover, according to the reports detailing the isotopic composition of the SLOWPOKE-2 cores, the difference between the two cores is approximately 2% [7]. The change in isotopic composition of the core can be seen in the SLOWPOKE-2 detector data. However, to properly graph and utilize the enhanced fuel monitoring system, accurate thermal power of the SLOWPOKE-2 and differences in thermal power between the two cores must be known.

4.3 Simulated Results

As mentioned in Chapter 3, pressure-based models are ideal for the simulation of the SLOWPOKE-2, however, some density models were also tested. It was found that density models were much more likely to result in unrealistic temperature values for multiple mesh densities. Tables 1 and 2 summarizes the various CFD models' quality and results. Models A through G vary by mesh density.

Table 1: Mesh information of CFD Models.

Model	Cells	Orthogonal Quality Average	Orthogonal Quality Min:	Aspect Ratio Max:	Fuel Pin Face Count	Core Volume mesh
A	12171151	0.923	0.144	411	1138798	9757005
B	19629240	0.924	0.06	1769	1138806	16679778
C	21914484	0.942	0.143	190	1138852	18416176
D	23230824	0.916	0.132	839	1138943	20059066
E	27216708	0.917	0.111	602	1306037	23456411
F	28217703	0.945	0.149	1118	1160303	23629314
G	30675541	0.920	0.126	534	1199849	26893439

Table 2: Temperature and Power of pressure-based CFD models.

Model	Inlet (°C)	Outlet (°C)	Delta T (°C)	Total Heat Transfer (W)	Computation Time	Contour Plot (Appendix B)
A	25.2	48.1	22.9	8369.2	10h 8m 35s	Figure 29
B	34.1	53.1	19	8369.6	10h 8m 1s	Figure 30
C	22.6	44.9	22.3	8369.4	17h 38m 51s	Figure 31
D	49.2	71.5	22.3	8369.6	20h 28m 50s	Figure 32
E	20.4	44.9	24.5	8369.2	21h 58m 11s	Figure 33
F	26.9	48.6	21.7	8349.5	23h 8min 33s	Figure 34
G	26.1	47.9	21.8	8349.3	24h 21m 44s	Figure 35

As seen from these two tables, the results are dependent on which mesh is used. To determine which model is most accurate a Grid Convergence Index (GCI) must be conducted. As seen in Table 2 the temperatures of the model are not convergent with refining mesh, however, the ΔT between the inlet and outlet appears to converge. However, because Models F and G have lower heat transfer by approximately 20 W, it cannot be determined that if these models had the same total heat transfer as the previous models, the ΔT would not be different.

First, the issue of temperatures in the model not converging must be addressed. When refining the volume mesh by reducing element sizes in Fluent, these refinements may occur at any point on the model. However, the idea behind a GCI is specifically refining the mesh in the areas of interest to ensure that the results of the model are not dependent on mesh resolution. That has clearly not been achieved using all models in Table 1. However, by investigating the core and inlet/outlet gap regions we can better understand the convergence behaviour of these models.

Density-based models were tested to be compared to pressure-based models. Models of mesh size matching Models A, and D were tested. The contour plot for density-based simulations of Model A and Model D are shown in Figure 17.

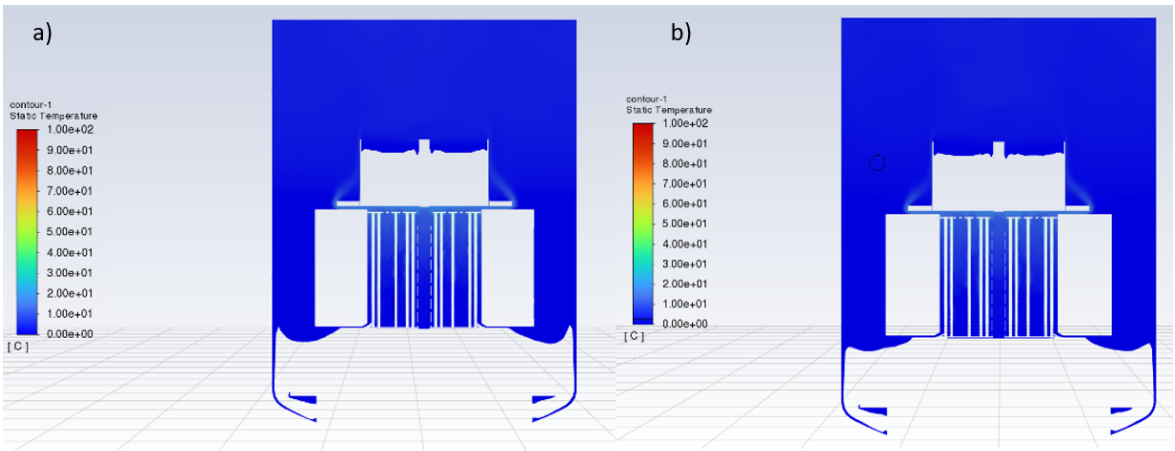

Figure 17: a) Model A density solution. b) Model D density solution.

As seen in Figure 17, the density model does not provide reasonable temperatures, note the contour plot has been limited to 0 and 100°C. While these models are loaded similarly to the pressure-based models, there is no energy under relaxation setting for the density-based models. It should also be noted that these models ran for the same number of iterations as the pressure-based models. From the density-based models tested in this project, it was evident that using pressure-based models would be easiest for this project and give the most reasonable results.

From the CFD simulations, the natural convection within the core is evident. As described in Chapter 1, the coolant movement in the core comes from changes in the density of the fluid leading to changes in the buoyant force. The movement of the water in the core can be seen in Figure 18, with areas of large velocity indicating large amounts of heat transfer or directional change of fluid movement, for example as the fluid enters the narrow inlet gap. This fluid behaviour is expected and convection can be seen.

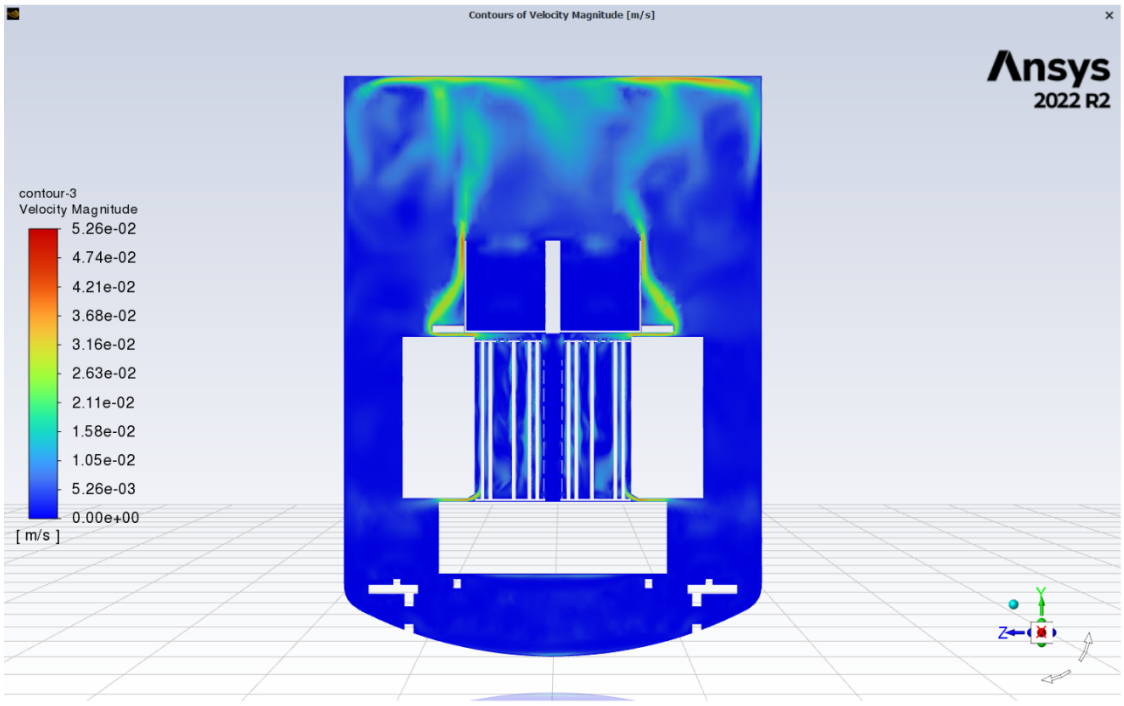

Figure 18: Velocity contour of SLOWPOKE-2 simulation.

As seen in Figure 18, as expected the velocity is higher at locations of rapid temperature change such as the outlet and inlet gaps as well as at the top and sides of the reactor container where the fluid cools. Importantly, heat transfer occurs at the wall of the reactor container as well, not just at the fuel pin surface. The reactor container is submerged in the external pool which has water kept at approximately 15 °C. Therefore, as the water inside the reactor container heats, heat transfer occurs at the surface of the reactor container as the pool water heats. It should be noted the pool has a much larger volume of water than the reactor container and heats very slowly. As stated earlier the heat transfer coefficient on the reactor container wall was set to 5 W/m^2K.

4.4 Numerical Stability

Model B, shown in Tables 1 and 2, was run once with default convergence conditions and then run again with no convergence conditions to compare between the two. Fluent calculated that the model converged based on its default convergence conditions at around 3250 iterations. For the model that continues to run after this point the residual plot oscillates noticeably and rapidly after 3250 iterations until it stops at the full 5000 iterations, notably, this causes Model A to have a slightly longer computation time than the refined Model B. This oscillation of residuals is a key indication of poor numerical stability in the model, this behaviour can also be seen in the Model A residuals that were run past default convergence conditions, shown in Figure 19. Furthermore, the temperature differences and model behaviour between the two exact same simulations with different convergence conditions are vast.

The stability of the models can often be seen by investigating the residual plots of the models. Usually having very small residuals with little to no change in the last 200 iterations indicates stability in the model. Figure 19 shows the residual plots corresponding to Model A. The residual plots of the rest of the models in Tables 1 and 2 is shown in Figure 20. The residual sum for the variables investigated in the simulation

(energy, velocity, continuity, etc.) is the difference between these values in a specific cell versus the neighbouring cell [15]. Theoretically when the residuals have reached zero the system has converged to a steady-state. In reality due to numerical and computational considerations, single precision solvers can reach residual values of $1x10^{-6}$ and double precision solvers can reach residual values $1x10^{-12}$ [15].

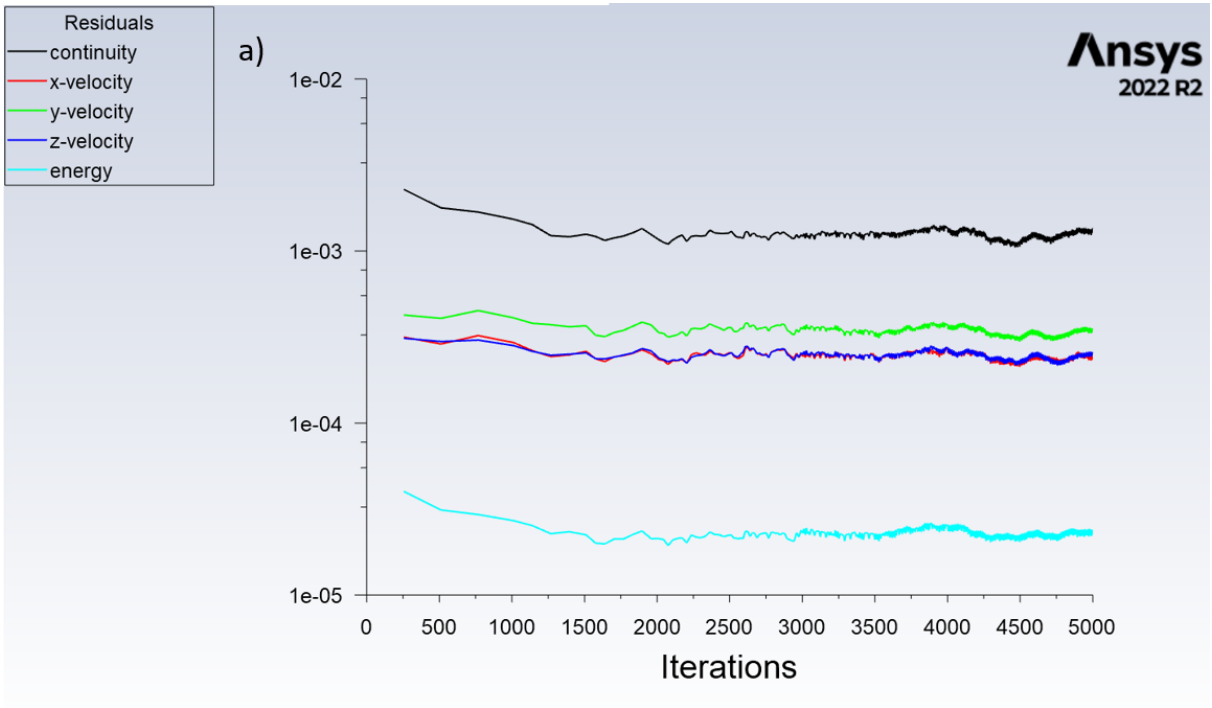

Figure 19: Model A residual plot showing numerical instability.

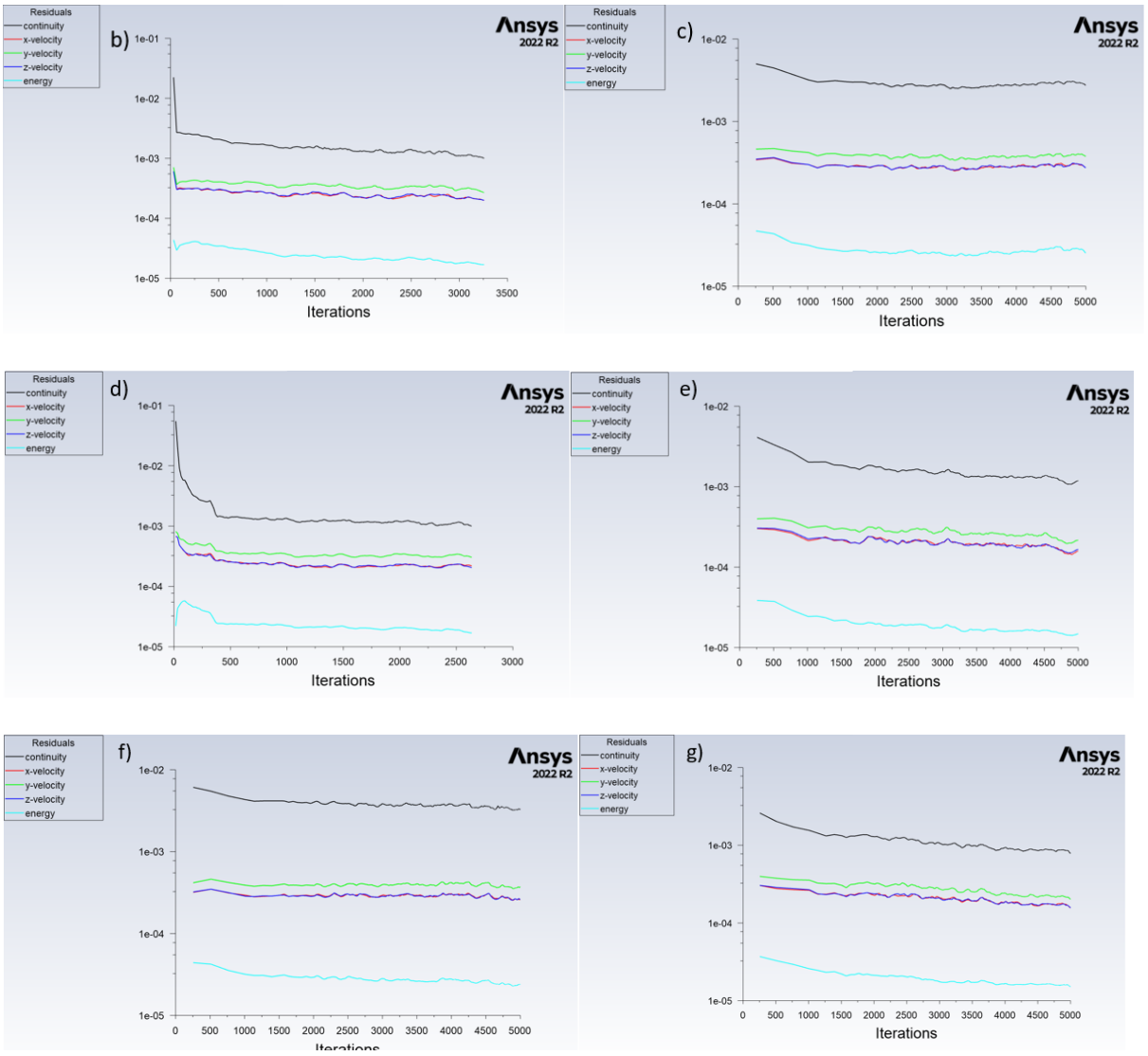

Figure 20: Residual plots labelled corresponding to CFD Model.

Many of these residual plots exhibit the same behaviour, rapidly decreasing before levelling out for the final iterations with small adjustments. However, as previously stated model A experiences continuous and visible oscillations towards the end of the simulation, indicating poor stability. Models B and D have rapid changes at

the beginning of the simulation but the residual plots level out as the simulation continues. These plots exhibit the importance of allowing CFD models, especially CFD models of complex systems such as the SLOWPOKE-2, to continue for many iterations. As a guideline, these models should run for at least 2000 iterations, and ideally for 5000 iterations to allow the system time to reach a reasonable solution. Notably models B and D also converge earlier due to reaching the Fluent default convergence conditions.

Chapter 5: Verification and Validation

Before post processing the CFD models, verification and validation of the model must be conducted. Verification is the process of determining computer programming errors and ensuring the correct implementation of the problem being solved. Verification ensures the equations are properly solved by the program. Validation determines the extent to which the model is accurate with real world data. Verification can therefore be thought of as the precision of the model, and validation as being the accuracy.

5.1 Grid Convergence Index

The temperature difference between the inlet and outlet temperatures has been decided as the parameter to converge upon. In part, this is due to the power of the SLOWPOKE-2 being uncertain, and therefore the temperatures expected from a half-power model may not be reflected in the simulation. Moreover, the temperature difference is an observable parameter of the reactor indicative of thermal power, whereas accurate thermal power (the main motivation behind the CFD model) is not. While the model should still converge on a temperature if the outlet probe was chosen as the parameter to converge upon, this temperature may be much different than what the experimental data predicts. While this may also be true for the ΔT, it is likely to vary less widely than the temperatures at the probe locations. The GCI test results are shown in Figure 21.

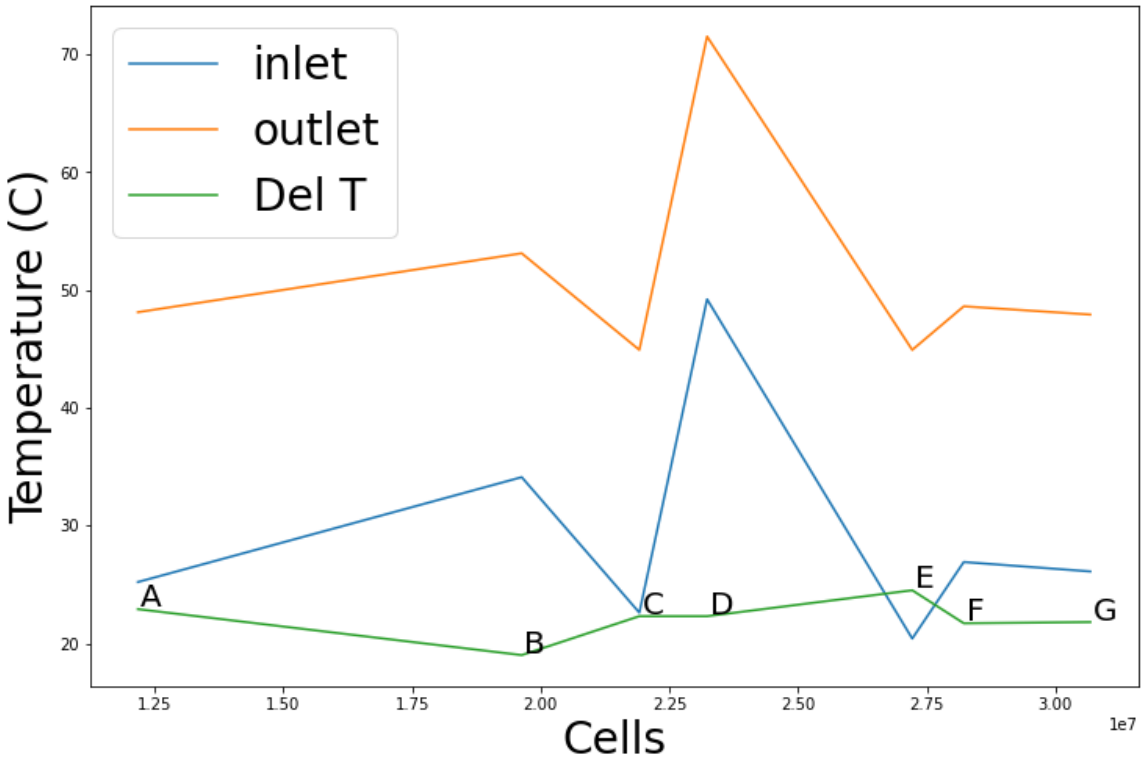

Figure 21: Grid convergence index of CFD models.

From this grid convergence plot, several observations can be made. First, the plot does not converge and therefore there is no converged model that can be used to compare simulated data to the experimental data. However, if models F and G are discarded because they have lower total heat transfer by approximately 20 W, and Model A is discarded due to the numerical instability of the residuals, then the plot appears to oscillate around inlet and outlet temperatures, while the ΔT converges towards 25 °C. Despite this, the oscillating inlet and outlet temperatures are a concern given the CFD model will be validated against the experimental data using these temperature measurements. Therefore, model D would indicate the SLOWPOKE-2 operating at a higher power as opposed to model C despite both models having the same ΔT.

As seen on the contour plots of the models with the highest cell counts (Figure 34 and 35 Appendix B), large local hotspots amid local cold spots can be seen at the top of the fuel cage. This behaviour is not expected in a correct CFD model as the temperatures

in Models F and G exceed boiling which is incorrect for the SLOWPOKE-2 system. While there may sometimes be small local hotspots in a CFD model that do not greatly affect the results, in these models it is clear that the local hotspots are too large indicative of poor modelling. Therefore, it appears refining the mesh too much also leads to modelling issues, although the overall temperatures at the probes do not seem to be influenced greatly by these local temperature hotspots.

Meaningful validation via comparing the simulated results to the experimental data from the SLOWPOKE-2 is not possible at this stage in the thesis. Once a mesh resolution has been properly converged upon the validation process can begin. However, there are a few comparisons that can be drawn from the CFD models presented in this paper to the CFD models created independently by CNL using STAR-CCM+ [13].

The converged upon model of the SLOWPOKE-2 according to CNL has a ΔT of approximately 22 °C. This temperature difference is common in many of the models presented in this paper as well. However, the CNL model uses 35 million cells and as stated previously, varies the temperature along the length of the fuel pin instead of assuming constant heat flux along the surface. Furthermore, according to initial results from the CNL model, the SLOWPOKE-2 power level is much lower than the reactor computer reads. The thermal power of the CNL model needed to be reduced to approximately 5.5 kW in order to match the temperatures shown in the experimental results of half-power runs. Therefore, the temperatures presented in this thesis, according to the CNL model, should be greater than what is expected at half-power. For reference, at half-power according to reactor data in the steady-state, the inlet should be slightly above 25 °C and the outlet should be slightly above 40 °C, this can be seen by looking at Figure 11.

Assuming the CNL model is correct and has been properly verified, Model D is closest to the CNL and the SLOWPOKE-2 models. The CNL model has a ΔT of approximately 22ºC, this ΔT is consistent with Model D. Importantly, the model created by CNL at 8.5kW had much higher inlet and outlet temperatures than the half power

experimental data showed. Model D is also consistent with this, having higher than expected inlet and outlet temperatures at 8.5 kW, again agreeing with the CNL model. Therefore, in Model D as in the CNL model, the thermal power of the core at "half-power" would need to be reduced in the simulation to match the experimental half power temperatures.

However, without proper verification via a GCI that gives reasonable results, models presented in this project could not be stated as accurate, and no hard proven conclusions could be drawn. The comparisons made in this thesis to CNL models are from initial reports from the CNL thermohydraulic modelling team [16].

Chapter 6: Error Analysis

Much of the error discussed in this Chapter is the systemic error of the temperature probes. The noise on the temperature probes that increases with reactor power indicates a flaw in the current temperature probe system leading to high uncertainties, especially at high reactor powers. As will be discussed in this Chapter it is unlikely this temperature probe noise comes from turbulence around the thermocouple, as at low powers there is very little noise. Furthermore, the temperature probe noise for the outlet levels out approaching full power. Therefore, there is likely some electrical noise or inherit flaw in the thermocouple system that leads to large uncertainties.

6.1 Probe Noise

As seen in Figures 10, 11 and 13 in the temperature results section, the temperature curve experimental data is very noisy. It is important to note the Figures shown in this project have not undergone any smoothing or averaging, they represent the SLOWPOKE-2 raw data. To understand the causes of the noise and how best to deal with this noise when comparing simulated data to experimental data, the raw data from the temperature probes was investigated.

The first step of this process is investigating if temperature probe noise can be seen when the reactor is inactive (power off). With no turbulence and the fluid in a steady-state temperature, if probe noise is seen, this would indicate the noise comes from the probe itself or electrical noise. Figure 22 shows the histogram of temperature values at each of the temperature probes. Note this data is not taken immediately after reactor shutdown, it has reached a steady-state after a long shutdown. If reactor data was taken during cooldown the noise would be difficult to separate from the natural standard deviation of the temperatures as the system cools.

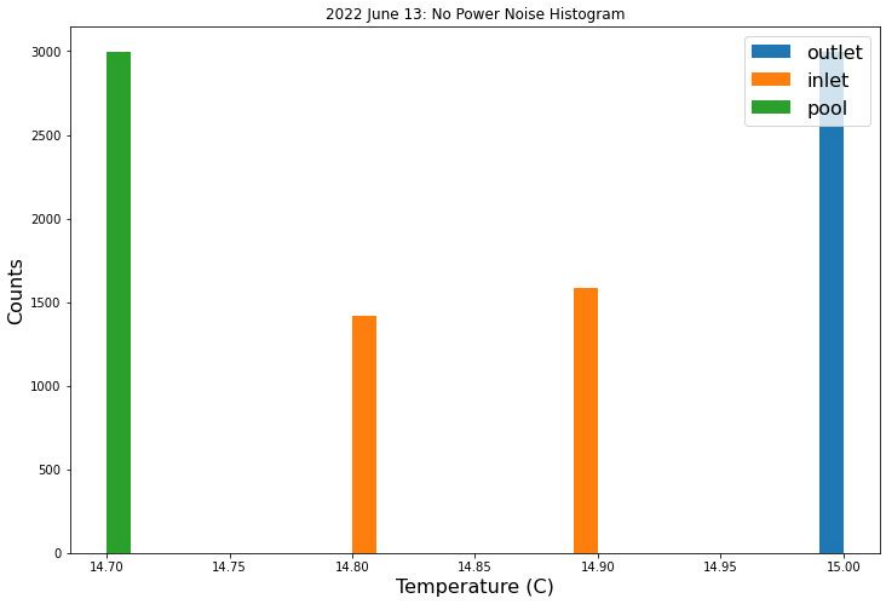

Figure 22: Temperature probe noise when the reactor is powered off.

From Figure 22 it is evident that there is little noise in the system while the reactor is inactive and has reached steady-state, as the outlet and pool temperature probes, record the same value for the duration investigated. The outlet and pool temperatures remain at a single value to one decimal place accuracy. The inlet probe however varies between two temperature values, perhaps due to the decimal accuracy to which the thermocouple and SIRCIS program is recording. Therefore, the thermocouple noise is dependent on reactor operation.

The next step in this investigation is to determine if the temperature probe noise changes with reactor power. To do this the reactor was run at several power levels, hundredth power, tenth power, quarter power, half-power and full power, the associated neutron flux setpoints for these values are $1x10^{10}$, $1x10^{11}$, $2.5x10^{11}$, $5x10^{11}$, and $1x10^{12}$ nv respectively. Figure 23 shows the temperature curves at these reactor powers (apart from full power and half power which were run on the following day) as well as the time intervals where the temperature probe noise was analyzed.

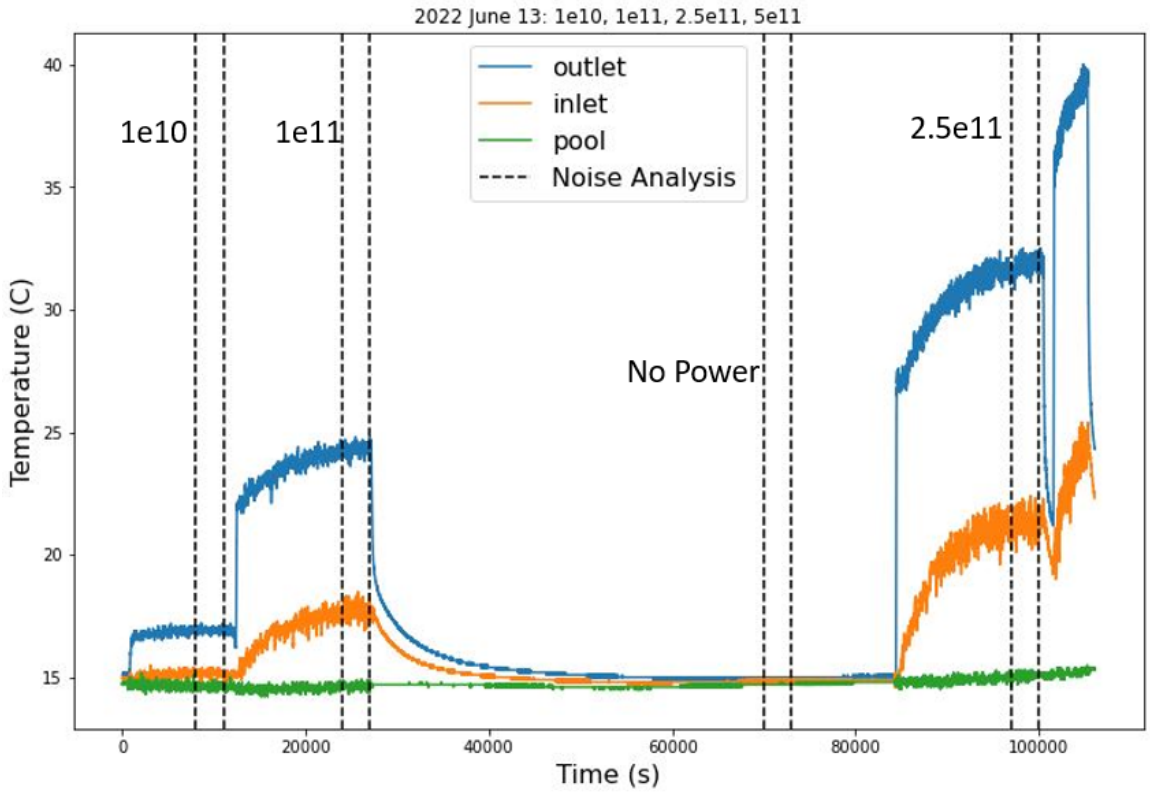

Figure 23: Temperature curves of the new core at multiple power levels.

As shown in Figure 23 all the time periods investigated for this temperature probe analysis occur in the quasi-steady-state. Although a half-power power run is shown in Figure 23 it was not used as it did not enter the quasi-steady-state for long enough to be reasonably compared to the other power levels. A half-power, and full power run from another day used for analysis is shown in Figure 24.

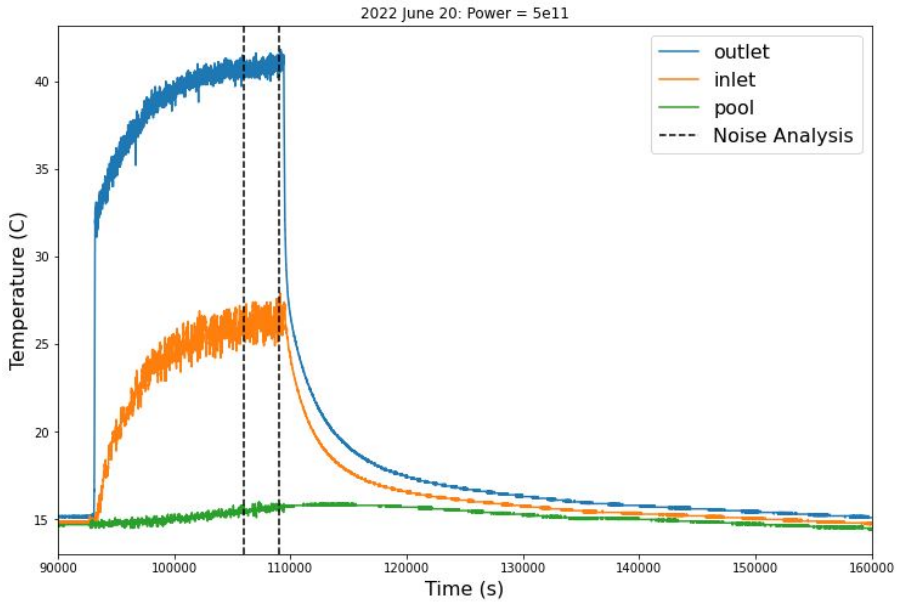

Figure 24: Half-power temperature curves.

Figure 25 shows temperature curves on June 20th, 2022, during full power reactor operation.

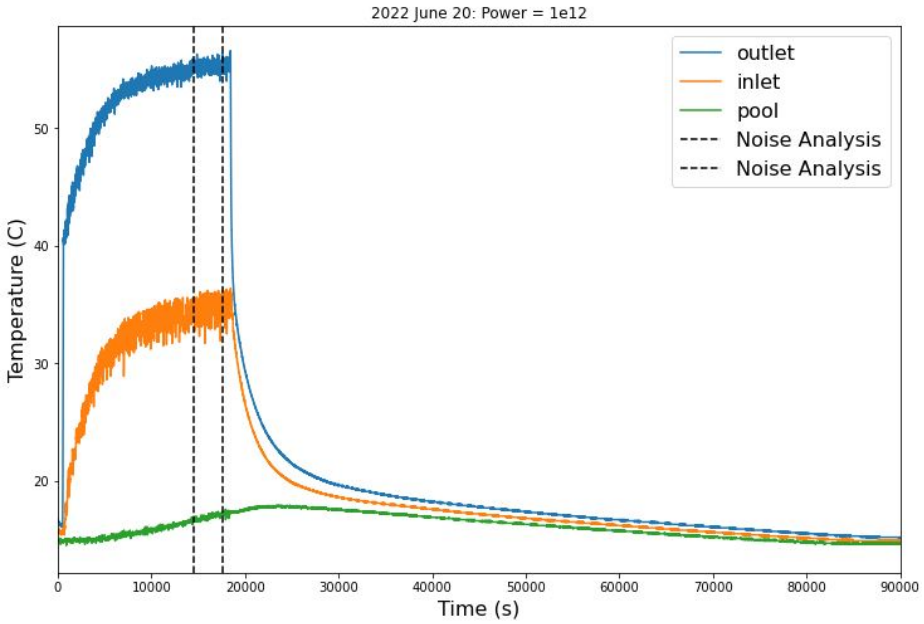

Figure 25: Temperature curves of the new core at full power for noise analysis.

Looking first at the $1x10^{10}$ reactor run, the first step was to plot the temperature curves in the region being investigated, this can be seen in Figure 26a. After ensuring the reactor was in a quasi-steady-state over the specified timeframe, the next step is to plot these temperature curves into a histogram. Visually from the line graph, there is little noise at this power level, and the histogram also indicates this with clusters of very tight bins, with a small standard deviation. The standard deviation has been written on the histogram plots for easy comparison.

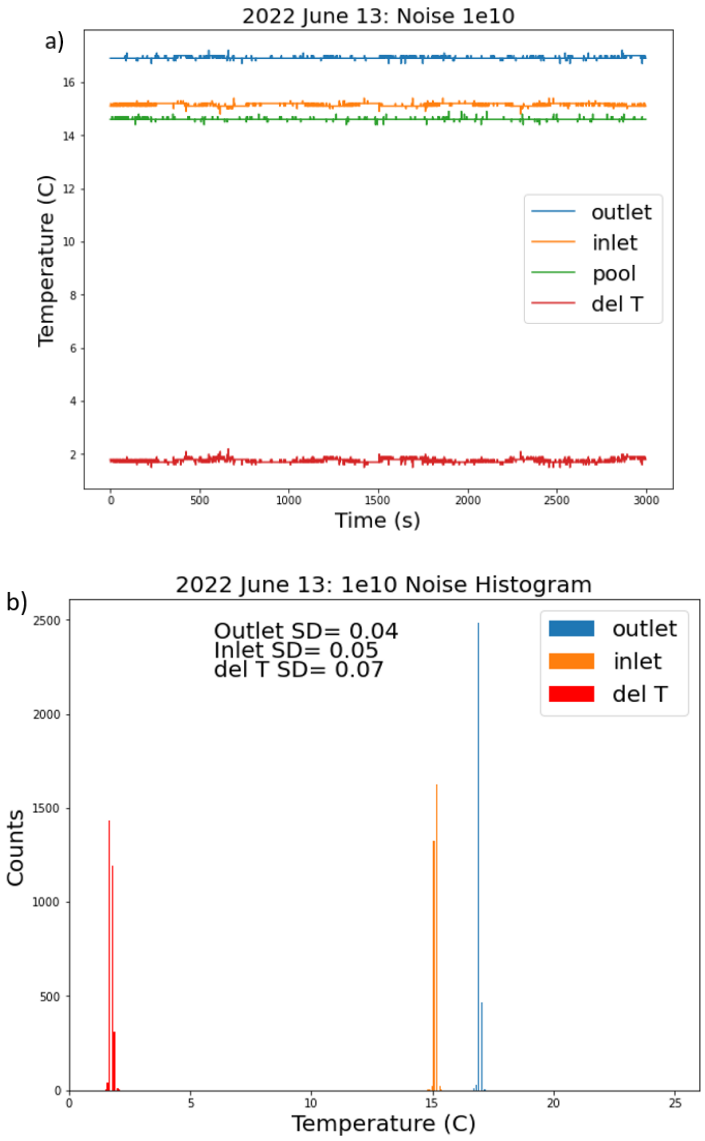

Figure 26: a) New core 1e10 noise b) temperature noise histogram.

Figure 26b shows the histogram of $1x10^{10}$ nv temperature probe data, several observations can be made from this figure. First, as indicated by the binning of the data and shown in the raw temperature probe data, the temperatures have been exported from SIRCIS with an accuracy of 1 decimal place. As such, there are some bins on the histogram that are not filled. The temperature seems to mostly fluctuate between two values, these being the two largest bins. It can also be seen that the outlet has the smallest standard deviation followed by the inlet, then ΔT. However, these standard deviation values are very small and close to each other, more power levels must be investigated before trends can be observed.

Other power levels must be investigated before concluding that the outlet has less noise than the inlet. The histogram and line plot for the next power level, one-tenth power $1x10^{11}$ nv, is shown in Figure 27. Note that for all noise line plots shown, the pool temperature probe noise is also shown. The pool thermocouple is not graphed via a histogram because of the very small standard deviation. However, looking at Figure 23 and 27b it can be seen that noise is present in the pool thermocouple. The pool, which does not rapidly change temperature and therefore has little turbulent flow around the thermocouple, further indicates the noise is caused by inherit electrical interference in the SLOWPOKE-2 system.

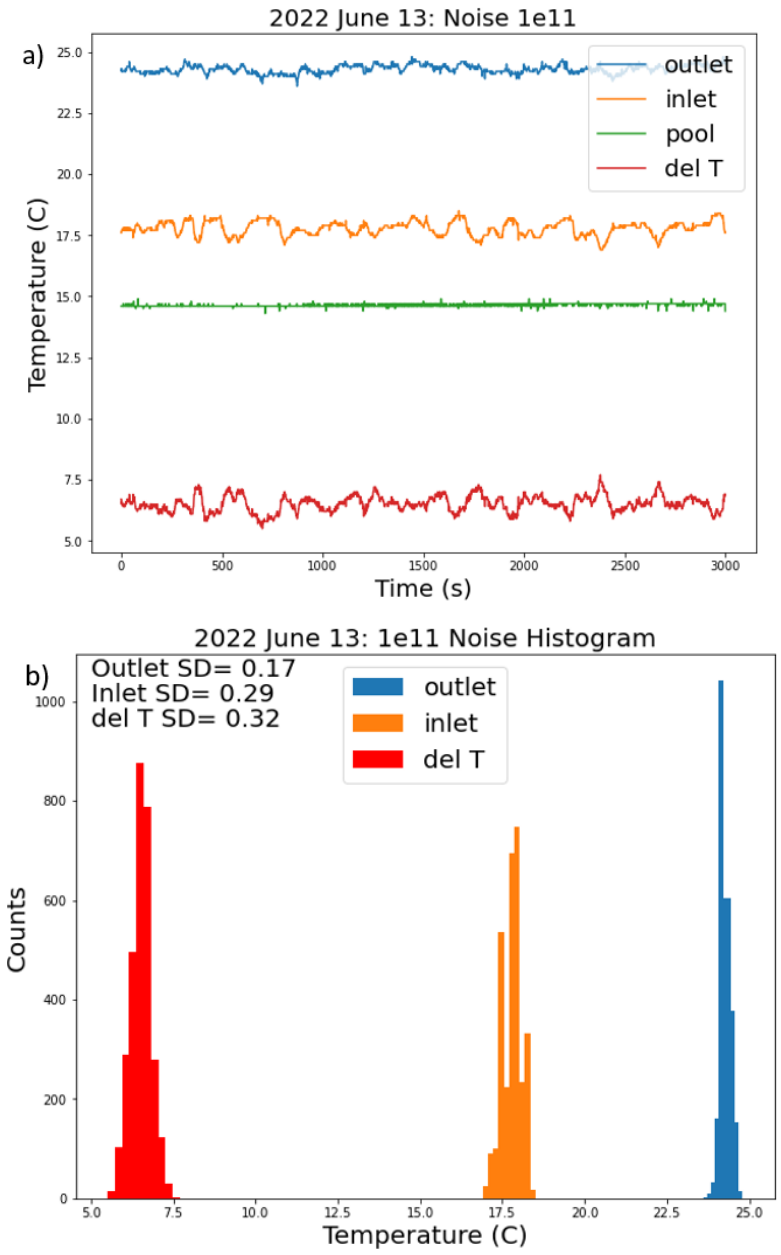

Figure 27: a) 1x10[11] nv temperature probe noise b) temperature probe noise histogram.

It is immediately evident from the line plot that there is more noise in this data than in the 1x10[10] nv data. The histogram for the temperature probe data follows the same trend seen in the 1x10[10] nv data. The inlet has a higher standard deviation than the outlet, and the ΔT having a similar yet slightly higher standard deviation than the inlet. This trend continues for the following power levels with standard deviations of the inlet and ΔT in

the full power data set being coincident. All histograms and line graphs can be seen in Appendix B.

To compare the standard deviations of the inlet, outlet and ΔT, Figure 28 shows the standard deviations of these values versus reactor power. At a neutron flux setpoint of 0 all points are coincident, and at a neutron flux setpoint of $1x10^{12}$ the inlet and ΔT points are coincident.

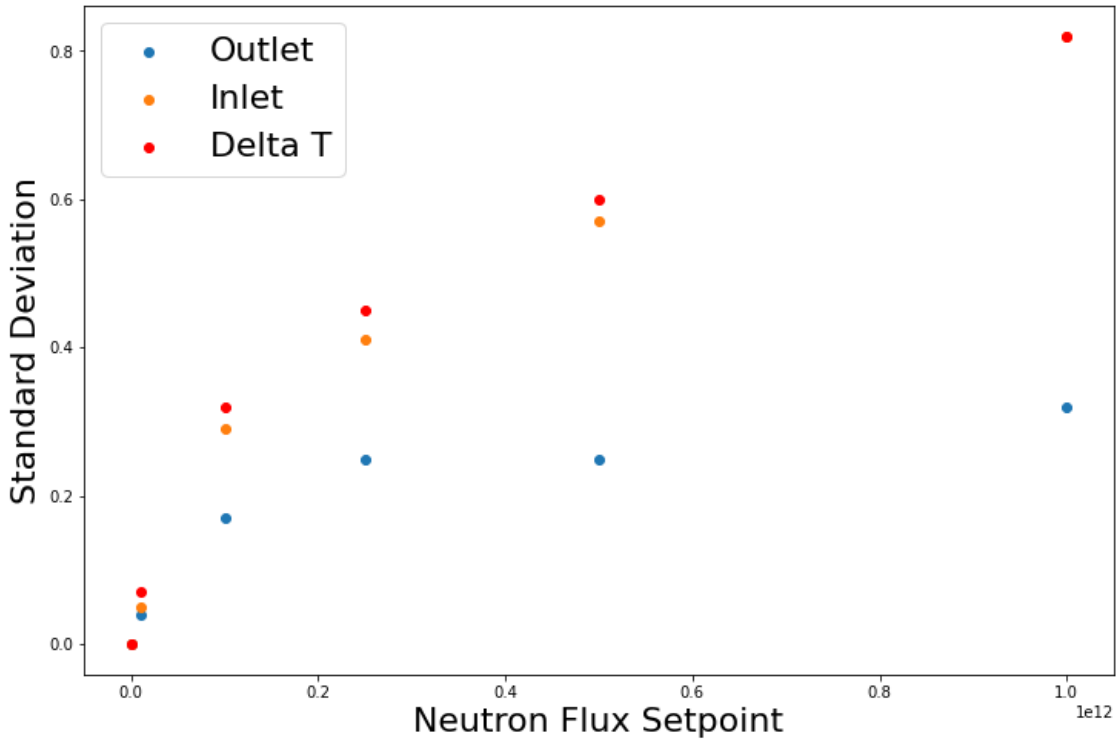

Figure 28: New core standard deviation of temperature probe data versus inner neutron flux.

From Figure 28 we can make several determinations about the SLOWPOKE-2 temperature probe noise, and how to mitigate this noise in future work on this project. First, it is evident that using the outlet temperature data will result in more accurate temperatures with less uncertainty. Therefore, when comparing simulated data to experimental data the outlet data should be the primary comparison, as opposed to the noisier inlet data. However, due to the lack of convergence in the models presented in

this thesis, outlet temperatures cannot be compared to the simulated results due to the large variation in simulated outlet temperatures. This further indicates the necessity of a converged model for meaningful comparisons. Furthermore, comparison of simulated data to experimental data should be done at low power, if possible, to reduce the effect temperature probe noise would have on the comparison.

Returning now to the Q value given in Section 4.1 to examine the uncertainty, the standard deviation of the June 30th, 2021, dataset is 0.566 and the standard deviation of the December 8th, 2021, dataset is 0.617 for the timeframe investigated. Note the average ΔT for the dataset before refuelling is 14.97 °C and the average ΔT of the data set after refuelling is 14.58 °C. Using the following error propagation formula for subtraction,

$$\sigma = \sqrt{(\sigma_{af})^2 + (\sigma_{bf})^2} \tag{9}$$

The final temperature difference between these two cores is found to be 0.40 ± 0.8 °C using significant digits. This finding exemplifies the temperature probe noise and therefore large uncertainty that is present on the ΔT half-power result. This reinforces the suggestion of using low power experimental outlet temperature data for comparison to the simulated data from Fluent.

6.2 Turbulence

In addition to a laminar simulation shown in Tables 1 and 2, Model D was also run with a Spalart-Allmaras turbulence model. The turbulence model was run twice, once with default convergence conditions, and once where the model was allowed to go past what Fluent considered converged and run the full 5000 iterations. The model converged when the turbulent kinetic viscosity residual dropped to 8×10^{-4}, after 1572 iterations. Stopping at this iteration the final temperature difference is 23.5 °C, whereas letting the model run for 5000 iterations has a final temperatures difference of 35.4 °C. At default convergence conditions, the turbulent Model D ΔT of 23.5 °C is very similar to the

laminar Model D ΔT of 22.3 °C. It is difficult to draw conclusions from this one model. It is uncertain, although unlikely that turbulent models will have a significant effect on the simulation over laminar flow. In future work once a model has been converged upon, more turbulent models should be tested, including two-equation turbulence model such as the k-epsilon, or k-omega turbulence models. Two equation models should calculate turbulence more accurately at the cost of computation time. While the flow is likely laminar given the fluid mechanics of the SLOWPOKE-2 system, and these models will not differ much from the one equation turbulence model it is worth considering in future work with a converged model.

6.3 Model Assumptions

As stated above one of the clear assumptions of the models used in this project is that the flow is laminar. Other assumptions include the use of the Boussinesq approximation. Since the SLOWPOKE-2 does not boil water and is kept at approximately 15 °C when the reactor is powered off and allowed to reach a steady-state this approximation is reasonable. The change in density of light water during reactor operation, divided by the density of light water will always be much smaller than 1, therefore the Boussinesq approximation is consistent with SLOWPOKE-2 operation. Another key assumption is that the convective heat transfer coefficient on the container walls is 5 W/m^2K, and this was only applied to the outer wall of the container, not the top or bottom. This heat transfer coefficient is likely the correct magnitude and may not affect the simulation results greatly, but more experiments need to be done on the SLOWPOKE-2 system to determine a more accurate value.

Chapter 7: Conclusions

In this project, a primary objective is to create a system capable of detecting changes in the fissile content of the SLOWPOKE-2 using only external neutron flux data and accurate thermal power. While this system has not yet been implemented, this project provided several positive developments including a demonstration that in part supports the theory behind the enhanced fuel monitoring system holds true at the SLOWPOKE-2 facility as well.

The SLOWPOKE-2 data first needed to be converted into useable file formats so that data analysis with Python was possible. After this, the data sets from before and after refuelling needed to be looked over to find two data sets that were comparable lengths and started at the same ambient initial conditions. This was done for all power levels and included neutron flux data. The noise of the raw data made drawing definitive conclusions difficult, and as such an error analysis on the temperature probe noise needed to be conducted. Similarly, appropriate data sets needed to be investigated to ensure the noise of various power levels was not artificially inflated due to the initial conditions or length of the reactor run at this power.

By investigating the neutron flux data and temperature data of the SLOWPOKE-2 before and after refuelling several observations were made. First, there is a clear temperature and therefore power difference between the two cores despite the SLOWPOKE-2 being operated at the same neutron flux setpoint, the only measure in the reactor of thermal power. As calculated in Chapter 4.1, the difference in energy between the two cores is estimated to be approximately 300 kJ ± 600 kJ with error. The large uncertainty on this figure, which was calculated from half-power operation, comes from the noise in the temperature probes which increases at higher reactor power is detailed in Section 6.1. The statistical measures on the ΔT values used to estimate the energy difference between the cores can be found in Section 4.1.

The data from the external He-3 detector in the SLOWPOKE-2 facility showed it is possible to differentiate between the two cores operating at the same power, as the newer core outputs slightly less neutron flux. Ideally, the external neutron count should remain the same between the old and new core, however possibly due to shim insertion, or a difference in fissile material of the core, the external neutron count of the new core is slightly lower. Neutrons populating the core are proportional to the external neutron flux and a change in the flux-to-power ratio can indicate changes in the fissile content of the core. However, for this theory to be tested further on the SLOWPOKE-2 the thermal power of the core must be reported with very little error.

There were many obstacles in creating an appropriate CFD model of the SLOWPOKE-2. Cleaning the CAD and ensuring the geometry was error-free was one such obstacle. Cleaning faults required the geometry to be meshed after, and if the mesh was not correctly capturing the geometry, more investigation into geometry faults needed to be conducted. This process repeated for some time before the geometry was fault free, and with proper meshing techniques could be appropriately captured.

Using appropriate meshing techniques also introduced an obstacle of correct mesh resolution to capture complex areas of the geometry. This was the main obstacle in this project. Refining the mesh by reducing both the maximum and minimum cell size did not guarantee the mesh would be of higher quality, or appropriately capture the areas of interest. As such many refining processes started the meshing process from the beginning, changing the meshing techniques required to refine the mesh in the fuel cage and thermocouple locations.

Loading the simulation appropriately, and setting material properties, turbulence equations, under-relaxation factors and other simulation parameters also had a steep learning curve. If the model was not loaded appropriately, it would take until the simulation was complete before it was discovered that the model had been solved incorrectly. Furthermore, it was not always clear what Fluent setting caused the model to solve incorrectly. It was also possible that the simulation appropriately solved the

SLOWPOKE-2 system, but it was the experimental power and temperatures that were incorrect. As the calibration of the SLOWPOKE-2 could be ± 25% inaccurate at best estimate, and the thermal power is determined via scaling of this neutron flux calibration it is possible the temperature curves of the experimental data are for different power levels than the SLOWPOKE-2 is reporting [4]. Conducting the GCI was to ensure the model was verified and solved the problem correctly, indicating that the SLOWPOKE-2 power level was incorrect; however, the GCI did not provide a useable converged model in this project. To fix this, more models of various mesh resolution should be tested with the same convergence and relaxation conditions. Models that do not output the same thermal power should immediately be discarded.

The motivation behind the CFD aspect of this project was to find an accurate thermal power of the SLOWPOKE-2. While this project succeeded in creating several models of varying mesh resolutions of the SLOWPOKE-2, the results of an initial GCI test suggest that more refining needs to be done to the models before a converged model is created. Some models shown in this project, such as Model D, have the same temperature difference and high inlet and outlet temperatures for half-power as the model created by CNL. Without a proper GCI indicating Model D is verified and has solutions independent of mesh resolution, further conclusions cannot be drawn.

The neutron analysis and CFD process shown in this thesis can be replicated for SMRs to implement the enhanced fuel monitoring system outlined in this thesis and originally presented by van der Ende et al. [5]. However, it should be noted a CFD model is only required for accurate thermal power. If the SMRs in question implementing the enhanced fuel monitoring system have accurate thermal power calibration, then a CFD model is not required. Therefore, following the external neutron flux methodology shown in this thesis and normalizing these values by the accurate thermal power of the reactor should be sufficient to begin enhanced fuel monitoring of SMRs.

Chapter 8: Future Work

The next step in this project is to verify a CFD model via a GCI and compare the simulated results of the model to experimental data and to the CFD model created by CNL. After this, the model's thermal power must be slowly adjusted until the temperature curves in a transient (not steady-state) simulation matches the SLOWPOKE-2 temperature curves. This should be done for all power levels to determine if the simulated temperature curves match the experimental temperature curves for startup and shutdown procedures. Due to the reactor being most frequently operated at half-power, comparisons should begin at half-power. The accurate power of the SLOWPOKE-2 would then be indicated by the thermal power of the CFD model that replicated the experimental data. For this thermal power to be checked, the thermal power required to simulate the SLOWPOKE-2 temperature curves should be compared to the thermal power required for the CNL model to simulate the experimental data as well. If the two models agree and have been verified through a GCI, it is a strong indication that the accurate thermal power of the SLOWPOKE-2 is the value given by the CFD simulations.

To reduce the uncertainty on the heat transfer coefficient assigned to the reactor container wall, experiments using a thermocouple placed beside the reactor container in the external pool are being conducted. These experiments involve operating the reactor at different power levels and adjusting the temperature probe location along the reactor container wall to investigate the temperatures and heat transfer behaviour. Once the heat transfer outside the reactor container is known it should also be set on the top and bottom walls of the reactor container.

Finally, the accurate thermal power can be used in tandem with the external neutron flux data presented in this paper to create a plot similar to Figure 4 where neutron flux to thermal power ratios before and after refuelling can be compared to determine if a change in the fissile content via refuelling can be detected. If so, the

change in fissile content according to this detection system should then be compared to the actual change in fissile content that occurred during refuelling.

In the future, neutron flux and thermal power of the new core can be investigated over time to determine if burnup, fission products, and shim addition change the results shown in this thesis, and to what degree.

To achieve the final objectives of this project, the following tasks are being proposed as a continuation of this thesis. Measuring reactor thermal power is important for analysis of the reactor core fissile content, based upon neutron flux data. It appears that the difference in inlet (T_i) and outlet (T_o) core temperatures may indicate thermal power to serve this purpose. A CFD model of the RMC SLOWPOKE-2 reactor has been created to accurately establish the relationship between $\Delta T = T_o - T_i$ and the reactor thermal power. The results of the RMC and CNL models are to be compared against each other. Due to intricacies and geometrical asymmetry in the design of the reactor, it has taken considerable time and effort to set up CFD models that produce realistic results. It is proposed that further refinement, benchmarking, and proper cross-comparison of the CFD models be completed. This modeling work, along with appropriate measured data and measured data error analysis sets a proper foundation for establishing a means of accurately measuring the thermal power in the core of the SLOWPOKE-2 reactor.

Measurement and analysis of changes in fissile content, before and after refueling of the RMC SLOWPOKE reactor, is to be completed using in-core and out-of-core neutron flux data being collected. Analysis of available data does demonstrate, although not completely align with the predictions of the model published, showing reduced external neutron count with changes in fissile isotope inventory. More in-depth analysis would be required for using the enhanced fuel monitoring system and to fully describe the changes in the SLOWPOKE-2 system from refuelling.

It is recommended that the procedures outlined in this thesis and the neutron flux analysis presented be applied to other thermal reactors, including SMR reactors to evaluate the viability of the enhanced fuel monitoring technique in other reactors.

Chapter 9: References

[1] S. PRASAD, A. Abdulla, M.G. Morgan, and I.L. Azevedo, "Nonproliferation Improvements and Challenges Presented by Small Modular Reactors," Progress in Nuclear Energy, vol. 80, pp. 102–109, Apr. 2015, doi: 10.1016/J.PNUCENE.2014.11.023

[2] J. WHITLOCK and J. Sprinkle, "Proliferation Resistance Considerations for Remote Small Modular Reactors," AECL Nuclear Review., vol. 1, no. 2, pp. 9–12, Dec. 2012, doi: 10.12943/ANR.2012.00013

[3] J.R.M PIERRE. Low enrichment uranium (LEU)-Fueled SLOWPOKE-2 nuclear reactor simulation with the Monte-Carlo based MCNP 4A code. Master's Thesis, Department of Chemistry and Chemical Engineering Royal Military College of Canada. Kingston (1996).

[4] J. C. DUCHESNE. RMC SLOWPOKE-2 Reactor Thermal Power Determination by Core Water Temperature Measurements. Master's Thesis, Department of Chemistry and Chemical Engineering Royal Military College of Canada. Kingston (1994).

[5] B. VAN DER ENDE, L. Li, D. Godin, and B. Sur. "Stand-off nuclear reactor monitoring with neutron detectors for safeguards and non-proliferation applications." *Nature Communications*, 10:1959 (2019).

[6] J. ATFIELD, L. Yaraskavitch, J. Spencer, S. Yue, P. Chan, and P. Samuleev. RMC SLOWPOKE-2 Reactor – core reload and commissioning tests. 15th International CANDU Fuel Conference. Ajax 2022.

[7] B. SUR. Personal Communication, Canadian Nuclear Laboratories, Chalk River. 2023.

[8] IAEA Department of Safeguards. Long-Term R&D Plan, 2012–2023, STR-375.

[9] R. T. DE WIT. "Reactivity calculations for the low enrichment uranium fueled SLOWPOKE-2 reactor at the Royal Military College of Canada." Master's Thesis, Department of Chemistry and Chemical Engineering Royal Military College of Canada. Kingston (1989).

[10] ANSYS Fluent Theory Guide, release 15.0. 2013.

[11] Ansys Fluent Fluid Simulation Software, available at https://www.ansys.com/products/fluids/ansys-fluent (accessed 2023 Feb. 28).

[12] COMSOL, available at https://www.comsol.com/cfd-module (accessed 2023 Mar. 10)

[13] Siemens PLM Software, Simcenter STAR-CCM+, available at https://star-ccm.com/ (accessed 2023 Feb. 28).

[14] P. H. OOSTHUIZEN, D. Naylor. An Introduction to convective heat transfer analysis. McGraw-Hill. (1999).

[15] ANSYS FLUENT 12.0 Documentation, available at https://www.afs.enea.it/project/neptunius/docs/fluent/html/ug/node812.htm (accessed 2023 Mar. 10)

[16] K. PODILLA. Personal Communication, Canadian Nuclear Laboratories, Chalk River. 2023.

Appendix A: Reactor Operation Time/Date Used in the Present Work

Date	Time	Power	Core
January 6th 2020	12:33:43 PM – 3:20:52 PM	$5x10^{11}$	Old
December 8th 2021	9:17:34 AM – 3:35:39 PM	$5x10^{11}$	New
June 13th 2022	10:40:18 AM – 4:08:09 PM	$1x10^{10}$, $1x10^{11}$, $2.5x10^{11}$, $5x10^{11}$	New
June 20th 2022	11:14:30 AM – 4:47:49 PM	$1x10^{12}$	New
June 30th 2021	11:06:54 AM – 6:24:37 PM	$5x10^{11}$	Old
May 17th 2021	9:55:49 AM – 4:17:18 PM	$5x10^{11}$, $1x10^{11}$, $1x10^{10}$	Old

Appendix B: Additional Figures

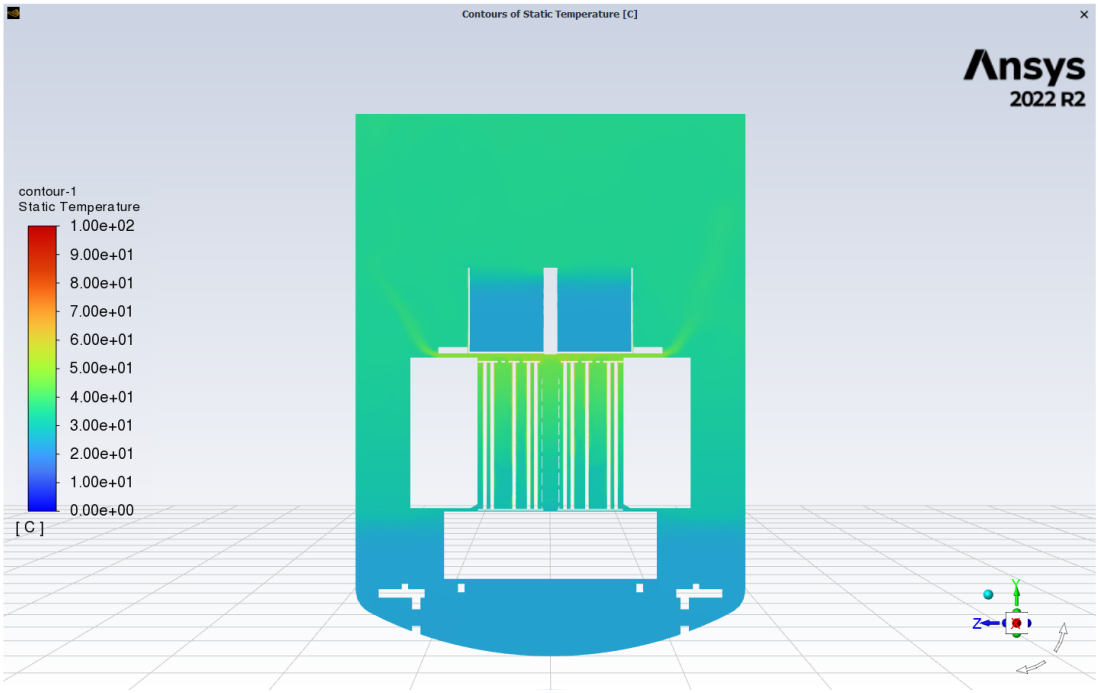

Figure 29: Model A temperature contour plot.

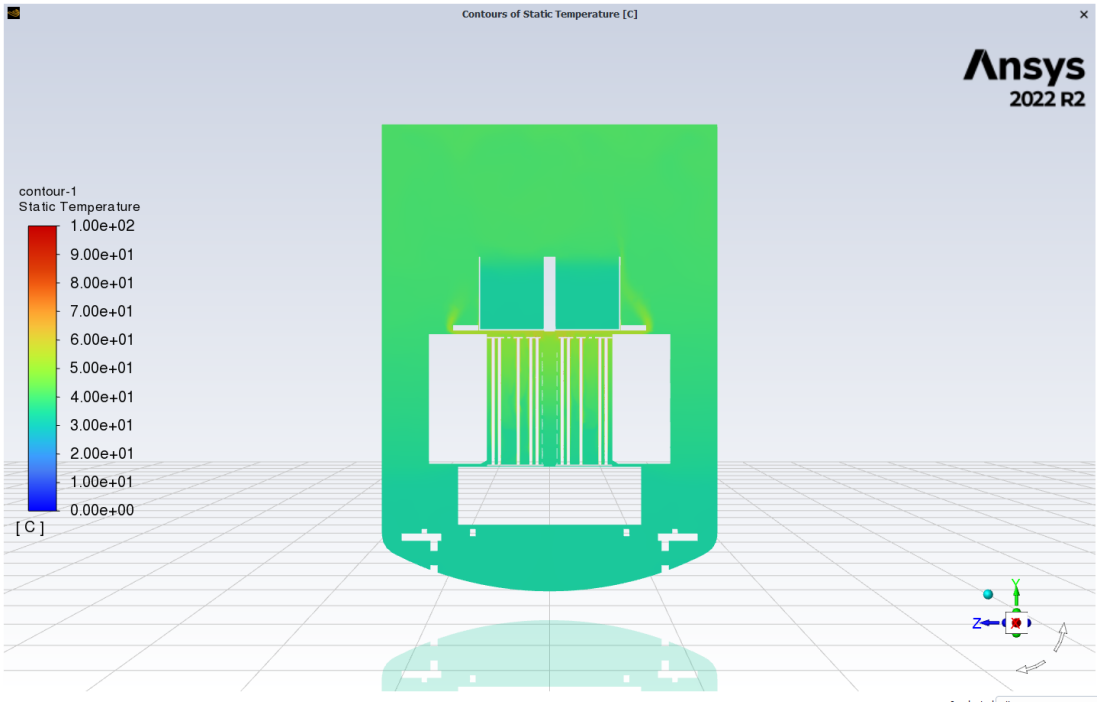

Figure 30: Model B temperature contour plot.

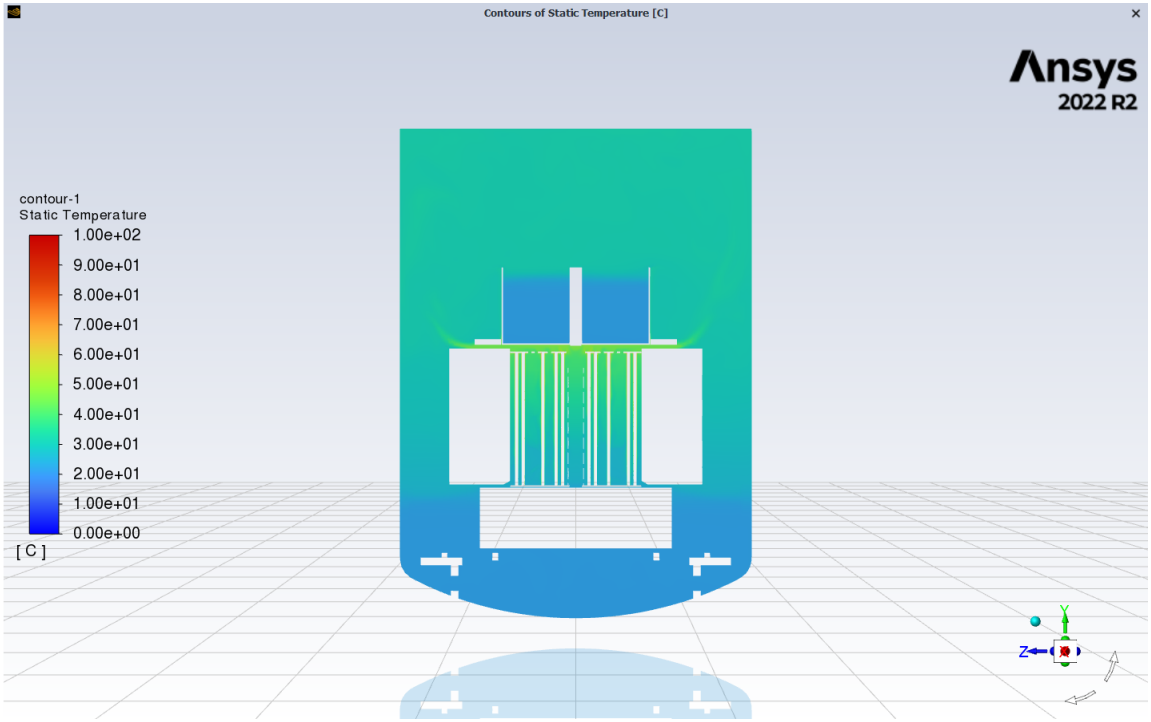

Figure 31: Model C temperature contour plot.

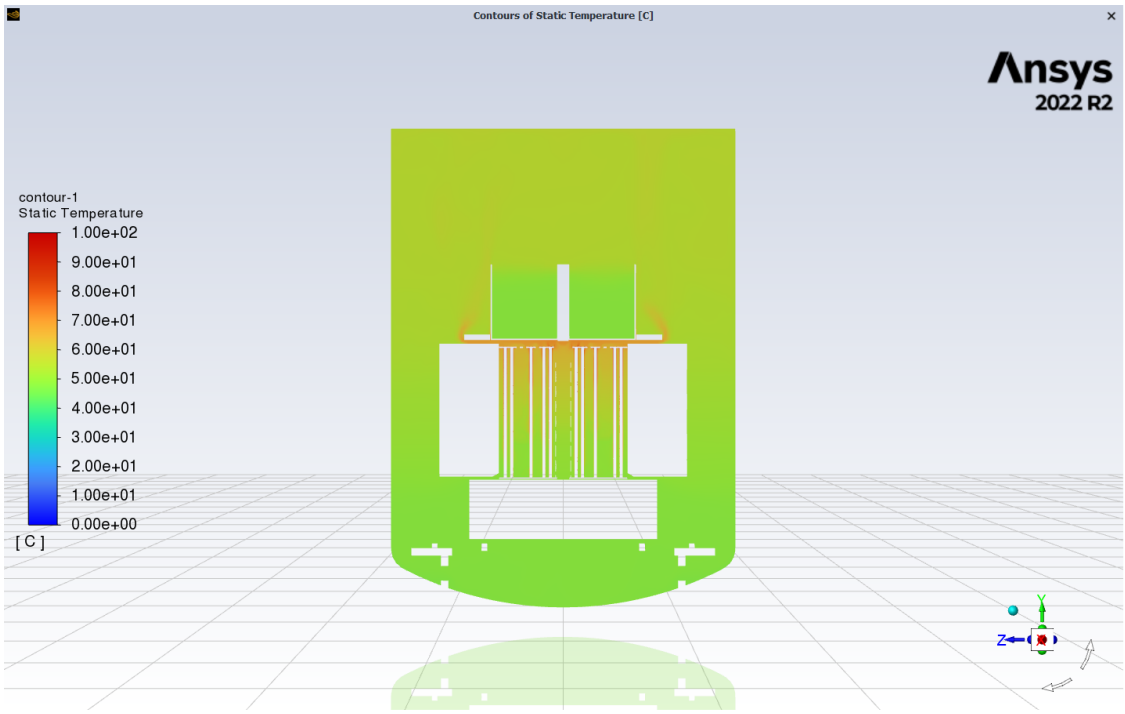

Figure 32: Model D temperature contour plot.

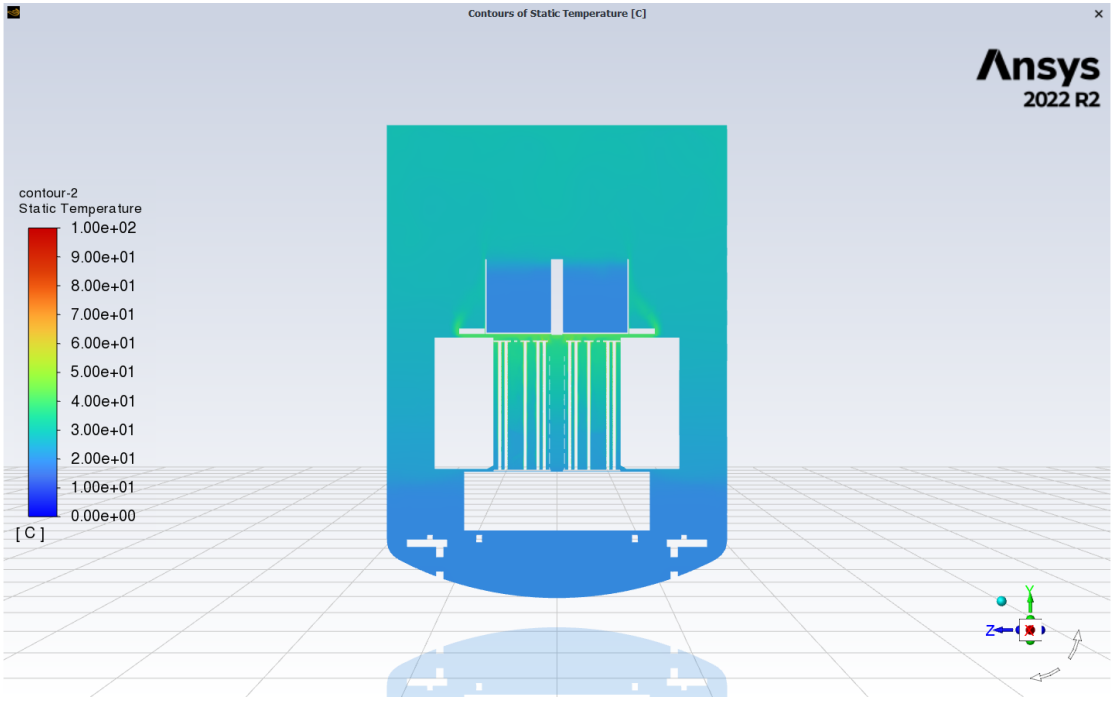

Figure 33: Model E temperature contour plot.

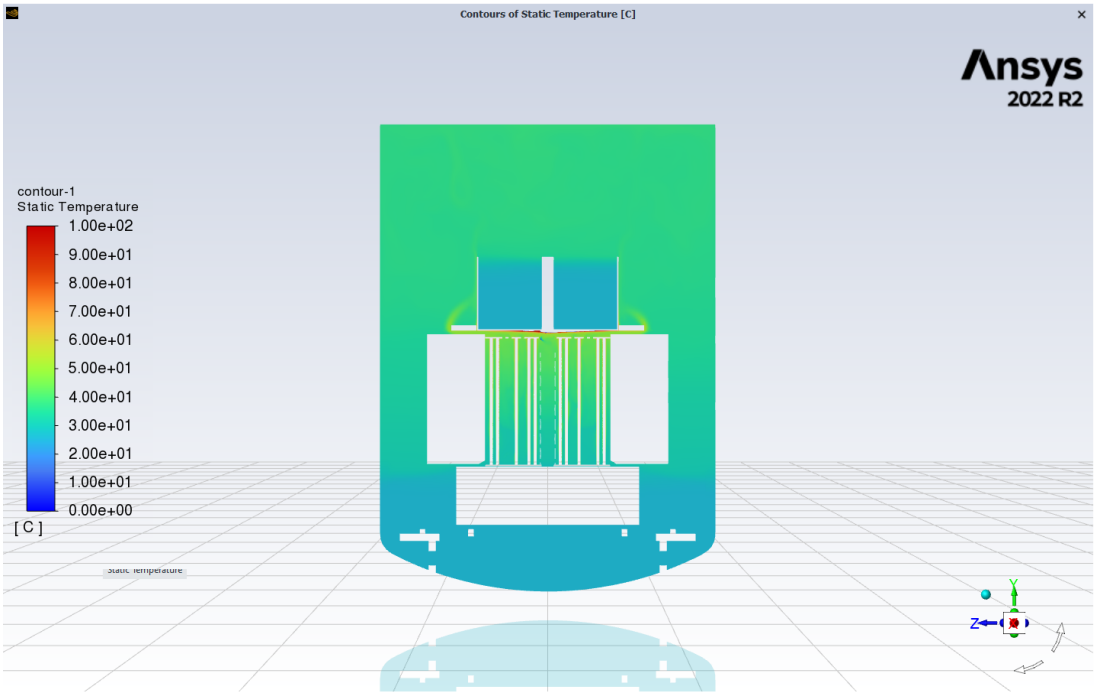

Figure 34: Model F temperature contour plot.

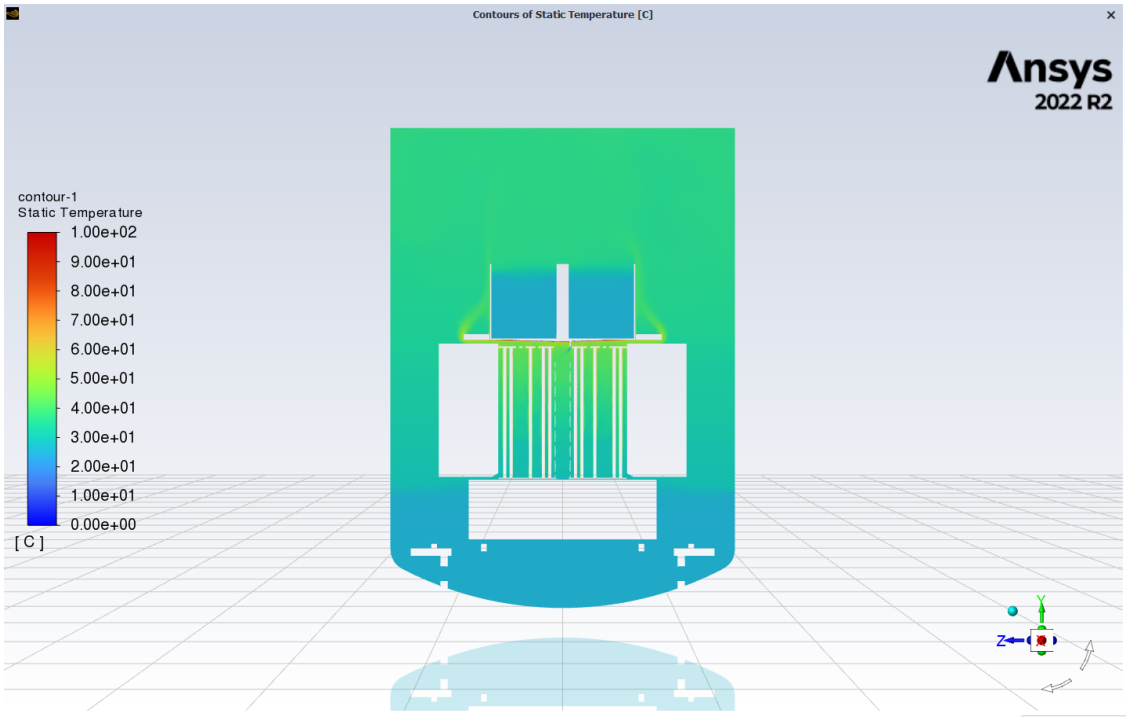

Figure 35: Model G temperature contour plot.

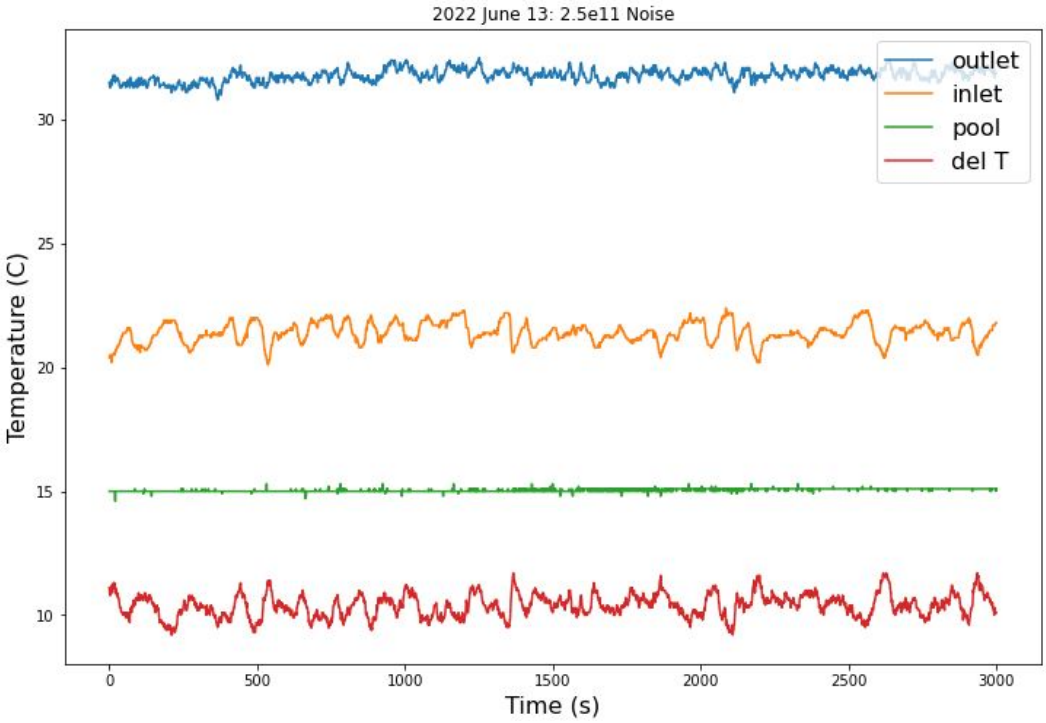

Figure 36: Temperature curves at the flux setting 2.5x10^{11} cm^{-2}s^{-1}.

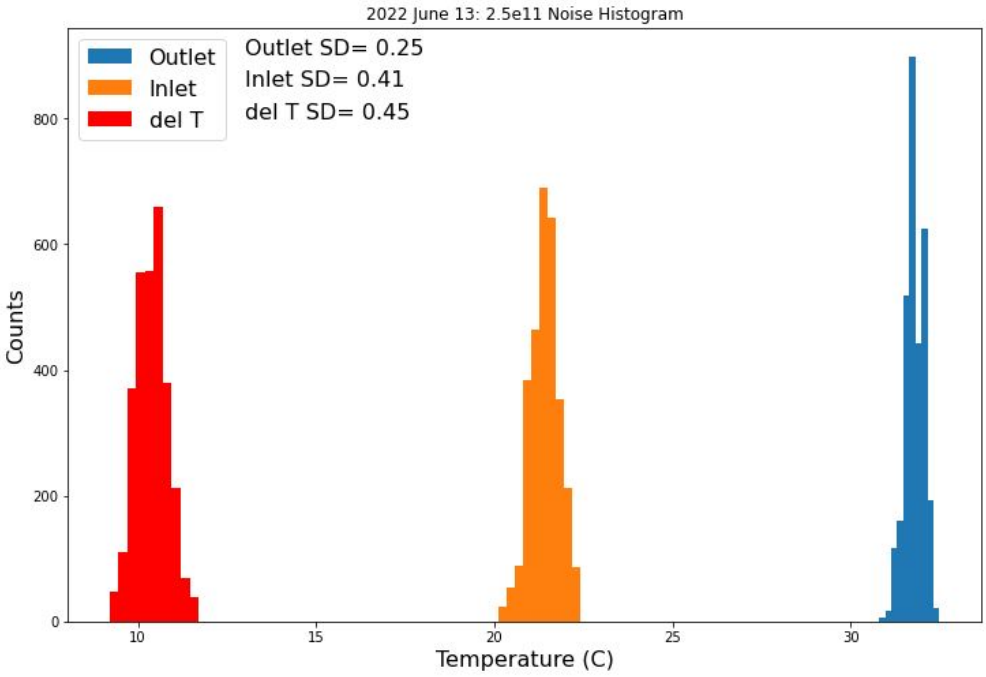

Figure 37: Temperature noise histograms at the flux setting 2.5x10^{11} cm^{-2}s^{-1}.

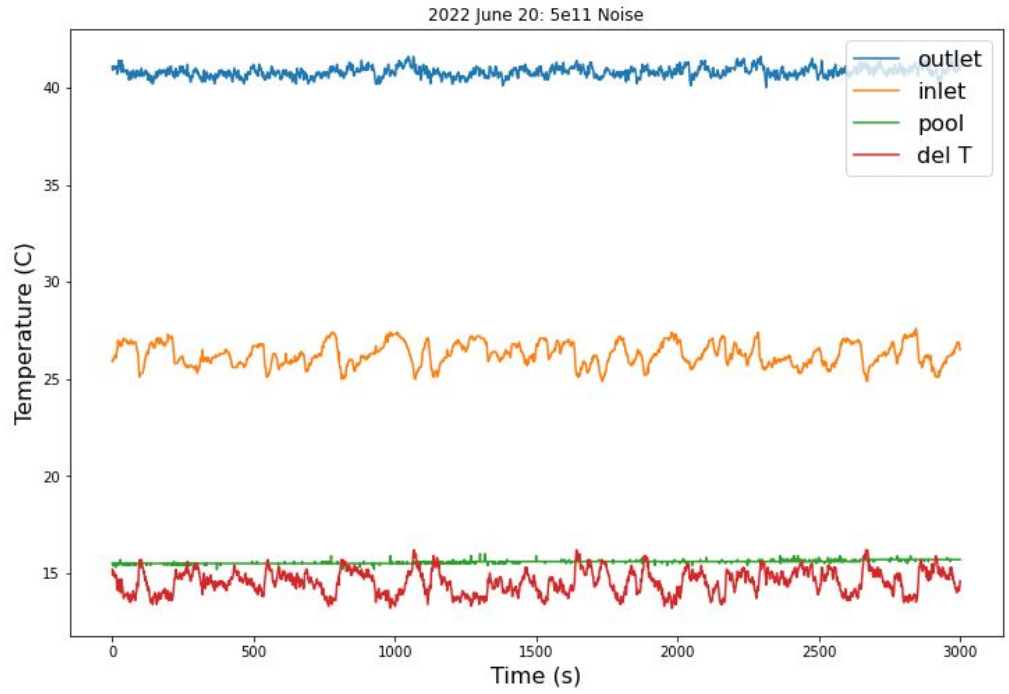

Figure 38: Temperature curves at the flux setting $5x10^{11}$ $cm^{-2}s^{-1}$.

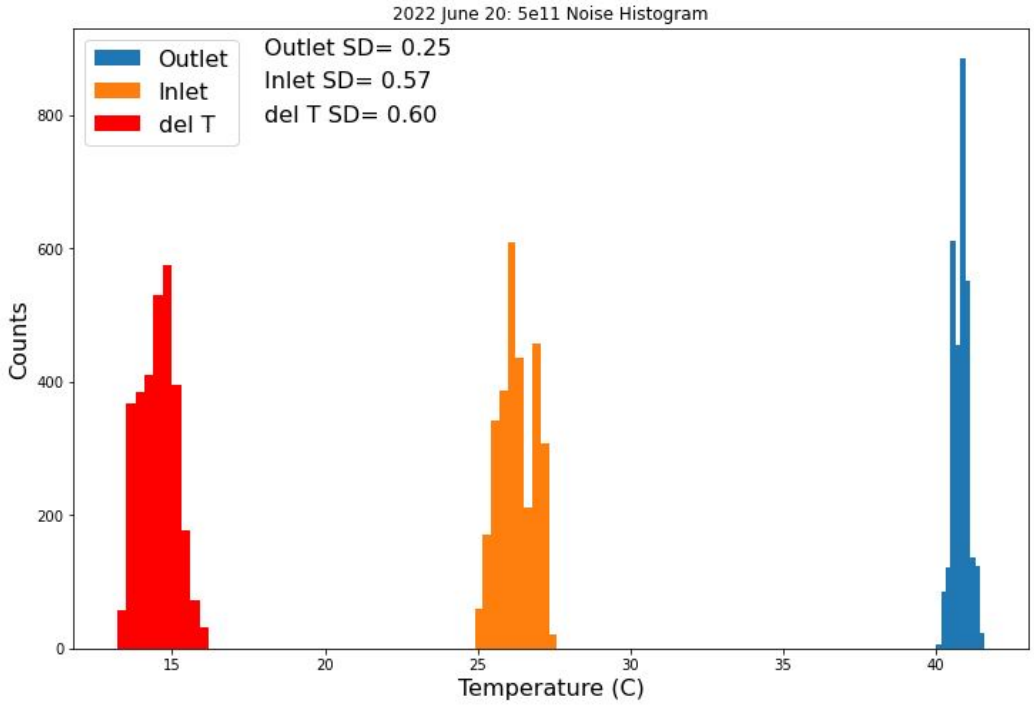

Figure 39: Temperature noise histograms at the flux setting $5x10^{11}$ $cm^{-2}s^{-1}$

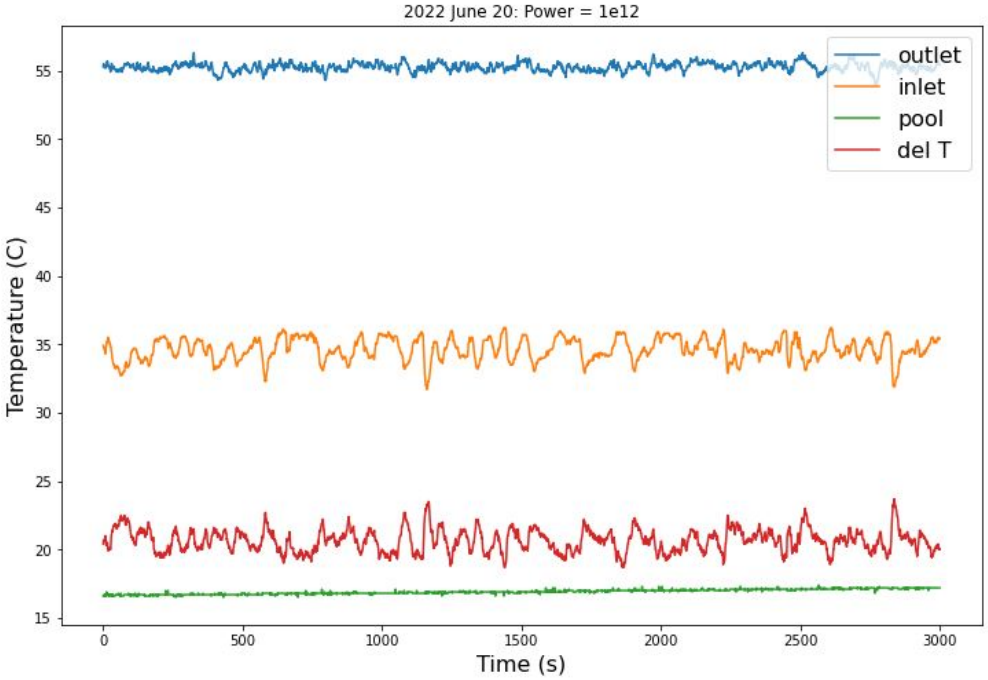

Figure 40: Temperature curves at the flux setting $1x10^{12}$ $cm^{-2}s^{-1}$

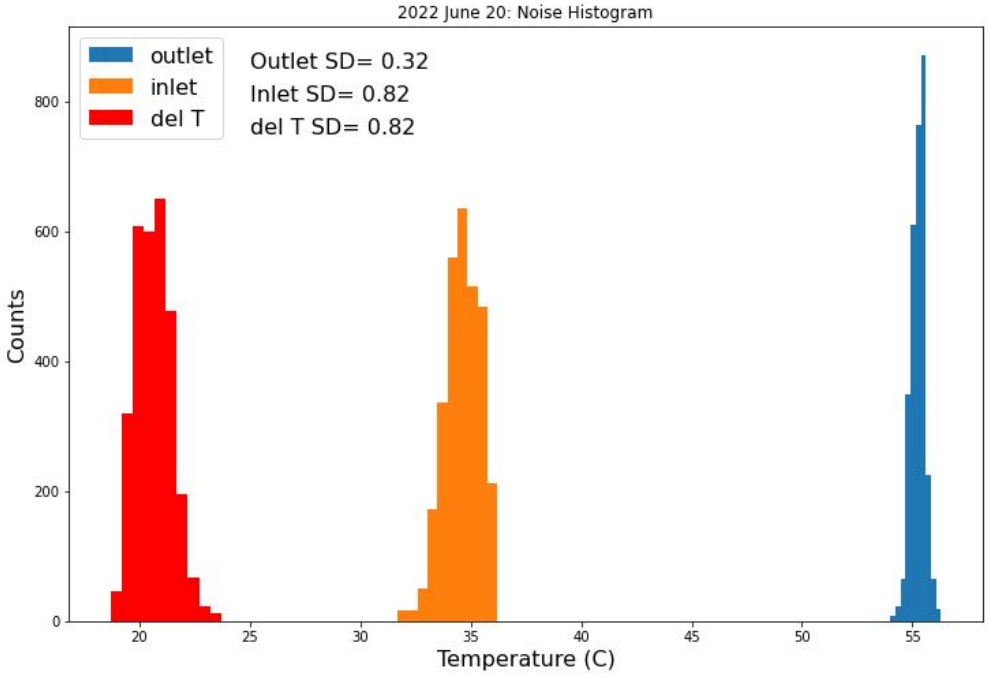

Figure 41: Temperature noise histograms at the flux setting $1x10^{12}$ $cm^{-2}s^{-1}$.

Appendix C: Shell Scripts & Journal Files

Example Journal File:

```
/file/set-tui-version "22.2"

/file/rc pres19.cas.gz

/solve/init/init/

/solve/iterate 5000

/wc pres19_res.cas.gz

/wd pres19_res.dat.gz

/exit yes
```

Example Shell Script:

```
#/bin/sh


## embedded options to bsub start with #BSUB


## — Name of the job —


#BSUB -J pres19


## — specify queue from the bqueues list —
```

```
#BSUB -q adept

# — specify the number of processors —

#BSUB -n 32

## — Specify the output and error files. %J is the job ID —

## — -o and -e mean append, -oo and-eo mean overwrite —

#BSUB -oo pres19%J.out

#BSUB -eo pres19%J.err

#!/bin/tcsh

fluent 3d -g -t32 -i pres19.jou -scheduler=lsf
```

Appendix D: Fluent Input Settings

Fluent

Version: 3d, dp, pbns, lam (3d, double precision, pressure-based, laminar)

Release: 22.2.0

Title:

Models

Model	Settings
Space	3D
Time	Steady
Viscous	Laminar
Heat Transfer	Enabled
Solidification and Melting	Disabled
Radiation	None
Species	Disabled
Coupled Dispersed Phase	Disabled
NOx Pollutants	Disabled

SOx Pollutants Disabled

Soot Disabled

Mercury Pollutants Disabled

Structure Disabled

Acoustics Disabled

Eulerian Wall Film Disabled

Potential/Li-ion Battery Disabled

Multiphase Disabled

Material Properties

Material: aluminum-1050a-h19 (solid)

Property	Units	Method	Value(s)
Density	kg/m^3	constant	2709.8
Cp (Specific Heat)	J/(kg K)	constant	895.61
Thermal Conductivity	W/(m K)	constant	236.67

Material: water-liquid (fluid)

Property	Units	Method	Value(s)
Density	kg/m^3	boussinesq	997
Cp (Specific Heat)	J/(kg K)	constant	4182
Thermal Conductivity	W/(m K)	constant	0.6
Viscosity	kg/(m s)	constant	0.001003
Molecular Weight	kg/kmol	constant	18.0152

Material: zr (solid)

Property	Units	Method	Value(s)
Density	kg/m^3	constant	6560
Cp (Specific Heat)	J/(kg K)	constant	285
Thermal Conductivity	W/(m K)	constant	21.5

Cell Zone Conditions

Zones

name id type

---

fluid1 22417 fluid

Setup Conditions

fluid1

Condition Value

Frame Motion? no

Boundary Conditions

Zones

name id type

---

a14977_inletthermocouplesocket 1820 wall

pipes:22320 22320 wall

pipes:22319 22319 wall

pipes:22318 22318 wall

pipes:22317 22317 wall

pipes:22316 22316 wall

rodwall 1824 wall

rodtf 1823 wall

a10713_vessel_lowershellassembly_bottom 1822 wall

a10754_shimtray 1821 wall

a18227_outerirradiationtubeguideplate 1819 wall

a10718_berylliumlowerplate 1818 wall

a10716_reflectorannulus 1817 wall

a10753_coreupperspacer_meshcontrol 1816 wall

a10753_coreupperspacer 1815 wall

a10718_berylliumplateroof 1814 wall

a10754_shimtray_topsupports 1813 wall

a18245_check_supports 1812 wall

a18245_bottomsupportplate 1811 wall

a18245_topsupportplate_bits 1810 wall

a18245_basket 1809 wall

a18245_topsupportplate 1808 wall

a17996_thermalcolumnassembly 1807 wall

a18228_annulussupportplateassembly 1806 wall

pipes 1805 wall

vesseltop_out 1804 wall

a10713_vessel_lowershellassembly 1803 wall

Setup Conditions

a14977_inletthermocouplesocket

Condition	Value
Thermal BC Type	Heat Flux
Wall Motion	Stationary Wall
Shear Boundary Condition	No Slip

pipes:22320

Condition	Value
Thermal BC Type	Heat Flux

Wall Motion Stationary Wall

Shear Boundary Condition No Slip

pipes:22319

Condition Value

Thermal BC Type Heat Flux

Wall Motion Stationary Wall

Shear Boundary Condition No Slip

pipes:22318

Condition Value

Thermal BC Type Heat Flux

Wall Motion Stationary Wall

Shear Boundary Condition No Slip

pipes:22317

Condition	Value
Thermal BC Type	Heat Flux
Wall Motion	Stationary Wall
Shear Boundary Condition	No Slip

pipes:22316

Condition	Value
Thermal BC Type	Heat Flux
Wall Motion	Stationary Wall
Shear Boundary Condition	No Slip

rodwall

Condition	Value
Material Name	zr
Thermal BC Type	Heat Flux
Heat Flux [W/m^2]	11668.3

Wall Motion	Stationary Wall
Shear Boundary Condition	No Slip

rodtf

Condition	Value
Material Name	zr
Thermal BC Type	Heat Flux
Wall Motion	Stationary Wall
Shear Boundary Condition	No Slip

a10713_vessel_lowershellassembly_bottom

Condition	Value
Thermal BC Type	Heat Flux
Wall Motion	Stationary Wall
Shear Boundary Condition	No Slip

a10754_shimtray

Condition	Value
Thermal BC Type	Heat Flux
Wall Motion	Stationary Wall
Shear Boundary Condition	No Slip

a18227_outerirradiationtubeguideplate

Condition	Value
Thermal BC Type	Heat Flux
Wall Motion	Stationary Wall
Shear Boundary Condition	No Slip

a10718_berylliumlowerplate

Condition	Value
Thermal BC Type	Heat Flux
Wall Motion	Stationary Wall

Shear Boundary Condition No Slip

a10716_reflectorannulus

Condition	Value
Thermal BC Type	Heat Flux
Wall Motion	Stationary Wall
Shear Boundary Condition	No Slip

a10753_coreupperspacer_meshcontrol

Condition	Value
Thermal BC Type	Heat Flux
Wall Motion	Stationary Wall
Shear Boundary Condition	No Slip

a10753_coreupperspacer

Condition	Value

Thermal BC Type Heat Flux

Wall Motion Stationary Wall

Shear Boundary Condition No Slip

a10718_berylliumplateroof

Condition Value

Thermal BC Type Heat Flux

Wall Motion Stationary Wall

Shear Boundary Condition No Slip

a10754_shimtray_topsupports

Condition Value

Thermal BC Type Heat Flux

Wall Motion Stationary Wall

Shear Boundary Condition No Slip

a18245_check_supports

Condition	Value
Thermal BC Type	Heat Flux
Wall Motion	Stationary Wall
Shear Boundary Condition	No Slip

a18245_bottomsupportplate

Condition	Value
Thermal BC Type	Heat Flux
Wall Motion	Stationary Wall
Shear Boundary Condition	No Slip

a18245_topsupportplate_bits

Condition	Value
Thermal BC Type	Heat Flux

Wall Motion	Stationary Wall
Shear Boundary Condition	No Slip

a18245_basket

Condition	Value
Thermal BC Type	Heat Flux
Wall Motion	Stationary Wall
Shear Boundary Condition	No Slip

a18245_topsupportplate

Condition	Value
Thermal BC Type	Heat Flux
Wall Motion	Stationary Wall
Shear Boundary Condition	No Slip

a17996_thermalcolumnassembly

Condition	Value
Thermal BC Type	Heat Flux
Wall Motion	Stationary Wall
Shear Boundary Condition	No Slip

a18228_annulussupportplateassembly

Condition	Value
Thermal BC Type	Heat Flux
Wall Motion	Stationary Wall
Shear Boundary Condition	No Slip

pipes

Condition	Value
Thermal BC Type	Heat Flux
Wall Motion	Stationary Wall
Shear Boundary Condition	No Slip

vesseltop_out

Condition	Value
Thermal BC Type	Heat Flux
Wall Motion	Stationary Wall
Shear Boundary Condition	No Slip

a10713_vessel_lowershellassembly

Condition	Value
Thermal BC Type	Convection
Convective Heat Transfer Coefficient [W/(m^2 K)]	5
Wall Motion	Stationary Wall
Shear Boundary Condition	No Slip

Solver Settings

Equations

Equation	Solved
Flow	yes
Energy	yes

Numerics

Numeric	Enabled
Absolute Velocity Formulation	yes

Pseudo Time Explicit Relaxation Factors

Variable	Relaxation Factor
Density	1
Body Forces	1
Energy	0.5
Explicit Momentum	0.5

Explicit Pressure 0.5

Linear Solver

Variable Solver Type Termination Criterion Residual Reduction Tolerance

---

Flow F-Cycle 0.1

Energy F-Cycle 0.1

Pressure-Velocity Coupling

Parameter Value

Type Coupled

Pseudo Time Method (Global Time Step) yes

Discretization Scheme

Variable Scheme

Pressure Second Order

Momentum Second Order Upwind

Energy Second Order Upwind

Solution Limits

Quantity	Limit
Minimum Absolute Pressure	1
Maximum Absolute Pressure	5e+10
Minimum Temperature	1
Maximum Temperature	5000